

**CHARACTERIZATION OF WOOD BIOCHAR AND EVALUATION OF ITS
ADSORPTION POTENTIAL FOR REMOVAL OF SULPHATE FROM
PRODUCED WATER IN OFFSHORE OIL AND GAS INDUSTRY**

by

© Yashodha Gayanthree Marambage

A Thesis submitted to the

School of Graduate Studies

in partial fulfilment of the requirements for the degree of

Master of Engineering

Faculty of Engineering and Applied Science

Memorial University of Newfoundland

May 2016

St. John's

Newfoundland

Abstract

This thesis analyses the potential of wood biochar as an adsorbent in removal of sulphate from produced water. In worldwide offshore oil and gas industry, a large volume of waste water is generated as produced water. Sulphur compounds present in these produced water streams can cause environmental problems, regulatory problems and operational issues. Among the various sulphur removal technologies, the adsorption technique is considered as a suitable method since the design is simple, compact, economical and robust. Biochar has been studied as an adsorbent for removal of contaminants from water in a number of studies due to its low cost, potential availability, and adsorptive characteristics. In this study, biochar produced through fast pyrolysis of bark, hardwood sawdust, and softwood sawdust were characterized through a series of tests and were analysed for adsorbent properties. Treating produced water using biochar sourced from wood waste is a two-fold solution to environmental problems as it reduces the volume of these wastes. Batch adsorption tests were carried out to obtain adsorption capacities of each biochar sample using sodium sulphate solutions. The highest sulphur adsorption capacities obtained for hardwood char, softwood char and bark char were 11.81 mg/g, 9.44 mg/g, and 7.94 mg/g respectively at 10 °C and pH=4. The adsorption process followed the second order kinetic model and the Freundlich isotherm model. Adsorption reaction was thermodynamically favourable and exothermic. The overall analysis concludes that the wood biochar is a feasible, economical, and environmental adsorbent for removal of sulphate from produced water.

Acknowledgements

I would like to thank my supervisor Dr Kelly Hawboldt for the guidance, encouragement and financial support provided. Without her precious support, it would not have been possible to conduct this research. Also, I greatly acknowledge the funding received by the Discovery grants program of the Natural Sciences and Engineering Research Council, Canada and the School of Graduate Studies, Memorial University.

I highly appreciate the support I was given by the staff in the Faculty of Engineering and Applied Science and the Department of Chemistry at Memorial University, especially Dr. Lenard Lye, Moya Crocker, Colleen Mahoney, Dr. Brent Myron, Christina Bottaro, Adam Beaton, Pam King, Lakmali Hewa, Kelly Leshane, Julie Collins, Dr. David Grant, Dr. Wanda Aylward, Alison Pye, Dr. Geert, Dr. Yan Zhang, Dr. Robert Helleur and everyone else who helped me in some way.

Besides the staff at Memorial University, I would like to thank Dr. Shantha Amarasinghe and Dr. Sanja Gunawardena who guided me and encouraged me to start my graduate studies at Memorial University. I would like to express my gratitude to all the faculty members at University of Moratuwa, Sri Lanka, where I completed my undergraduate degree in Chemical and Process Engineering. I would like to thank all of my friends who supported me from the beginning. Finally, I would like to thank my wonderful husband Gayan Jayasundara and my family for all the love and support. Thank you!

Table of Contents

Abstract	ii
Acknowledgements	iii
Table of Contents	iv
List of Tables	viii
List of Figures	x
List of Symbols, Nomenclature or Abbreviations	xii
List of Appendices	xv
Introduction and Overview	1
Co-authorship Statement.....	4
Chapter 1. Removal of Sulphur Compounds from Offshore Produced Water -Review	5
1.1 Introduction.....	6
1.2 Composition of produced water	8
1.2.1 Natural compounds of oil/gas present in produced water.....	8
1.2.2 Production chemicals added in produced water.....	11
1.3 Produced water treatment processes	12
1.3.1 Chemical treatment	13
1.3.2 Biological treatment.....	13
1.3.3 Physical treatment	14
1.4 Adsorption processes in produced water treatment	16
1.5 Treatment of Sulphur Compounds in Produced Water.....	17

1.6	Adsorption of sulphur compounds from aqueous solutions	22
1.7	Adsorption kinetics	29
1.7.1	Pseudo first order kinetic model	30
1.7.2	Pseudo Second order kinetic model	30
1.8	Adsorption Capacity and isotherms	35
1.8.1	Freundlich isotherm model	37
1.8.2	Langmuir isotherm model.....	38
1.8.3	BET isotherm model	39
1.9	Thermodynamics of Adsorption	45
1.10	Conclusion	48
1.11	Bibliography- Chapter 1	50
Chapter 2.	Characterization of Biochar - Review.....	56
2.1	Introduction.....	57
2.2	Pyrolysis of biomass	58
2.3	Biochar as an Adsorbent in Water Treatment.....	61
2.4	Characterization of Biochar	67
2.4.1	Surface area, total pore volume and pore size distribution.....	67
2.4.2	Biochar Density (solid /true density and bulk density).....	72
2.4.3	Char particle structure and surface topography	74
2.4.4	Moisture, ash, volatile matter, and fixed carbon content.....	77
2.4.5	Elemental composition.....	78
2.4.6	Functional groups/ Surface functionality	81

2.4.7	Crystalline structure and mineralogical composition.....	86
2.5	Conclusion	88
2.6	Bibliography –Chapter 2.....	90
Chapter 3.	Biochar Characterization Results and Discussion	95
3.1	Introduction.....	96
3.2	Materials and methods	96
3.3	Results and discussion	99
3.3.1	N ₂ adsorption isotherms, specific surface area, pore characteristics	99
3.3.2	Biochar density	101
3.3.3	SEM analysis	101
3.3.4	pH of biochar	103
3.3.5	Thermo gravimetric analysis.....	103
3.3.6	Elemental composition.....	105
3.3.7	ATR (Attenuated Total Reflection)-FTIR Results.....	107
3.3.8	X-Ray Diffraction analysis	109
3.4	Conclusion	111
3.5	Bibliography- Chapter 03	113
Chapter 4.	Adsorption of Sulphate Using Wood Biochar	115
4.1	Introduction.....	116
4.2	Materials and methods	118
4.2.1	Characterization of biochar.....	118
4.2.2	Batch adsorption experiments.....	119

4.2.3	Adsorption kinetic studies.....	120
4.2.4	Adsorption isotherm studies	121
4.2.5	Adsorption thermodynamic studies	122
4.3	Results and discussion	124
4.3.1	Effect of the biochar type and the temperature	124
4.3.2	Adsorption Kinetics	127
4.3.3	Adsorption isotherms	134
4.3.4	Adsorption thermodynamics	137
4.4	Conclusion	139
4.5	Bibliography- Chapter 04	141
Chapter 5.	Summary	143
5.1	Future work and recommendations.....	145
5.2	Challenges.....	145

List of Tables

Table 1-1: Produced water generation at offshore operations (Lee and Neff 2011).....	6
Table 1-2 Concentrations of naturally occurring compounds in produced water (Neff, 2002)	10
Table 1-3 Production chemicals in produced water (Igunnu, 2012).....	11
Table 1-4 :Major sulphate removal processes in aqueous media (Silva et al., 2010).....	19
Table 1-5 : Pseudo-second order kinetic model linear forms(Oboh et al., 2013).....	31
Table 1-6 Kinetic parameters obtained from different adsorption systems with biochar ..	32
Table 1-7 Summary of coefficients of Freundlich and Langmuir adsorption isotherms of some aqueous anion adsorption systems.....	42
Table 1-8 Thermodynamic parameters for some biomass based adsorption systems	46
Table 2-1 Availability, suitability of waste materials for biochar production (Lehmann, Gaunt and Rondon, 2006).....	57
Table 2-2 Typical product yields (dry basis) obtained by different modes of pyrolysis (Herbert et al. 2012 ; Duku et al. 2011; Maschio et al. 1992 ; Ahmad, Rajapaksha, et al. 2014 ;Bolan et al. 2013).....	59
Table 2-3 Biochar source, production method, and application for removal of aqueous contaminants	62
Table 2-4 BET Surface area, pore size and total pore volume of different biochar	69
Table 2-5 Particle density and bulk density of some biochar in literature.....	73
Table 2-6 Pore Categories (Wildman et al. 1991; Lehmann and Joseph 2010).....	74

Table 2-7 Proximity Analysis using TGA studied in some of the literature	77
Table 2-8 CHNSO Analysis in some biochar found in literature	79
Table 2-9 Bonding groups and structures according to the wave number (Fu et al. 2009)	83
Table 2-10 Functional groups of biochar samples determined by the FTIR analysis (Özçimen and Ersoy-Meriçboyu, 2010)	84
Table 3-1 Results of BET analysis.....	100
Table 3-2 Elemental analysis results of biochar and the comparison of aromaticity and polarity	105
Table 3-3 XRD Results	110
Table 4-1 Effect of the temperature on adsorption of sulphate by different biochar types	124
Table 4-2 Effect of mixing time on adsorption of sulphate by different biochar types ...	127
Table 4-3 First order kinetic model plots.....	130
Table 4-4 Second order kinetic model plots	131
Table 4-5 Comparison of the first and second order adsorption rate constants and calculated and experimental q_e values	132
Table 4-6 Adsorption capacities obtained from different initial sulphate concentrations	134
Table 4-7 Freundlich and Langmuir equation constants and correlation coefficients for adsorption of sulphate by biochar	136
Table 4-8 Thermodynamic parameters	138

List of Figures

Figure 1-1 : Natural components of oil/gas present in produced water.	9
Figure 1-2 : Simple Schematic of the Sulf-IX™ process(Lopez et al., 2009)	21
Figure 1-3 : Sulphate adsorption capacity on γ -Al ₂ O ₃ with respect to the solution pH, based on the effect of NaNO ₃ concentration (0.01, 0.05, and 0.1 M) and simulation by triple- layer modelling (TLM) (Wu et al., 2000)	25
Figure 1-4 : Sulphate adsorption isotherms on goethite determined at different pH (Geelhoed et al., 1997).....	27
Figure 1-5 : Types of adsorption isotherms (Rouquerol, 1999).....	36
Figure 1-6 : Isotherm Models(Rouquerol, 1999)	40
Figure 2-1 Yields of slow pyrolysis of wood (% wt)(Maschio et al., 1992)	60
Figure 2-2 Yields of fast pyrolysis of hazel nut shells (% wt) (Maschio et al., 1992)	60
Figure 2-3 BET surface areas of pine wood char as a function of production temperature under various ramp rates (Brown et al., 2006).....	68
Figure 2-4 Solid density as a function of final temperature of pyrolysis process (Brown et al., 2006).	72
Figure 2-5 SEM image of wood biochar produced by slow pyrolysis (Downie, 2011). ...	75
Figure 2-6 SEM images of biochar obtained at 500 °C (Lee et al., 2013).....	76
Figure 2-7 FTIR spectra for holm-oak wood char (EnC) and ceucalyptus wood char (EuHC) (Pastor-Villegas et al., 2007).....	82

Figure 2-8 XRD Patterns of three types of Rice Husk Biochar (Arc=Archerite, Cal=Calcite, Cris=Cristobalite, Kali = Kalicinite, Pyro=Pyrocoprote, Syl=Sylvite, Tri=Tridymite). (Prakongkep et al., 2013).....	87
Figure 3-1 Comparison of BET- N ₂ adsorption isotherms for bark, hardwood and softwood biochar.....	99
Figure 3-2 SEM images of biochar from (a) Bark, (b) Hardwood, (c) Softwood	102
Figure 3-3 TGA plots for the weight percentage and the derivative weight percentage vs. temperature	104
Figure 3-4 ATR-FTIR results for bark, hardwood and softwood charin the wavelength range of 4000 cm ⁻¹ to 400 cm ⁻¹	107
Figure 3-5 XRD patterns of biochar obtained with Cu- K α radiation (40 kV,40 mA) and 0.1° step size within 5° - 100°)	109
Figure 4-1 Adsorption capacity vs. Temperature and biochar type.....	126
Figure 4-2 Adsorption capacity vs. Mixing time and biochar type	128
Figure 4-3 Sulphate adsorption isotherm data at pH=4 and 10°C for different biochar.	135
Figure 4-4 Van't Hoff plot for adsorption of sulphate on biochar.....	137

List of Symbols, Nomenclature or Abbreviations

ΔG	Gibbs free energy change of adsorption
ΔH	Enthalpy change
ΔS	Entropy change
$\gamma\text{-Al}_2\text{O}_3$	Gamma Alumina
AE	Anion Exchanger
AMD	Acid Mine Drainage
ASTM	American Society for Testing and Materials
ATR	Attenuate Total Reflectance
BET	Brunauer–Emmett–Teller
BTEX	Benzene, Toluene, Ethyl benzene and Xylenes
BOD	Biological Oxygen Demand
CaCO_3	Calcium carbonate
CaSO_4	Calcium Sulphate
C-CART	Centre for Chemical Analysis, Research and Training
C_2HCl_3	Trichloroethylene
COD	Chemical Oxygen Demand
CREAIT	Core Research Equipment and Instrument Training Network
DAP	Dissolved Air Precipitation (DAP)
EA	Elemental Analyzer
ED	electrodialysis

FeS ₂	Iron Sulphide
FTIR	Fourier Transform Infrared Spectroscopy
GAC-FBR	Granular activated carbon- Fixed Bed Reactor
HCl	Hydrochloric acid
ICP-AES	Inductively Coupled Plasma Atomic Emission Spectrometry
ICP-OES	Inductively Coupled Plasma Optical Emission Spectrometry
ICP-MS	Inductively Coupled Plasma Mass Spectrometry
IUPAC	International Union of Pure and Applied Chemistry
K ₂ O	Potassium Oxide
MB	Methylene Blue
MF	Micro Filtration
MgO	Magnesium Oxide
MoO ₄ ²⁻	Molybdate
NaOH	Sodium Hydroxide
NaNO ₃	Sodium Nitrate
Na ₂ O	Sodium Oxide
Na ₂ SO ₄	Sodium Sulphate
NF	Nano Filtration
NO ₃ ⁻	Nitrate
NORM	Naturally Occurring Radioactive Materials
NPD	Naphthalene, Phenanthrene and Dibenzothiophene
ppm	Parts per million
xiii	

PAH	Polycyclic Aromatic Hydrocarbons
PO_4^{3-}	Phosphate
P_2O_5	Phosphorous Pentoxide
RHB	Rice Husk Biochar
R^2	Correlation Coefficient
RO	Reverse Osmosis
SeO_4^{2-}	Selenate
SEM	Scanning Electron Microscope
SO_4^{2-}	Sulphate
SRB	Sulphate Reducing Bacteria
TDS	Total Dissolved Solids
TERRA	The Earth Resources Research and Analysis Facility
TLM	Triple Layer Modelling
TGA	Thermal Gravimetric Analysis
TOC	Total Organic Carbon
TSR	Thermal Sulphur Reduction
UF	Ultra Filtration
XRD	X-ray Diffraction
ZnCl_2	Zinc Chloride
ZrO_2	Zirconium Oxide

List of Appendices

Appendix A: Characterisation of produced water from various studies148

Introduction and Overview

Produced water is a by product with more than 80% of the volume of wastes generated by exploration and production activities of the oil and gas industry (Hayes, 2004). Typically the targeted compound in produced water is “oil” in water; however, other compounds such as sulphur compounds can have an impact on operations and the environment. Sulphur compounds identified in produced water include sulphate, thiosalts, polysulphides, bisulphite, hydrogen sulphide, and elemental sulphur (Lee and Neff, 2011). Removal of all or part of these compounds would be beneficial, however, space on offshore platforms is limited and therefore any treatment system must be compact. One possible bulk removal technology is biochar based adsorbent. Biochar is a by-product from pyrolysis of biomass. In this study, the characteristic of biochar derived from the pyrolysis of wood residues and possible application to remove sulphate from wastewaters are assessed. This study has the capability to aid the oil and gas industry in treatment of sour waste water streams introducing a more environment friendly, compact and economical treatment technique.

This thesis is written in the manuscript style with five chapters and each chapter is briefly outlined in the following paragraphs.

Chapter 1 is the main literature review on removal of sulphur compounds present in produced water. This chapter discusses the composition of produced water and its significance in offshore oil and gas industry and also reviews some current produced

water treatment technologies. It explains the advantage of using adsorption technology in water treatment especially for offshore platforms. The chapter consists of a detailed review on past research studies on biochar adsorbents in water treatment for different target contaminants including compounds containing sulphur. Adsorption kinetics, different isotherm models, adsorption capacity calculations, and thermodynamic parameters are also reviewed with examples from past research papers.

Chapter 2 is a comprehensive review on characterization of biochar as an adsorbent in water treatment. This chapter discusses the important characteristics of biochar based adsorbents used in past research studies in water treatment and also the optimum adsorption parameters have been obtained. It also describes different pyrolysis processes and the change in the chemical and physical structure of biomass due to carbonization. Chemical, physical and thermal properties are reviewed such as surface area, total pore volume and pore size distribution, biochar density, particle structure and surface topography, moisture, ash, volatile matter, and fixed carbon content, elemental composition, functional groups/ surface functionality, crystalline structure, and mineralogical composition by giving examples from past studies.

Chapter 3 is based on biochar characterisation experiments. Three types of wood biochar were subjected to a series of characterisation experiments (bark, hardwood sawdust, and softwood sawdust). Physical properties such as surface area, porosity, total pore volume, pore width and surface morphology are discussed which were obtained using BET-N₂

analysis and SEM analysis. Density, pH, thermal properties which were determined by TGA analysis, and CHNSO analysis of biochar samples are also taken into consideration when analysing the suitability of biochar as an adsorbent. Results of ATR-FTIR analysis and XRD which were performed to find out functional groups and mineralogical composition are also discussed in detail.

Chapter 4 is a discussion on experiments carried out in treatment of aqueous sulphate using wood biochar as an adsorbent. Suitability of bark, hardwood sawdust, and softwood sawdust biochar as adsorbents are analysed based on a series of batch adsorption experiments. The optimum adsorption parameters are concluded by the experiments carried out varying the temperature, solution pH, and the initial concentration of sulphate solution. The suitable adsorption isotherm model, kinetic parameters, and the thermodynamic parameters are determined using the test results.

Chapter 5 is the summary of the thesis and it includes the suggestions for future work, recommendations, challenges faced during the research work, and the overall conclusion.

Co-authorship Statement

All the first drafts of each chapter were written by the candidate, Yashodha Gayanthree Marambage, who is the principal author and her supervisor Dr. Kelly Hawboldt provided theoretical and technical guidance, revised the drafts and the final editing of this thesis was based on the comments and revision of the supervisor.

Chapter 1. Removal of Sulphur Compounds from Offshore Produced Water -Review

Yashodha G. Marambage, Kelly A. Hawboldt

Faculty of Engineering and Applied Science, Memorial University of Newfoundland,

St. John's, NL, Canada. A1B3X5

Abstract

Produced water streams generated from offshore oil and gas operations can contain high concentrations of sulphur compounds if the source reservoir is sour or soured due to enhanced oil recovery methods such as seawater injection. Sulphur compounds can cause corrosion, safety issues, and environmental issues on the platform. As such, removal of all or part of the sulphur compounds is required, however, the space on offshore platforms is limited and therefore any treatment system must be compact. Further, offshore treatment processes should be simple and operationally robust due to the remote location of the platforms. The by-products from the treatment process should be environmentally friendly to minimize the effect on the marine environment. This chapter discusses the composition of produced water, the treatment technologies employed in offshore oil and gas industry and the possibility of biochar based adsorbent processes. Biochar based adsorbents used in removal of different contaminants from waste water are analysed according to their adsorption isotherm models, adsorption kinetics, and thermodynamics. Current treatment processes used to remove aqueous sulphur compounds are reviewed.

1.1 Introduction

Produced water is the largest waste stream with respect to the volume in the production phase of offshore operations in the petroleum industry (Neff et al., 2011). As the reservoir ages, the volume of produced water increases and during the later stage of production, produced water can account for a significant volume of produced fluids (Judd et al., 2014). It is predominantly made up of formation water and/or seawater depending on the production processes, and a variety of organic and inorganic compounds. It has been estimated that more than 25,000m³ of water is discharged per day from large facilities with several platforms (Neff, 2002). Table 1-1 summarizes produced water volumes worldwide.

Table 1-1: Produced water generation at offshore operations (Lee and Neff 2011)

Offshore location	Produced water generation (m ³ /day)
US offshore waters	256,000
Norwegian continental shelf	370,000
Atlantic Canada, Hibernia field	20,300
Canadian Scotia Shelf	100–600
North American offshore platforms	57,808
World	2,200,000

Produced water contains dispersed oils, dissolved minerals, grease, heavy metals, cations and anions, treating chemicals, formation solids, dissolved gases, naturally occurring radioactive materials (NORM), microorganisms, and dissolved oxygen. Sulphur compounds identified in produced water include but are not limited to sulphate, thiosalts, polysulphides, bisulphite, hydrogen sulphide, and elemental sulphur (Lee and Neff, 2011). Upon discharge of produced water, these compounds can change the natural sulphur cycle and also can affect plant and animals causing environmental issues (Cao *et al.*, 2011; Silva, Cadorin and Rubio, 2010). In addition to that, the acidity caused by these sulphur compounds can cause corrosion in equipment and pipelines, violate industrial regulations, and also can cause safety issues during the production process (Grant *et al.*, 2006; Silva, Cadorin and Rubio, 2010).

Development of an effective treatment process for the produced water streams is important in maintaining overall marine environment. On offshore oil and gas producing platforms and/or remote locations where infrastructure and space is limited, the treatment of all effluent streams using conventional systems is challenging. Daigle *et al.* (2012) has proposed compact water treatment units should be installed in offshore platforms in future and proper control and monitoring systems should be established in order to ensure the effectiveness of the process (Daigle *et al.*, 2012). In addition to the environmental impact, costs of water handling in offshore platforms have become a major concern. Produced water treatment and disposal costs in offshore production platforms have been reported to

be more than \$400 million per year (Khatib and Verbeek, 2002). As such, modern offshore oil and gas industry should emphasize green processes that contribute to the sustainable development and reduce costs of traditional water treatment methods(Khatib and Verbeek, 2002). Adsorption processes consume less energy, giving nearly 100% of product water recovery, and no chemicals are required for a normal adsorptive process (RPSEA, 2009). Adsorbents derived from waste derived biochar would make the process environmentally friendly and cost effective (Yao, 2013).

1.2 Composition of produced water

The contaminants in produced water originate from two sources: natural compounds in production liquids (oil/gas) and from the chemicals added during the production process.

Appendix A summarizes the characterisation of produced water obtained from various studies and summarized in the sections below

1.2.1 Natural compounds of oil/gas present in produced water

Produced water contains dispersed oil and dissolved organic and inorganic compounds: primarily the compounds listed below in figure 1-1. These contaminants are categorized in groups due to the number of compounds and variability from field to field (Husain et al. 2008; OGP 2002).

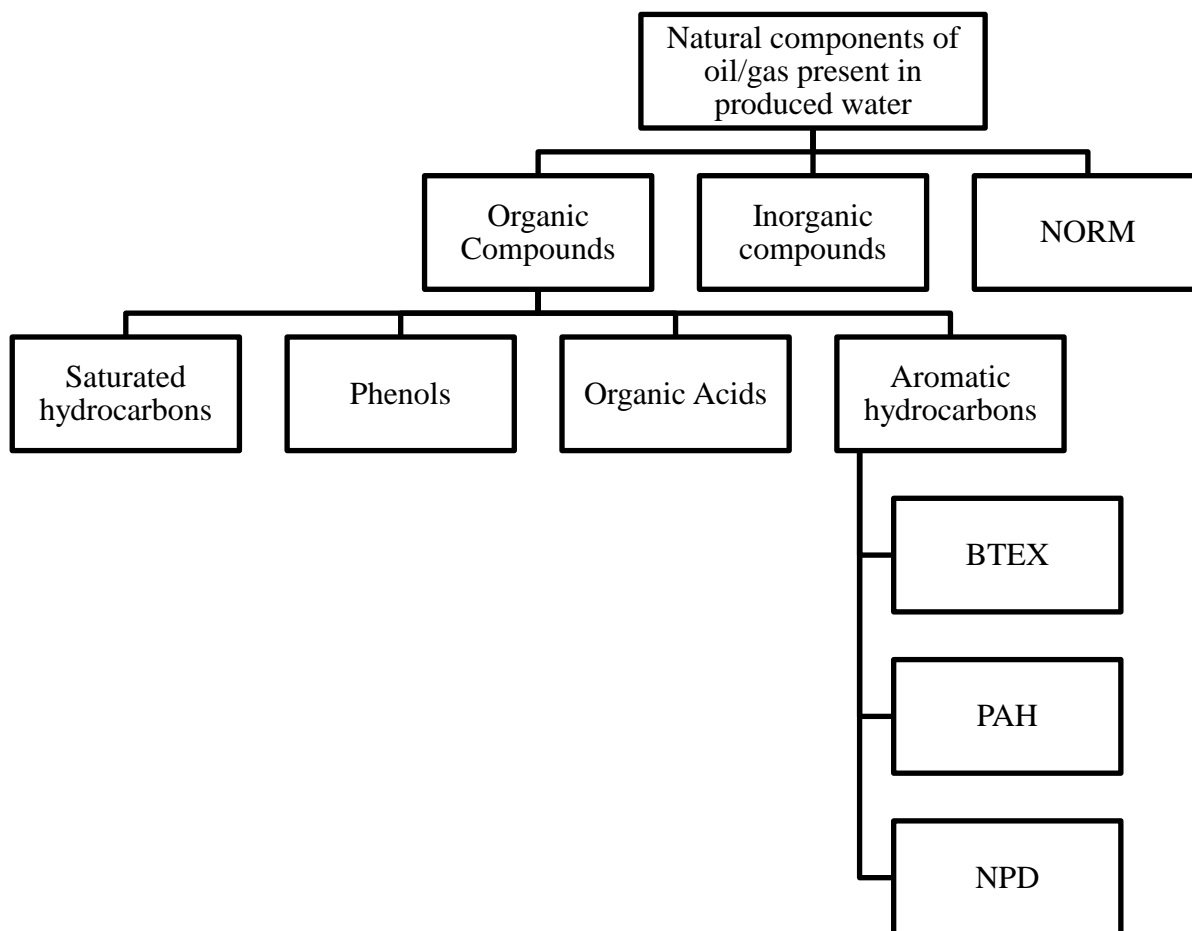


Figure 1-1 : Natural components of oil/gas present in produced water.

(NORM- Naturally Occurring Radioactive Materials, BTEX - Monocyclic aromatic compounds; Benzene, Toluene, Ethyl Benzene, and Xylenes (ortho, meta and para isomers), PAH - Polycyclic aromatic hydrocarbons (except Naphthalene, Phenanthrene, and Dibenzothiophene, which are included in the NPD-group; these are 3-

6 ring aromatic compounds), NPD- Naphthalene, Phenanthrene and Dibenzothiophene including their C1-C3 alkyl homologues; these are 2-3 ring aromatic compounds).

The amount of each group in produced water depends on several factors such as the reservoir's geology, type of oil/gas, and variations within the lifetime of the production process of a particular field and volume of water production (Neff, 2002). Table 1-2 gives the concentrations of selected naturally occurring compounds in produced water

Table 1-2 Concentrations of naturally occurring compounds in produced water (Neff, 2002)

Compound	Concentration (mg/L)	Compound	Concentration (mg/L)
Saturated hydrocarbons	17-30	Cadmium	trace-0.49
BTEX	0.068-578	Chromium	trace-18
PAH	0.04-3.0	Copper	trace-55
NPD	0.14-0.175	Iron	trace-465
Phenols	0.6-23	Lead	trace-18
Organic acids	<0.001-10000	Manganese	trace-7
Total organic carbon	<0.1-11000	Mercury	trace-0.075
Sulphate	<1-8000	Nickel	trace-1.67
Arsenic	0.000004-0.32	Zinc	trace-200
Barium	<0.001-2000	NORM	0-5.15 (pCi/L)

1.2.2 Production chemicals added in produced water

Through the oil and gas production process, chemicals may be added to prevent corrosion, foam production, scale deposition, hydrate formation, wax deposition, gas dehydration, emulsion breaking, and bacterial growth. Treatment chemicals can generally be put into three categories: production treatment chemicals, gas processing chemicals, and stimulation and work over chemicals (Ray and Engelhardt, 1992). Production chemicals can be pure compounds or compounds containing active ingredients dissolved in a solvent or a co-solvent (Igunnu, 2012). Approximately 19% of these production chemicals remain in the discharged produced water in offshore platforms (Neff, 2002). Most of the production chemicals are dissolved in the oil phase and the others are left in the produced water stream in very small concentrations as summarized in table 1-3 (Igunnu, 2012).

Table 1-3 Production chemicals in produced water (Igunnu, 2012)

Chemical	Concentration (mg/L)	
	Oil Field	Gas Field
Corrosion inhibitor	2-10	2-10
Scale inhibitor	4-30	-
Demulsifier	1-2	-
Polyelectrolyte	0-10	-
Methanol	-	1000-15000
Glycol (DEG)	-	500-2000

1.3 Produced water treatment processes

Water treatment processes are employed in various process stages; before injection of produced water back to the reservoir, before reusing produced water as process water, irrigation (onshore), and wetlands etc. When discharging produced water to the environment (offshore or onshore), treatment is required to meet regulatory standards (Fakhrul Razi et al., 2009).

The technical and economic feasibility of treatment technologies depends on the initial composition of the produced waters, the type of processing to be used, quality of the effluent, infrastructure required for the process (chemical storage, operational complexity) and in the case of offshore, equipment footprint (Hayes, 2004). Therefore, the modern oil and gas industry may use physical, chemical and/or biological treatment techniques to enhance the removal or separation of dispersed oil or grease, suspended solids, dissolved gases, organics and salts, microorganisms, and NORM in their wastewater streams.

Fakhrul Razi et al (2009) reviewed processes in produced water treatment. According to the paper, various parameters such as produced water chemistry, cost- effectiveness, space availability, reuse and discharge plans, durable operation, and behaviour of by-products should be taken into consideration when designing a treatment procedure.

1.3.1 Chemical treatment

Processes using chemicals include chemical precipitation, chemical oxidation, electrochemical process, photo catalytic treatment, Fenton Process, treatment with ozone, room temperature ionic liquids (for very small scale remediation), and demulsifier (Fakhrul Razi et al., 2009). Chemical oxidation is a widely used technology for the removal of COD, BOD, organic and some inorganic compounds present in produced water, and it is applicable to all types of produced water irrespective of TDS and salt concentration (Igunnu, 2012). Chemical treatment processes have the disadvantage of increased sludge generation and increased effluent streams with chemicals.

1.3.2 Biological treatment

Biological treatment is a more environmentally friendly and robust method to purify many produced water streams. Both aerobic and anaerobic bacteria are being used in these units and can be operated in the anaerobic, denitrifying, and aerobic modes. The GAC-FBR (Granular activated carbon- Fixed Bed Reactor) is a commercially available unit, that can treat produced waters up to 15,000 mg/L TDS (Hayes, 2004). Biological Aerated Filter (BAF) uses aerobic conditions to remove oil and organic substances from produced water (Igunnu, 2012). Biological processes have been used to remove ammonia, suspended solids, nitrogen, chemical oxygen demand (COD), biological oxygen demand (BOD), heavy metals, iron, soluble organics, trace organics, and hydrogen sulphide from produced water (Igunnu, 2012). However, these processes typically require long retention

times and resulting larger volume systems which translates into a large equipment footprint, which is a disadvantage on offshore platforms where space is limited (Judd et al. 2014; ERIN Consulting Ltd. and OCL Services Ltd. 2003). In addition, in harsh, cold offshore regions biological activity will be further reduced requiring additional energy for temperature control.

1.3.3 Physical treatment

Physical treatment processes such as filtration, membrane separation, dissolved air precipitation (DAP), electro dialysis (ED), ion exchange, and adsorption are common in produced water treatment. Suspended solids, oil particles, and some metals can be removed using filters (e.g. filters, shell filters, and membrane filters). At the tertiary separation stage, compact centrifuges and cyclones are used to separate dissolved gas, oil, and some water, especially particles with smaller diameters.

Deep bed filters and hydroclones are common oil removal units where hydroclone can reach below 10 ppm free oil levels and removes particles larger than 15 μm (Hayes, 2004). However, solids in waste water can both block the hydroclone inlet and lead to scale formation and a disposal procedure is required for the waste generated (Igunnu, 2012). Induced gas floatation method can result in oil removal of greater than 93% with chemical addition, but cannot remove dissolved oil components, is not suitable for high-temperature feed water, and a disposal procedure is required for sludge generated (Hayes, 2004; Igunnu, 2012).

Membrane separation is an effective treatment process as less energy is consumed, fewer additional chemicals required, and stringent effluent standards can be achieved (Iggunu 2012; Fakhrul Razi et al. 2009). Membrane separation can be categorized as microfiltration (MF), ultra filtration (UF), reverse osmosis (RO), and nanofiltration (NF). MF has the largest pore size (0.1–3 mm) and is typically used for the removal of suspended solids and turbidity reduction (Iggunu, 2012). UF removes macromolecules, colour, odour, viruses, and colloidal organic matter and NF is used in removal of multivalent ions (Iggunu, 2012). UF is the most effective method for oil removal from produced water in comparison with traditional separation processes. (Iggunu 2012; Fakhrul Razi et al. 2009). The membranes require periodic cleaning and waste generated during backwash and cleaning processes must be either disposed of or treated further (Iggunu, 2012). NF and RO are highly sensitive to organic and inorganic compounds in the feed water and membranes are not suitable for feed temperatures above 45°C (Iggunu, 2012).

Electrodialysis is used to remove dissolved ions from produced water with moderate TDS values up to 15,000 mg/L (Hayes, 2004). By introducing selectively permeable membranes with the Electrodialysis reversal process, a wide range of different ions present in produced water can be simultaneously separated (e.g. sodium, calcium, magnesium, chloride, sulphide, sulphate, bicarbonate, barium, heavy metal cations, and

most of the dissolved organic compounds) (Hayes, 2004). This method is costly and suitable for treating relatively low saline produced water (Igunnu, 2012).

Ion exchange method is especially useful in the removal of monovalent and divalent ions and metals by resins from produced water. (Doran et al. 1997; Igunnu 2012). Studies have shown that two beds of strong acid ion-exchange resin in series can remove calcium and magnesium in oil free water when the effluent TDS is less than 50,000ppm (Fakhrul Razi et al., 2009). Limitations are high operating cost, high chemical cost, and the sensitivity to fouling (Igunnu, 2012)

1.4 Adsorption processes in produced water treatment

Adsorption is a physical treatment process which is usually employed in the latter stage of the treatment process to remove manganese, iron, total organic carbon (TOC), BTEX, oil, and heavy metals present in produced water (Igunnu, 2012). Typical adsorbents include activated carbon, organoclays, activated alumina, and zeolite. Activated carbon can remove dissolved organic compounds very effectively, but not dispersed oil particles (Hayes, 2004). It is an excellent adsorbent for some inorganic contaminants and trace organics, as an example, BTEX removal can exceed 99% (Hayes, 2004). Organoclay (a combination of sodium montmorillonite clay with a cationic quaternary amine salt) can remove dispersed (free) oil particles from produced water (Fakhrul Razi et al., 2009). Modified Silica or zeolite resins, which are hydrophobic, are used in the removal of dispersed or dissolved hydrocarbons and in the removal of dissolved chemicals in oil field

waste water streams. These adsorbents provides a very high surface area and also a weak bonding with contaminants which results in high removal rates and the absorbent media can be regenerated (Igunnu, 2012). Adsorption processes can be used irrespective of the salinity level of water and can remove 80% of heavy metals achieving nearly 100% water recovery (Igunnu, 2012).

1.5 Treatment of Sulphur Compounds in Produced Water

In oil and gas operations, sulphur sources include the reservoir as metal sulphides (e.g. pyrite or FeS_2 and gypsum or CaSO_4), hydrogen sulphide in gas and organosulfides or as sulphate in injected seawater (Sánchez-Andrea et al., 2014). Reservoir souring is the process where sulphur compounds are converted to hydrogen sulphide through biological and/or chemical activity. Biological souring occurs due to the action of sulphate reducing bacteria (SRB) which are anaerobic microorganisms and consume sulphate, thiosulphate, or elemental sulphur to produce sulphide while oxidizing electron donors (Gieg et al., 2011). Chemical souring can occur as a result of various mechanisms such as thermal sulphur reduction (TSR), direct thermo-chemical reduction of sulphate from seawater, maturation of sulphur-containing organic matter; dissolution of sulphide minerals and reduction of FeS_2 (pyrite or marcasite) followed by the dissolution of sulphide minerals and also due to the conversion of injected sulphite, which is used as an oxygen scavenger (Ligthelm et al., 1991)

Injection and water flooding can introduce SRB and/or enhance SRB growth by introducing nutrient sulphide concentration and labile carbon sources from sea water (Gieg et al., 2011). In production fields associated with sour gas or oil with high sulphur content, produced water is usually contaminated with sulphur species. As produced water in reservoir is in its reduced state, some of sulphur may be present as sulphides or elemental sulphur (Neff, 2002). Therefore, in addition to organic compounds, produced water consists of inorganic sulphur species including sulphate, thiosalts, polysulphides, bisulphite, hydrogen sulphide, and elemental sulphur which are in concentrations of μM - mM (Witter and Jones, 1999). Sulphur compounds such as sulphates and sulphides have been reported within the range of 2-1650 mg/L and 0-10 mg/L respectively (Fakhrul Razi et al., 2009). In production fields where lime (calcium hydroxide) is used to mitigate acidity and remove metal cations, the sulphate concentration is usually higher (1,600 – 1,800 mg/L) (Lopez et al., 2009). Sulphur compounds can cause physical/chemical corrosion, odour, and increased effluent chemical oxygen demand in produced water (Hulshoff Pol et al., 1998).

In both natural water and industrial water streams, sulphate is a common substance removed when the concentration does not comply with standards. Sulphate removal from aqueous streams is one of the most challenging tasks in the industry (Silva et al., 2010). A number of processes have been proposed to remove sulphate compounds from water as outlined in table 1-4.

Table 1-4 :Major sulphate removal processes in aqueous media (Silva et al., 2010)

Treatment Process	Advantages	Disadvantages
Biological reduction Anaerobic systems	Low costs Easy to operate	Long residence time Organic material residuals Large area
Membrane filtration Reverse Osmosis Ultra filtration	High efficiency Short time	High costs Large wastewater volume
Adsorption and/or ion exchange Sulf-IX™ process (Lopez et al., 2009)	High efficiency Sulphate levels lower than 250 mg/L	Requires frequent bed regeneration
Alternative sorbents (Chitosan)	Costs are lower than reverse osmosis processes	Handling difficulties of chitosan Tailing generated in the regeneration of resins
Chemical precipitation Barium sulphate precipitation Crystallisation of sulphate salts	Short time High kinetics	High costs Large sludge generation
Ettringite precipitation ($3\text{CaO} \cdot 3\text{CaSO}_4 \cdot \text{Al}_2\text{O}_3 \cdot 31\text{H}_2\text{O}$)	Low solubility Independent of pH	Residual concentration of barium

The challenge in all of these processes when the target contaminant is sulphate, is the high solubility and stability of sulphate ions in aqueous solutions (Namasivayam and Sangeetha, 2008). When the sulphate concentration is high, ion exchange processes are the most suitable, followed by chemical precipitation processes (addition of barium or calcium salts) (Silva et al., 2002). Addition of 80 g /L of barium can achieve a sulphate removal up to 61.4% while calcium addition can achieve 99% sulphate removal from waste water (Benatti et al., 2009). The process requires a proper sludge separation (filtration or centrifugation) and disposal which may involve high costs. Reverse osmosis, electrodialysis, and nanofiltration or membrane filtration can be used but are limited as waste water volumes increase.

Anion exchange processes have been studied as an adsorbent to remove sulphate from aqueous solution. Cao et al. (2011), converted rice straw (an agricultural residue), into a strong basic anion exchanger (RS-AE) for removal of sulphate (Cao et al., 2011). They treated the straw with NaOH, after partially removing water, and reacting with epichlorohydrin and trimethylamine. The sulphate adsorption efficiency was 79.2% for an initial concentration of 100 mg/L of sulphate solution containing 0.1g adsorbent at 25⁰C and pH of 6.4 (Cao et al., 2011). The study showed that after four cycles of adsorption and regeneration, the sulphate adsorption efficiency of RS-AE decreased less than 10% from 74.7% to 66.2% emphasizing the potential of RS-AE for repeatedly use in the removal of sulphate ions from waste water (Cao et al., 2011).

Lopez et al. (2009) reviewed “green” processes used in industry to remove sulphates and metals from wastewater. Sulf-IX™ process is a sulphate removal process based on ion exchange principle and can reduce the sulphate concentration of wastewater below 250 mg/L (Lopez et al., 2009). The only by-product is clean gypsum, which is not hazardous and can be sold as a construction material or safely disposed of in land-fill (Lopez et al., 2009). The schematic diagram of the Sulf-IX™ process is shown in figure 1-2.

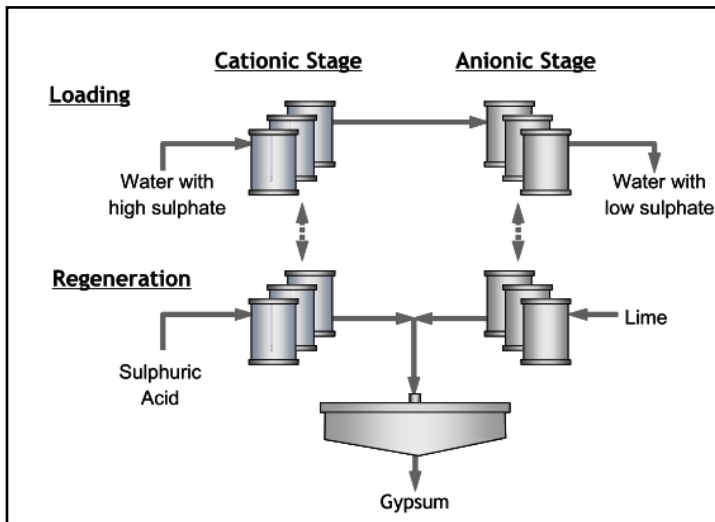


Figure 1-2 : Simple Schematic of the Sulf-IX™ process(Lopez et al., 2009)

The system consists of anion exchange resins to remove sulphate ions and since those resins have finite capacity, a regeneration process is required. This process is proposed for the removal of sulphate from lime plant effluent and for the treatment of wastewater streams high in Total Dissolved Solids (TDS) and Ca/Mg hardness (Lopez et al., 2009).

1.6 Adsorption of sulphur compounds from aqueous solutions

Adsorption processes for produced water treatment use a variety of materials such as zeolite, organoclay, biochar, activated alumina, and activated carbon (Guerra et al., 2011). The most popular adsorbent is activated carbon, which can be prepared from different materials such as biochar by controlled combustion and then activating them to enhance adsorptive characteristics.

Activated carbon from coconut coir pith, activated using ZnCl_2 has been investigated as an adsorbent for removal of sulphate from water. Based on experimental data, the equilibrium monolayer adsorption capacity of sulphate was 4.9mg/g on 500mg of adsorbent. The optimal agitation was 200 rpm at 35°C with a pH of 4 (Namasivayam and Sangeetha, 2008). The amount of sulphate adsorbed (mg/g), increased with increasing adsorbent dose, temperature and initial sulphate concentration until the equilibrium adsorption capacity was reached. Sulphur removal varied from 54% to 90% in the optimum pH range of 3.0–9.0. At higher pH values (>9), OH^- ions compete with sulphate ions and also electrostatic repulsion can occur between the negatively charged adsorbent surface and sulphate ions. At lower pH values (<3), the sulphate adsorption is inhibited by Cl^- ions which have been added externally as HCl to adjust pH (Namasivayam and Sangeetha, 2008). The high surface area and high micropore area of the ZnCl_2 activated carbon were responsible for the high adsorption capacity while the addition of foreign

competitive anions such as perchlorate, chloride, molybdate, nitrate and phosphate in the solution reduced sulphate adsorption (Namasivayam and Sangeetha, 2008).

Hong et al. (2014) studied removal of sulphate from acid mine drainage water (AMD) using wood based activated carbon, modified by grafting polypyrrole under a nitrogen atmosphere. This process resulted in polypyrrole-grafted activated carbon (GAC) media that could be electrically switched from a net positive charge to a net neutral charge (Hong et al., 2014). The positively charged GAC would adsorb sulphate, and when it is switched to neutral state, it would release sulphate (Hong et al., 2014). Standard aqueous phase batch adsorption isotherm experiments with a range of varying concentrations of sulphate in the solution were performed. Sulphate adsorption capacity increased as pyrrole treated GAC increased from 0.02mol/L to 1mol/L pyrrole solution and 2mol/L pyrrole solution (Hong et al., 2014). However, for GAC sample synthesised with 5mol/L solution, the sorption capacity declined due to decrease in pore volumes and surface areas (excessive amounts of polypyrrole blocked the pores and reduced the number of active sites available for sulphate adsorption) (Hong et al., 2014). A maximum of 44.7 mg/g of sulphate adsorption was achieved when the initial sulphate dose was 250 mg/L, using the GAC sample synthesised with 2mol/L pyrrole solution (Hong et al., 2014). The adsorption isotherm data was fitted to the Langmuir model and correlation coefficient was shown in between 0.93–0.99 (Hong et al., 2014). Both pore volume and positively-charged polypyrrole functional density were identified as the important parameters for

sulphate capture and there should be an adequate porosity for the sulphate to diffuse to the nitrogen-functionalized sites (Hong et al., 2014). A rapid small scale column test was also performed using AMD water and ground water with 773mg/L and 500mg/L sulphate concentration where the highest corresponding sulphate loadings at full breakthrough were obtained as 41mg/g for AMD water and 44mg/L for groundwater using GAC synthesised with 2 mol/L pyrrole solution(Hong et al., 2014). The GAC appeared to have high affinity for sulphate even though AMD water and groundwater contain various competing anions.

Sulphate adsorption on laboratory synthesised magnetite from aqueous solutions was investigated by Roonasi and Holmgren (2009).The pH range studied was 4–9 to avoid formation of HSO_4^- from SO_4^{2-} which occurs at very low pH which may complicate the analysis of the results (Roonasi and Holmgren, 2009). A Langmuir isotherm model gave an affinity constant of $1.2344 \times 10^4 \text{ M}^{-1}$ implying a moderate affinity of sulphate for the magnetite surface(Roonasi and Holmgren, 2009). It was proposed that the sulphate ions covalently attach to the magnetite surface (Roonasi and Holmgren, 2009). The effect of calcium ions on sulphate adsorption on magnetite indicated the increase in surface charge due to the calcium addition can improve the adsorption of sulphur at pH 8.5 on magnetite (Roonasi and Holmgren, 2009).

Competitive adsorption of different anions (sulphate, molybdate, chromate, selenate, and selenite) on $\gamma\text{-Al}_2\text{O}_3$ (gamma alumina) has been examined by Wu et al. 2000. In the

single anion systems, removal rates were high, but when other competitive ions were present in the aqueous media, removal rates were low. Sulphate adsorption percentages (in the single anion system) on 30 g/L of γ -Al₂O₃ in a 5×10^{-3} M of initial sulphate solution in the presence of three different NaNO₃ electrolyte concentrations are presented in figure 1-3. The results show that the sulphate adsorption percentage is high in an acidic environment and impacted by NaNO₃ concentration (Wu et al., 2000). As the sulphate adsorption is strongly dependent on background electrolyte concentration, it is assumed that sulphate ions form an outer-sphere complex: sulphate ion remains bounded to the hydration shell and does not bind directly to the γ -Al₂O₃ surface.

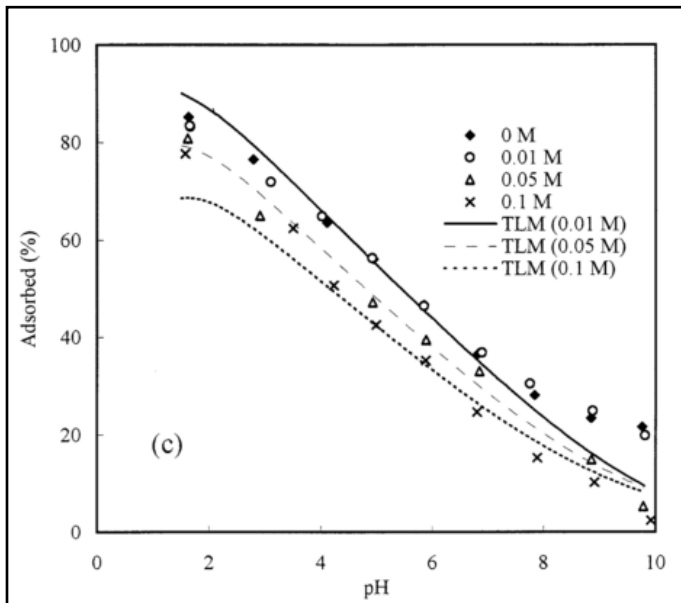


Figure 1-3 : Sulphate adsorption capacity on γ -Al₂O₃ with respect to the solution pH, based on the effect of NaNO₃ concentration (0.01, 0.05, and 0.1 M) and simulation by triple-layer modelling (TLM) (Wu et al., 2000)

Adsorption of sulphate and molybdate ions on a chitin-based material (from an industrial shrimp shell waste after demineralisation, deproteinisation and deacetylation) has been investigated by Moret and Rubio (2003). Adsorption pH and time, adsorbent/adsorbate ratio, and feed concentration of sulphate ions were varied. The adsorption was fit to the Langmuir isotherm with a capacity of 156 mg/g (Moret and Rubio, 2003). The optimum pH value was in the range of 4-4.5 (Moret and Rubio, 2003). Experiments were extended to find the maximum adsorption capacity on effluents from a porphyry Cu–Mo sulphide flotation mill which contains molybdate and sulphate anions and on acid mine drainage (AMD) effluents from coal mines. For the effluent from Cu–Mo sulphide flotation mill, the sulphate adsorption percentage was 71% for a feed concentration of 1590 mg/L and from the coal mining AMD effluent, 80% of sulphate ions was adsorbed for a feed concentration of 1540 mg/L (Moret and Rubio, 2003).

Geelhoed et al. (1997) studied the adsorption of sulphate ions on goethite and a decrease in sulphate was observed with increasing pH, indicating that the adsorption is hindered when the goethite surface becomes less positively charged (Geelhoed et al., 1997). A maximum adsorption capacity around $1.75\mu\text{mol}/\text{m}^2$ was observed in a sulphate solution concentration of 4.0 mM and a pH of 3.0. The presence of phosphate ions in the solution decreased the adsorption of sulphate, as phosphate is a strong competitor for adsorption of sulphate on goethite (Geelhoed et al., 1997). Sulphate adsorption isotherms on goethite as a function of pH are shown in figure 1-4.

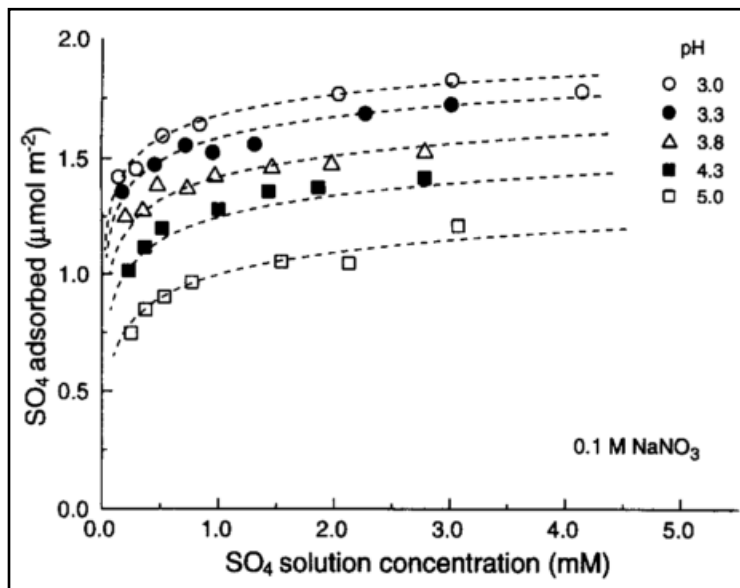


Figure 1-4 : Sulphate adsorption isotherms on goethite determined at different pH (Geelhoed et al., 1997)

Sugarcane bagasse, a residue produced in large quantities in sugar and alcohol industries, has been studied as the starting material for a potential adsorbent in sulphate removal (Mulinari and da Silva, 2008). After a series of chemical modifications, a cellulose/hydrous zirconium oxide hybrid material, (Cell/ZrO₂.nH₂O) was produced and adsorption of sulphate was analysed at 298 K. Approximately 0.2 g of adsorbent was mixed with 50mL of Na₂SO₄ solution with varying initial concentrations for five minutes. A sulphate adsorption capacity of 38.4mol/g has been achieved for initial Na₂SO₄ concentration of 3×10⁻⁴ to 5×10⁻⁴ mol/ L. The adsorption was attributed to the high

specific surface area and the adsorption reaction was between the sulphate ions and the zirconium reactive centre, designated as Zr-OH (Mulinari and da Silva, 2008).

In summary, activated carbon from coconut coir pith has showed a 4.9 mg/g of sulphate adsorption capacity and polypyrrole-grafted activated carbon (GAC) has given a sulphate adsorption capacity of 44.7 mg/g (Namasivayam and Sangeetha, 2008; Hong et al., 2014). Maximum sulphate adsorption capacities of $1.75\mu\text{mol}/\text{m}^2$ and $0.4\text{mol}/\text{g}$ were observed for goethite and modified sugarcane bagasse respectively (Geelhoed et al., 1997; Mulinari and de Silva, 2008). Magnetite has exhibited a moderate affinity of sulphate for the magnetite surface and it was shown that sulphate adsorption is strongly dependent on background electrolyte concentration after a study of sulphate adsorption on $\gamma\text{-Al}_2\text{O}_3$ surface (Roonasi and Holmgren, 2009; Wu et al., 2000). Adsorption of sulphate on a chitin-based material from an industrial shrimp shell waste showed an adsorption capacity of 156 mg/g and even was successful in removal of sulphate from industrial waste streams (Moret and Rubio, 2003). All these studies showed that sulphate adsorption capacity is increased with the increase in temperature and decrease in solution pH.

In order to establish a proper adsorption system for an industrial application, adsorption kinetics, adsorption isotherms, and thermodynamics should be taken into consideration.

1.7 Adsorption kinetics

Liquid-Solid adsorption takes place in three stages, external mass transfer, internal mass transfer, and adsorption (Chowdhury, 2012). External mass transfer (boundary layer or film diffusion) occurs between the external surface of the adsorbent and the surrounding fluid phase and is driven by the concentration difference across the boundary layer around adsorbent (Lazaridis and Asouhidou, 2003). Internal mass transfer takes place within the particle, governed by either pore diffusion where adsorbate molecules leave the adsorbent surface or solid diffusion when pores are very small so that adsorbate remains on the surface of the adsorbent (Lazaridis and Asouhidou, 2003). In the final stage, adsorption and desorption takes place between the adsorbate and active sites and the rate of the process depends on the reaction kinetics (Qiu et al., 2009). Based on the kinetic information, adsorption reaction mechanism, solute uptake rate and the residence time required for adsorption process can be determined to develop the experimental adsorption column (Qiu et al., 2009). Kinetic analysis also provides information to develop possible reaction mechanisms for a particular adsorption reaction. In order to describe the adsorption kinetics at different temperatures, two mathematical kinetic models have widely been used in adsorption studies; pseudo first order model and pseudo second order model.

1.7.1 Pseudo first order kinetic model

The first-order rate expression is outlined below (Qiu et al., 2009).

$$\log(q_e - q_t) = \log q_e - \frac{K_1 t}{2.303} \quad (1-1)$$

Where q_t (mg/g) is the amount of the adsorbate adsorbed at time t (min), K_1 (min^{-1}) is the rate constant of pseudo first order adsorption and q_e (mg/g) is the adsorption capacity at equilibrium.

1.7.2 Pseudo Second order kinetic model

The second-order kinetic model is as follows (Qiu et al., 2009).

$$\frac{t}{q_t} = \frac{1}{K_2 q_e^2} + \frac{t}{q_e} \quad (1-2)$$

Where q_t (mg/g) is the amount of the adsorbate adsorbed at time t (min), K_2 (min^{-1}) is the rate constant of pseudo second order adsorption and q_e (mg/g) is the adsorption capacity at equilibrium. A linear relationship in the plot of t/q_t versus t is expected if second-order kinetics is applicable. The initial adsorption rate h ($\text{mg g}^{-1}\text{min}^{-1}$) when t approaches 0, can be determined from K_2 and q_e value using the following equation:

$$h = K_2 q_e^2 \quad (1-3)$$

Equation (1-2) is the most common linear form used for pseudo-second order kinetic model and can be changed into four different linear forms using some mathematical adjustments which are shown in table 1-5. (Obboh et al., 2013).

Table 1-5 : Pseudo-second order kinetic model linear forms(Oboh et al., 2013)

Type	Linear form	Plot
Type 1	$\frac{t}{q_t} = \frac{1}{K_2 q_e^2} + \frac{t}{q_e}$	t/q _t vs. t
Type 2	$\frac{1}{q_t} = \left(\frac{1}{K_2 q_e^2} \right) \frac{1}{t} + \frac{1}{q_e}$	1/q _t vs. 1/t
Type 3	$q_t = q_e - \left(\frac{1}{K_2 q_e^2} \right) \frac{q_t}{t}$	q _t vs. q _t /t
Type 4	$\frac{q_t}{t} = K_2 q_e^2 - K_2 q_e^2 q_t$	q _t /t vs. q _t

The different linear forms of the same model give significantly different kinetic parameters and correlation coefficients (Oboh et al., 2013). The pseudo second order kinetic model has been widely applied to the adsorption of pollutants from aqueous solutions(Ho, 2006). The main advantages of using this model is that the equilibrium adsorption capacity and the initial adsorption rate can be calculated from the model (Ho, 2006).

Kinetic modelling of adsorption on biochar in past studies have been investigated and summarized in the table 1-6.

Table 1-6 Kinetic parameters obtained from different adsorption systems with biochar

Biochar	Adsorbate	Kinetic model	Parameters			Reference
			K (min^{-1})	q_e (mg/g)	R^2	
Sugar beet tailings char (600°C for 2h)	Phosphate	1 st order	0.0026	23.474	0.9968	(Yao et al., 2011)
Clay–biochar composites (600°C for 1h)	Methylene blue (MB)	1 st order	0.0155	6.888	0.769	(Yao et al., 2014)
Corn straw (600°C for 2h)	Copper	1 st order	0.083	8.93	0.865	(Chen et al., 2011)
Corn straw (600°C for 2h)	Zinc	1 st order	0.130	7.11	0.921	(Chen et al., 2011)
Hardwood (450°C for 5s)	Copper	1 st order	0.100	3.70	0.876	(Chen et al., 2011)
Hardwood (450°C for 5s)	Zinc	1 st order	0.141	2.63	0.923	(Chen et al., 2011)
Corn stover (650°C for 0.3h)	Nitrate	1 st order	0.0468	0.005	0.99	(Chintala et al., 2013)

Biochar	Adsorbate	Kinetic model	Parameters			Reference
			K (min ⁻¹)	q _e (mg/g)	R ²	
pine wood (650°C for 18min)	Nitrate	1 st order	0.0587	0.003	0.97	(Chintala et al., 2013)
Switch grass (650°C for 18min)	Nitrate	1 st order	0.0472	0.00558	0.98	(Chintala et al., 2013)
clay–biochar composites (600°C for 1h)	Methylene blue (MB)	2 nd order	0.0033	7.265	0.852	(Yao et al., 2014)
Corn straw (600°C for 2h)	Copper	2 nd order	0.003	10.76	0.996	(Chen et al., 2011)
Corn straw (600°C for 2h)	Zinc	2 nd order	0.006	8.20	0.999	(Chen et al., 2011)
Hardwood (450°C for 5s)	Copper	2 nd order	0.011	4.31	0.999	(Chen et al., 2011)
Hardwood (450°C for 5s)	Zinc	2 nd order	0.009	3.14	0.988	(Chen et al., 2011)

Biochar	Adsorbate	Kinetic model	Parameters			Reference
			K (min ⁻¹)	q _e (mg/g)	R ²	
coconut coir pith char (700°C)	Sulphate	2 nd order	0.170	1.93	0.997	(Namasivayam and Sangeetha, 2008)
coconut coir pith char (700°C)	Sulphate	1 st order	0.088	0.79	0.988	(Namasivayam and Sangeetha, 2008)
sugar beet tailings-char (600°C for 2h)	Phosphate	2 nd order	0.0868	28.771	0.994	(Yao et al., 2011)

In most of the studies, a 1st order kinetic model has been used to determine adsorption kinetics. According to the study of Namasivayam and Sangeetha(2008), sulphate adsorption of coconut coir pith char fits a 2nd order model and shows a R² value of 0.997 which is greater than that of 1st order kinetic model (Namasivayam and Sangeetha, 2008). The study shows that the calculated q_e values from 1st order kinetic model do not agree with the experimental q_e values but the calculated q_e values from 2nd order model agree with experimental q_e values. These calculations confirm that the adsorption of sulphate follow the 2nd order kinetic model. The adsorption capacity increased with time, and then

showed saturation, indicating monolayer coverage of sulphate on the surface of the adsorbent. The rate constant (K) increased on increasing the temperature from 35 °C to 60 °C.

1.8 Adsorption Capacity and isotherms

Adsorption capacity is the amount of adsorbate taken up by the adsorbent, per unit mass (or volume) of the adsorbent (Knaebel, 2004). The capacity depends on the temperature, fluid-phase concentration, pressure, contact time, viscosity and surface tension, initial condition of the adsorbent and the extent of surface exposed (Rice, 1934). At a fixed temperature, adsorption capacity at equilibrium is measured against the equilibrium concentration of the adsorbate in the solution to draw equilibrium adsorption isotherm. This illustrates the distribution of adsorbate molecules in equilibrium between liquid and solid (Yao et al., 2014).

$$q_e = \frac{\text{Amount of solute adsorbed}}{\text{Mass of adsorbant}} = f(C_0) \quad (1-4)$$

C_0 = Equilibrium concentration of the solute remaining in solution

Adsorption isotherms for physical adsorption are grouped into six classes as shown below, according to IUPAC classification (Rouquerol, 1999).

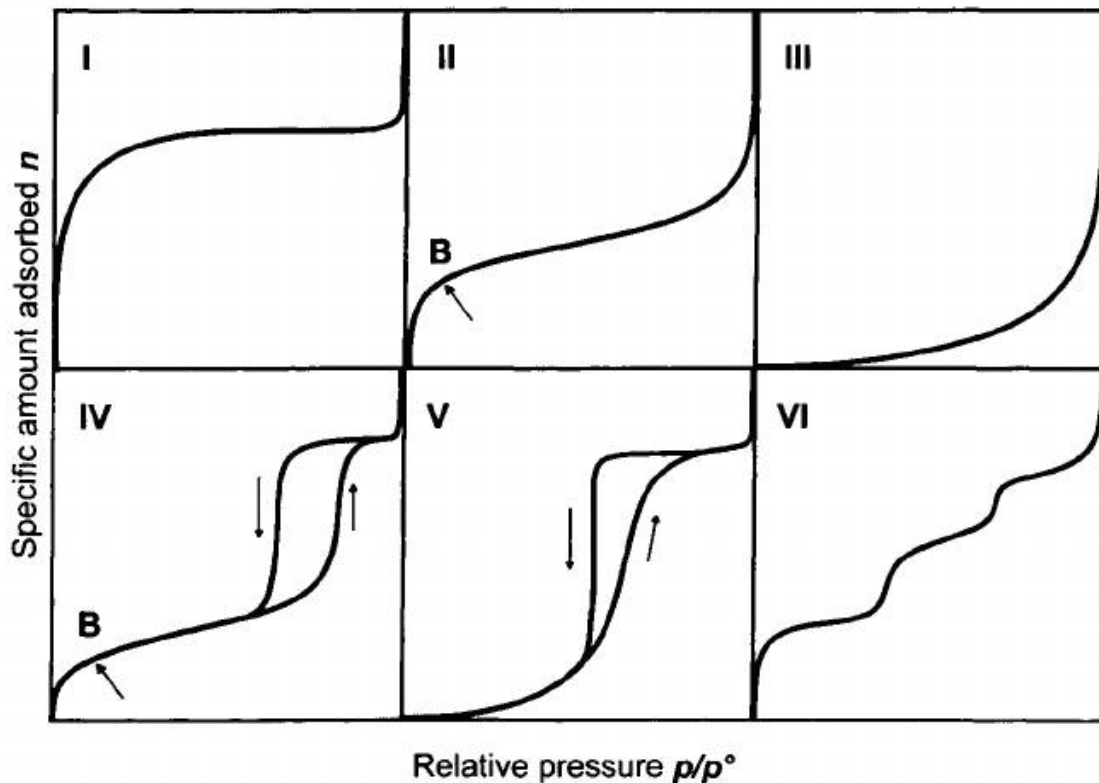


Figure 1-5 : Types of adsorption isotherms (Rouquerol, 1999)

At low concentration of adsorptive, liquid- solid adsorption isotherms fall into two different categories, “type L” and “type S” which are analogous to “type I” and “type III or V” respectively in the above IUPAC classification (Rouquerol, 1999). Empirical isotherms have been developed and typically apply to type I, II and IV which are favourable isotherms as those concave downwards (Knaebel, 2004). Type IV and V exhibit a hysteresis loop where adsorption and desorption occur in different isotherms due to capillary condensation in mesopores(Rouquerol, 1999). Usually experimental

isotherms have a combination of those shapes and data from isotherm experiments are analyzed based on linearization of the isotherm models. The most commonly used isotherms in activated carbon/char treatment of water and wastewater treatment are the Freundlich and Langmuir isotherms. In wastewater treatment, where multi-component systems are common, the Freundlich isotherm has the best fit for a variety of wastewater treatment processes (Sheindorf et al., 1980).

1.8.1 Freundlich isotherm model

The Freundlich Isotherm is empirical and widely used but only applicable over a narrow range of temperatures and concentrations. It assumes a heterogeneous adsorbent surface composed of adsorption sites with different adsorption potentials.

$$q_e = K_F C_e^{\frac{1}{n}} \quad (1-5)$$

q_e = Amount of solute adsorbed per unit weight of adsorbent at equilibrium (mg/g dry weight)

C_e = Equilibrium concentration of the solute in the solution (mg/L)

' K_F ' and 'n' are temperature dependent specific constants which are determined experimentally. K_F is Freundlich constant, an indicator of adsorption capacity (mg/g), higher K_F indicate higher adsorbent capacity. The inverse of n ($1/n$) is a measure of intensity of adsorption. Higher $1/n$ values indicate enhanced adsorption. The n parameter

also relates to degree of heterogeneity on the adsorption sites. Values of n close to 1 indicate greater heterogeneity on the surface of the adsorbent (Ahmad et al., 2014b).

Linearization of the Freundlich model gives

$$\log(q_e) = \log(K_F) + \frac{1}{n} \log(C_e) \quad (1-6)$$

A log-log plot of q_e versus C_e gives an intercept of $\log K_F$ and a slope of $1/n$.

1.8.2 Langmuir isotherm model

The Langmuir isotherm assumes monolayer coverage of molecules on the adsorbent surface and all adsorption sites are equally probable (all atoms in adsorbent surface have the same capability of adsorbing gas molecules).

$$q_e = \frac{Q_a^0 K_L C_e}{1 + K_L C_e} \quad (1-7)$$

q_e = Amount of solute adsorbed per unit weight of adsorbent at equilibrium (mg/g dry weight)

C_e = Equilibrium concentration of the solute in the solution (mg/L)

K_L is Langmuir constant related to the affinity of the binding sites (L/mg) and Q_a^0 is the maximum adsorption capacity for forming monolayer (mg/g).

Linearization of the Langmuir model gives:

$$\frac{C_e}{q_e} = \frac{1}{K_L Q_a^0} + \frac{C_e}{Q_a^0} \quad (1-8)$$

A Langmuir system exhibits a straight line when plotting $\frac{C_e}{q_e}$ versus C_e with intercept $\frac{1}{K_L Q_a^0}$ and a slope of $\frac{1}{Q_a^0}$.

1.8.3 BET isotherm model

The BET (Brunauer, Emmett and Teller) model is a more general, multi-layer isotherm model which assumes that molecules can be adsorbed as several layers on the adsorbent surface which is composed of fixed individual sites. The Langmuir isotherm applies to each layer where no transmigration occurs between layers. It also assumes that there is equal energy of adsorption for each layer except for the first layer and the energy required to adsorb the first particle layer is adequate to hold the monolayer in place (USACE, 2001).

$$q_e = \frac{Q_a^0 K_B C_e}{(C_s - C_e)[1 + (K_B - 1)\frac{C_e}{C_s}]} \quad (1-9)$$

q_e = Amount of solute adsorbed per unit weight of adsorbent at equilibrium (mg/g dry weight)

C_e = Equilibrium concentration of the solute in the solution (mg/L)

C_s = saturation (solubility limit) concentration of the solute (mg/L)

K_B is a parameter related to the binding intensity for all layers and Q_a^0 is the maximum adsorption capacity. When $C_e \ll C_s$ and $K_B \gg 1$ and $K_{ad} = K_B/C_s$ the BET isotherm approaches Langmuir isotherm.

BET model linearization gives:

$$\frac{C_e}{(C_s - C_e)q_e} = \left(\frac{K_B - 1}{K_B Q_a^0} \right) \frac{C_e}{C_s} + \frac{1}{K_B Q_a^0} \quad (1-10)$$

A plot of $\frac{C_e}{(C_s - C_e)q_e}$ versus C_e gives a straight line with intercept $\frac{1}{K_B Q_a^0}$ and a slope

of $\frac{K_B - 1}{K_B Q_a^0 C_s}$.

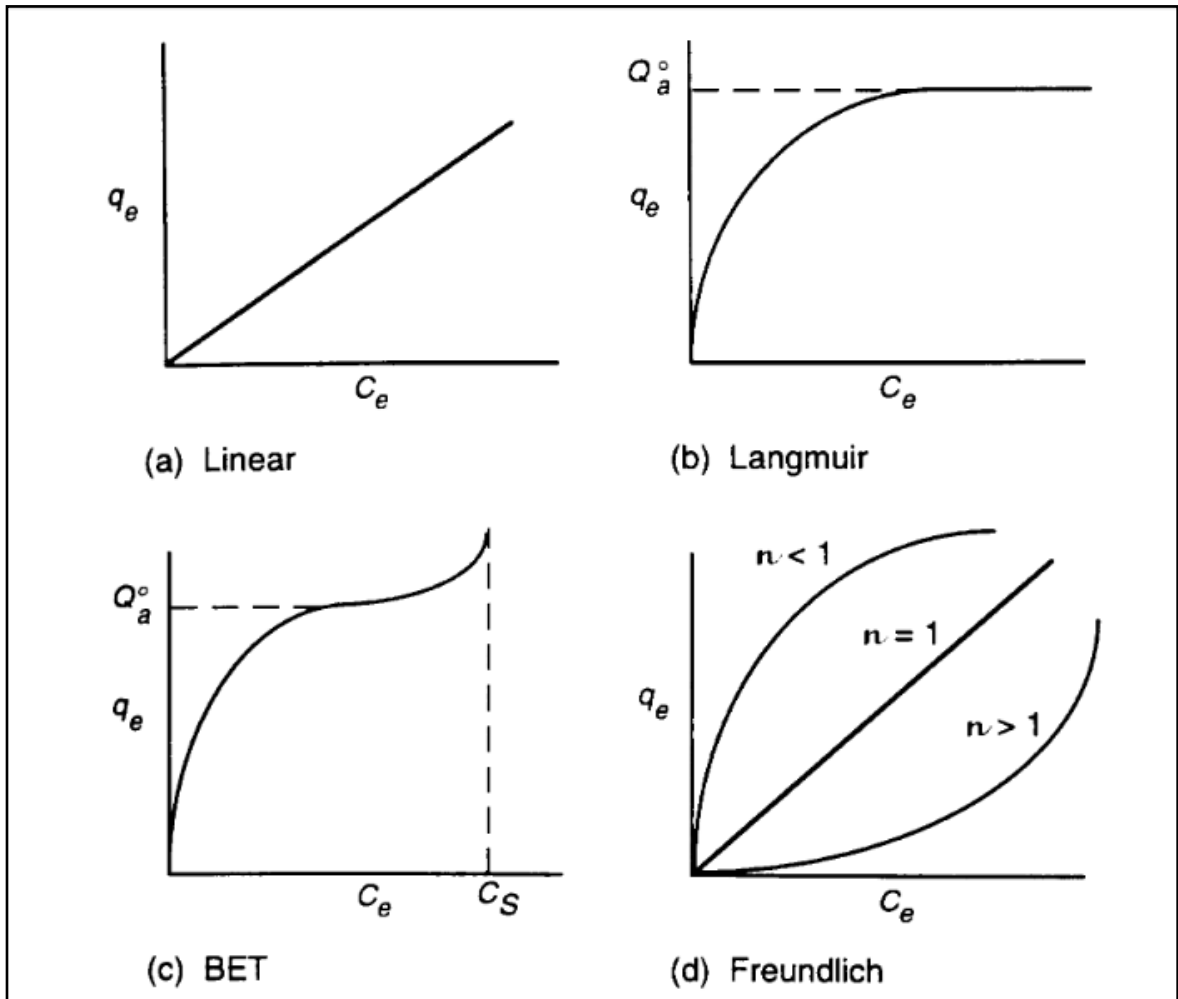


Figure 1-6 : Isotherm Models(Rouquerol, 1999)

In a study on bamboo biochar for adsorption of metal-complex dyes, the Freundlich model has shows better agreement with the adsorption process than Langmuir isotherm, indicating multilayer adsorption of acid black 172 on a heterogeneous bamboo biochar surface (Yang et al., 2013). The tests were done at 20 °C, 30 °C and 40 °C with corresponding 'n' values of 2.69, 2.52 and 2.26 with 'K_F' values of 37.61, 36.09, 48.54 L/g (Yang et al., 2013). Biochar derived from buffalo-weed for trichloroethylene removal from water also fit well to the Freundlich model with a correlation coefficient of approximately 0.9 (Ahmad et al., 2014b). Two biochars were tested (one produced at 300 °C the other at 700 °C). The obtained 'n' values were 0.343 and 0.931, and 'K_F' values of 0.038 and 5.461 mg/g for 300°C and 700°C biochar respectively (Ahmad et al., 2014b).

Langmuir and Freundlich isotherm models were used to describe heavy metal removal using magnetic biochar (Harikishore et al., 2014). The Langmuir isotherm gave a higher correlation coefficient and lower chi-square value than Freundlich isotherm. The Langmuir isotherm for Pb(II) and Cd(II) adsorption gave maximum adsorption capacities of 25.294 and 14.960 respectively. The K_L values were 2.470 and 1.726 respectively (Harikishore et al., 2014). For the same metal removal, the Freundlich isotherm has given '1/n' values of 0.040 and 0.187 with 'K_F' values of 0.912 and 8.867 mg/g respectively (Harikishore et al., 2014)

Plant biomass (bamboo, bagasse, hickory chips), treated with clay (montmorillonite and kaolinite) were investigated as an adsorbent to remove methylene blue (MB), from an

aqueous solution. The Freundlich model showed the best fit with a R^2 of 0.940 (Yao et al., 2014). The 'n' value was 0.169 and a K_F of $5.640 \text{ mg}^{1-n} \text{ L}^n \text{ g}^{-1}$ with a maximum adsorption capacity of 11.940 mg/g (Yao et al., 2014).

Table 1-7 Summary of coefficients of Freundlich and Langmuir adsorption isotherms of some aqueous anion adsorption systems

Adsorbent	Anion	Langmuir			Freundlich			Reference
		Isotherm parameters			Isotherm parameters			
		Q_{\max} (mg/g)	B (L/mg)	R^2	K_f (mg/g)	N	R^2	
Coconut coir pith char	SO_4^{2-}	4.9	0.22	0.9	1.96	4.02	0.996	(Namasivayam and Sangeetha, 2008)
Wood AC	SO_4^{2-}	38.02	0.039	0.99	-	-	-	(Hong et al., 2014)
Shrimp shells	SO_4^{2-}	156	0.0292	0.999	-	-	-	(Moret and Rubio, 2003)
Rice straw	SO_4^{2-}	11.68	0.037	0.65	3.70	5.38	0.74	(Cao et al., 2011)
$\gamma\text{-Al}_2\text{O}_3$	SO_4^{2-}	7.696	0.1135	0.906	2.771	0.123	0.918	(Wu et al.,2002)

Adsorbent	Anion	Langmuir			Freundlich			Reference
		Isotherm parameters			Isotherm parameters			
		Q _{max} (mg/g)	B (L/mg)	R ²	K _f (mg/g)	N	R ²	
Modified wheat straw	NO ₃ ⁻	128.96	0.0045	0.966	2.69	1.73	0.995	(Wang et al., 2007)
γ-Al ₂ O ₃	MoO ₄ ²⁻	30.87	0.0398	0.915	2.438	0.328	0.996	(Wu et al., 2002)
γ-Al ₂ O ₃	SeO ₄ ²⁻	12.30	0.105	0.849	3.064	0.179	0.944	(Wu et al., 2002)
γ-Al ₂ O ₃	SeO ₃ ²⁻	20.85	0.084	0.921	3.063	0.246	0.995	(Wu et al., 2002)
Sleet Furnace Slag	PO ₄ ³⁻	1.43	3673	0.795	2.44	218	0.770	(Sakadevan and Bavor, 1998)
Zeolite	PO ₄ ³⁻	2.15	462	0.872	0.91	2.29	0.852	(Sakadevan and Bavor, 1998)
Blast Furnace Slag	PO ₄ ³⁻	44.247	442	0.967	2.23	677	0.972	(Sakadevan and Bavor, 1998)

The Langmuir model assumes a monolayer adsorption and the Freundlich model assumes a heterogeneous adsorption due to the functionality of the sorption sites or the adsorbate molecules (Namasivayam and Sangeetha, 2008). In most of the adsorption systems shown in table 1-7, Freundlich isotherm model shows more agreement with the results than Langmuir isotherm. In sulphate adsorption systems, two of the studies have considered only Langmuir isotherm. Sulphate adsorption capacity is highest on shrimp shells with Langmuir adsorption capacity of 156 mg/g with $R^2=0.999$, concluding that the nature of sulphate ions adsorption on shrimp shells is a result of a monolayer formation on the adsorbent surface and an interaction with the surface amino groups (Moret and Rubio, 2003). Sulphate adsorption on coconut coir pith char followed both Langmuir and Freundlich isotherms for all the temperatures studied suggesting both the monolayer adsorption mechanism and the heterogeneous adsorption mechanism respectively. For the adsorption of sulphate on $\gamma\text{-Al}_2\text{O}_3$, the isotherm data were best fitted in Freundlich equation than Langmuir, because at low sulphate concentrations used, the Freundlich equation closely represents adsorption results theoretically, since many adsorption sites are available (Wu et al., 2002).

1.9 Thermodynamics of Adsorption

Obtaining a mechanism for an adsorption process starts with calculation of distribution coefficient at different temperatures.

$$K_D = \frac{q_e}{C_e} \quad (1-11)$$

K_D = distribution coefficient (L/kg)

q_e = quantity of the adsorbate adsorbed per unit mass of solid (mg/kg)

C_e = equilibrium concentration of adsorbate in the solution (mg/L)

The K_D values can be used to determine the thermodynamic parameters such as standard Gibbs free energy change, enthalpy change (ΔH), and entropy change (ΔS):

$$\Delta G = \Delta H - T\Delta S \quad (1-12)$$

$$\Delta G = -RT\ln K_D \quad (1-13)$$

R = universal gas constant (8.314 Jmol⁻¹K⁻¹)

T = absolute temperature (K)

The ΔH and ΔS can be obtained from the intercept and slope of Van't Hoff equation of ΔG vs. T

$$\ln K_D = \frac{\Delta S}{R} - \frac{\Delta H}{R} \times \frac{1}{T} \quad (1-14)$$

ΔG , ΔH , and ΔS obtained through above equations are extremely important when understanding the thermodynamic nature of a particular adsorption process. Adsorption is

a spontaneous process and therefore the total free energy of the system should decrease during the process ($\Delta G < 0$). Therefore, a negative value of the standard Gibbs free energy change shows that it is a favourable spontaneous adsorption process. The ΔH and ΔS can either be positive or negative according to the adsorption system characteristics. During adsorption, when the degree of freedom of the molecule or the randomness of the molecule decreases, ΔS becomes negative, but positive entropy change is also possible due to the affinity of adsorbent and increasing randomness at the solid solution interface (Bhatnagar et al., 2011). Positive ΔH represents the endothermic nature of an adsorption, where the adsorption capacities increase with increasing temperature (Yang et al., 2014). Adsorption processes can also be exothermic as molecules are adsorbed on the adsorbent, heat can be generated due to the forces of attraction. Thermodynamic parameters for some biomass based adsorption systems are shown in table 1-8.

Table 1-8 Thermodynamic parameters for some biomass based adsorption systems

Adsorption system	Thermodynamic parameters			Reference
	$\Delta G(\text{kJmol}^{-1})$	$\Delta S(\text{Jmol}^{-1}\text{K})$	$\Delta H(\text{kJmol}^{-1})$	
As(III) on Modified chestnut shell	-6.7928	-103.816	-314.36	(Targan and Tirtom, 2014)
Sulphate on coconut coir pith char	-28.8	132.7	15.4	(Namasivayam and Sangeetha, 2008)

Adsorption system	Thermodynamic parameters			Reference
	$\Delta G(\text{kJmol}^{-1})$	$\Delta S(\text{Jmol}^{-1}\text{K})$	$\Delta H(\text{kJmol}^{-1})$	
Cadmium on biochar from root of rose	-14.77	69.40	6.26	(Khare et al., 2013)
Chromium on biochar from root of rose	-14.74	88.19	11.99	(Khare et al., 2013)
Copper on biochar from root of rose	-14.75	67.44	5.68	(Khare et al., 2013)
Lead on biochar from root of rose	-14.41	63.11	4.72	(Khare et al., 2013)
As(III) on iron rich sludge	-16.5 to -18.9	77	6.18	(Yang et al., 2014)
As(V) on iron rich sludge	-17.4 to -21.0	122.7	18.4	(Yang et al., 2014)
Copper on Corn straw char	-0.80	88.21	25.27	(Chen et al., 2011)

The negative values for ΔG in all adsorption systems show that a favourable spontaneous adsorption process has been taken place. ΔH and ΔS values are positive except in adsorption of As(III) on modified chestnut shell which has a very high negative value for ΔH and ΔS compared to other systems. Comparatively high positive ΔS value in sulphate adsorption on coconut coir pith char shows that the degree of freedom/randomness of the sulphate molecule is higher than that of other adsorbates. Positive ΔH values for most adsorption systems indicate that the reaction is endothermic; adsorption capacities increase with increasing temperature.

1.10 Conclusion

A large volume of waste stream is generated as produced water in worldwide offshore oil and gas industry. Produced water consists of dispersed oil and various other chemical compounds which require treatment. Among those contaminants, sulphur compounds present such as sulphate, thiosalts, polysulphides, bisulphite, hydrogen sulphide, and elemental sulphur which can cause environmental problems, regulatory problems and operational issues. Current industrial produced water treatment methods can be identified in chemical, biological and physical categories but there are limitations when applied in offshore environment, such as space and human resources. Adsorption technique is considered as a suitable method since the design is simple, compact, economical and robust. In the designing of adsorption unit for an industrial application, and for the

selection of a suitable adsorbent, adsorption kinetics, isotherm models and thermodynamics of the adsorption process are required to be assessed.

Industrial adsorbents such as activated carbon, organoclay, zeolite, magnetite, biochar produced from waste streams, and other by products from different industries have been widely used in many research studies for the removal of contaminants from waste water. There are few studies concentrated on the removal of sulphur compounds from aqueous solutions using adsorbents. Activated carbon from coconut coir pith, polypyrrole-grafted activated carbon (GAC), Magnetite, $\gamma\text{-Al}_2\text{O}_3$, an industrial shrimp shell waste, goethite, and modified sugarcane bagasse have been studied as potential adsorbents in removal of sulphate from water. Biochar, which has similar adsorption characteristics can be a potential adsorbent for the removal of sulphur compounds from produced water. Design of a suitable compact, robust and remotely operated sulphur adsorption unit, using biochar could be an excellent solution for the offshore produced water treatment.

1.11 Bibliography- Chapter 1

Ahmad, M., Moon, D. H., Vithanage, M., Koutsospyros, A., Lee, S. S., Yang, J. E., Lee, S. E., Jeon, C. and Ok, Y. S. (2014) 'Production and use of biochar from buffalo-weed (*Ambrosia trifida* L.) for trichloroethylene removal from water', *Journal of Chemical Technology and Biotechnology*, 89(1), pp. 150–157. doi: 10.1002/jctb.4157.

Benatti, C. T., Tavares, C. R. G. and Lenzi, E. (2009) 'Sulfate removal from waste chemicals by precipitation.', *Journal of environmental management*, 90(1), pp. 504–11. doi: 10.1016/j.jenvman.2007.12.006.

Bhatnagar, A., Vilar, V. J. P., Botelho, C. M. S. and Boaventura, R. a R. (2011) 'A review of the use of red mud as adsorbent for the removal of toxic pollutants from water and wastewater.', *Environmental technology*, 32(3-4), pp. 231–49. doi: 10.1080/09593330.2011.560615.

Cao, W., Dang, Z., Zhou, X.-Q., Yi, X.-Y., Wu, P.-X., Zhu, N.-W. and Lu, G.-N. (2011) 'Removal of sulphate from aqueous solution using modified rice straw: Preparation, characterization and adsorption performance', *Carbohydrate Polymers*. Elsevier Ltd., 85(3), pp. 571–577. doi: 10.1016/j.carbpol.2011.03.016.

Chen, X., Chen, G., Chen, L., Chen, Y., Lehmann, J., McBride, M. B. and Hay, A. G. (2011) 'Adsorption of copper and zinc by biochars produced from pyrolysis of hardwood and corn straw in aqueous solution', *Bioresource Technology*, 102(19), pp. 8877–8884. doi: 10.1016/j.biortech.2011.06.078.

Chintala, R., Mollinedo, J., Schumacher, T. E., Papiernik, S. K., Malo, D. D., Clay, D. E., Kumar, S. and Gulbrandson, D. W. (2013) 'Nitrate sorption and desorption in biochars from fast pyrolysis', *Microporous and Mesoporous Materials*. Elsevier Inc., 179, pp. 250–257. doi: 10.1016/j.micromeso.2013.05.023.

Chowdhury, Z. K. (2012) *Activated Carbon: Solutions for Improving Water Quality*. American Water Works Association.

Daigle, T., Phillips, B., Hantz, S. and Janjua, R. (2012) 'Advanced produced Water Treatment', *American Institute of Chemical Engineers*.

Doran, G., Carini, F. and Fruth, D. (1997) 'Evaluation of Technologies to Treat oil Field Produced Water or Reuse Quality.'

ERIN Consulting Ltd. and OCL Services Ltd. (2003) *Sheens Associated with Produced Water Effluents – Review of Causes and Mitigation Options*.

Fakhrul Razi, A., Pendashteh, A., Abdullah, L. C., Biak, D. R. A., Madaeni, S. S. and Abidin, Z. Z. (2009) 'Review of technologies for oil and gas produced water treatment.', *Journal of hazardous materials*, 170(2-3), pp. 530–551. doi: 10.1016/j.jhazmat.2009.05.044.

Geelhoed, J. S., Hiemstra, T. and Van Riemsdijk, W. H. (1997) 'Phosphate and sulfate adsorption on goethite: Single anion and competitive adsorption', *Geochimica et Cosmochimica Acta*, 61(12), pp. 2389–2396. doi: 10.1016/S0016-7037(97)00096-3.

Gieg, L. M., Jack, T. R. and Foght, J. M. (2011) 'Biological souring and mitigation in oil reservoirs.', *Applied microbiology and biotechnology*, 92(2), pp. 263–82. doi: 10.1007/s00253-011-3542-6.

Grant, M. T., Rowe, B., Foy, M., Theriault, S. and Card, H. (2006) *Atlantic Canada Wastewater Guidelines Manual for Collection, Treatment, and Disposal*.

Guerra, K., Dahm, K. and Dunderf, S. (2011) *Oil and Gas Produced Water Management and Beneficial Use in the Western United States*.

Harikishore Kumar Reddy, D. and Lee, S.-M. (2014) 'Magnetic biochar composite: Facile synthesis, characterization, and application for heavy metal removal', *Colloids and Surfaces A: Physicochemical and Engineering Aspects*. Elsevier B.V., 454, pp. 96–103. doi: 10.1016/j.colsurfa.2014.03.105.

Hayes, T. (2004) 'Overview of Emerging Produced Water Treatment Technologies.'

Ho, Y.-S. (2006) 'Review of second-order models for adsorption systems.', *Journal of hazardous materials*, 136(3), pp. 681–9. doi: 10.1016/j.jhazmat.2005.12.043.

Hong, S., Cannon, F. S., Hou, P., Byrne, T. and Nieto-delgado, C. (2014) 'Sulfate removal from acid mine drainage using polypyrrole-grafted granular activated carbon', *Carbon*. Elsevier Ltd, 73(29), pp. 51–60. doi: 10.1016/j.carbon.2014.02.036.

Hulshoff Pol, L. W., Lens, P. N., Stams, a J. and Lettinga, G. (1998) 'Anaerobic treatment of sulphate-rich wastewaters.', *Biodegradation*, 9(3-4), pp. 213–24. Available at: <http://www.ncbi.nlm.nih.gov/pubmed/10022065>.

Husain, T., Veitch, B., Hawboldt, K., Niu, H., Adams, S. and Shanaa, J. (2008) 'Produced Water Discharge Monitoring', (May), pp. 5–8.

Igunnu, E. T. (2012) 'Produced water treatment technologies', *International Journal of Low-Carbon Technologies*, pp. 1–21. doi: 10.1093/ijlct/cts049.

Judd, S., Qiblawey, H., Al-Marri, M., Clarkin, C., Watson, S., Ahmed, a. and Bach, S. (2014) 'The size and performance of offshore produced water oil-removal technologies for reinjection', *Separation and Purification Technology*. Elsevier B.V., 134, pp. 241–246. doi: 10.1016/j.seppur.2014.07.037.

Khare, P., Dilshad, U., Rout, P. K., Yadav, V. and Jain, S. (2013) 'Plant refuses driven biochar: Application as metal adsorbent from acidic solutions', *Arabian Journal of Chemistry*. King Saud University. doi: 10.1016/j.arabjc.2013.11.047.

Khatib, Z. and Verbeek, P. (2002) 'Water to Value – Produced Water Management for Sustainable Field Development of Mature and Green Fields.'

Knaebel, K. S. (2004) 'Adsorbant Selection', *Adsorption Research Inc.*

Lazaridis, N. K. and Asouhidou, D. D. (2003) 'Kinetics of sorptive removal of chromium(VI) from aqueous solutions by calcined Mg-Al-CO(3) hydrotalcite.', *Water research*, 37(12), pp. 2875–82. doi: 10.1016/S0043-1354(03)00119-2.

Lee, K. and Neff, J. (2011) *Produced Water-Environmental Risks and Advances in Mitigation Technologies.*

Ligthelm, D. J., Boer, R. B. De, Brint, J. F. and Schulte, W. M. (1991) 'Transportation in an Oil Reservoir Owing to Bacterial Activity.'

Lopez, O., Sanguinetti, D., Bratty, M. and Kratochvil, D. (2009) 'Green Technologies for Sulphate and Metal Removal in Mining and Metallurgical Effluents.'

Moret, a. and Rubio, J. (2003) 'Sulphate and molybdate ions uptake by chitin-based shrimp shells', *Minerals Engineering*, 16(8), pp. 715–722. doi: 10.1016/S0892-6875(03)00169-9.

Mulinari, D. R. and da Silva, M. L. C. P. (2008) 'Adsorption of sulphate ions by modification of sugarcane bagasse cellulose', *Carbohydrate Polymers*, 74(3), pp. 617–620. doi: 10.1016/j.carbpol.2008.04.014.

Namasivayam, C. and Sangeetha, D. (2008) 'Application of coconut coir pith for the removal of sulfate and other anions from water', *Desalination*, 219(1-3), pp. 1–13. doi: 10.1016/j.desal.2007.03.008.

Neff, J. (2002) *Bioaccumulation in marine organisms: effect of contaminants from oil well produced water*. Amsterdam; Boston: Elsevier, 2002. Available at: [http://books.google.ca/books?id=ABIQ_FGKOZcC&lpg=PP2&ots=v0lQIJZVW-&dq=J.M.Neff%2C Bioaccumulation in Marine Organisms%3A Effect of Contaminants from OilWell ProducedWater%2C Elsevier%2C The Netherlands%2C 2002&lr&pg=PP2#v=onepage&q=J.M.Neff, Bioaccumulation in Marine Organisms: Effect of Contaminants from OilWell ProducedWater, Elsevier, The Netherlands, 2002&f=false](http://books.google.ca/books?id=ABIQ_FGKOZcC&lpg=PP2&ots=v0lQIJZVW-&dq=J.M.Neff%2C%20Bioaccumulation%20in%20Marine%20Organisms%3A%20Effect%20of%20Contaminants%20from%20OilWell%20ProducedWater%2C%20Elsevier%2C%20The%20Netherlands%2C%202002&lr&pg=PP2#v=onepage&q=J.M.Neff,%20Bioaccumulation%20in%20Marine%20Organisms%3A%20Effect%20of%20Contaminants%20from%20OilWell%20ProducedWater,%20Elsevier,%20The%20Netherlands,%202002&f=false).

Neff, J., Lee, K. and Deblois, E. M. (2011) 'Produced Water : Overview of Composition , Fates , and Effects', *Produced Water*, pp. 3–54. doi: 10.1007/978-1-4614-0046-2.

Oboh, I. O., Aluyor, E. O. and Audu, T. O. K. (2013) 'Second-order kinetic model for the adsorption of divalent metal ions on *Sida acuta* leaves', 8(34), pp. 1722–1728. doi: 10.5897/IJPS09.146.

OGP (2002) *Aromatics in produced water: occurrence, fate & effects, and treatment*.

Qiu, H., Lv, L., Pan, B., Zhang, Q., Zhang, W. and Zhang, Q. (2009) 'Critical review in adsorption kinetic models', *Journal of Zhejiang University SCIENCE A*, 10(5), pp. 716–724. doi: 10.1631/jzus.A0820524.

Ray, J. and Engelhardt, R. (1992) *Produced Water: technological, environmental issues and solutions*. California. Available at: [http://books.google.ca/books?id=0BFDzWFL8t8C&lpg=PA1&ots=Xc3OtOIC-k&dq=J. Carey, A. Zaidi and J. Ribo, Specific toxic organics in produced waters from in-situ heavy oil recovery operations in western Canada, In Produced water technological~Environmental Issues and Solutions \(Edited by J.P. Ray and F.R. Engelhardt\), Plenum Pre&lr&pg=PP8#v=onepage&q&f=false](http://books.google.ca/books?id=0BFDzWFL8t8C&lpg=PA1&ots=Xc3OtOIC-k&dq=J.Carey,%20A.Zaidi%20and%20J.Ribo,%20Specific%20toxic%20organics%20in%20produced%20waters%20from%20in-situ%20heavy%20oil%20recovery%20operations%20in%20western%20Canada,%20In%20Produced%20water%20technological~Environmental%20Issues%20and%20Solutions%20(Edited%20by%20J.P.%20Ray%20and%20F.R.%20Engelhardt),%20Plenum%20Press&lr&pg=PP8#v=onepage&q&f=false).

Rice, R. (1934) 'Adsorption of strychnine sulphate by various charcoals and by Lloyd ' s reagent.'

Roonasi, P. and Holmgren, A. (2009) 'An ATR-FTIR study of sulphate sorption on magnetite; rate of adsorption, surface speciation, and effect of calcium ions.', *Journal of colloid and interface science*. Elsevier Inc., 333(1), pp. 27–32. doi: 10.1016/j.jcis.2008.12.080.

Rouquerol, F. (1999) *Adsorption by Powders and Porous Solids*. San Diego: Academic Press, San Diego.

RPSEA (2009) *An Integrated Framework for Treatment and Management of Produced Water*.

Sakadevan, K. and Bavor, H. J. (1998) 'Phosphate adsorption characteristics of soils, slags and zeolite to be used as substrates in constructed wetland systems', *Water Research*, 32(2), pp. 393–399. doi: 10.1016/S0043-1354(97)00271-6.

Sánchez-Andrea, I., Sanz, J. L., Bijmans, M. F. M. and Stams, A. J. M. (2014) 'Sulfate reduction at low pH to remediate acid mine drainage.', *Journal of hazardous materials*. Elsevier B.V., 269(3), pp. 98–109. doi: 10.1016/j.jhazmat.2013.12.032.

Sheindorf, C., Rebhun, M. and Sheintuch, M. (1980) 'A Freundlich Type Multicomponent Isotherm.'

Silva, A. ., Varesche, M. ., Foresti, E. and Zaiat, M. (2002) 'Sulphate removal from industrial wastewater using a packed-bed anaerobic reactor', *Process Biochemistry*, 37(9), pp. 927–935. doi: 10.1016/S0032-9592(01)00297-7.

Silva, R., Cadorin, L. and Rubio, J. (2010) 'Sulphate ions removal from an aqueous solution: I. Co-precipitation with hydrolysed aluminum-bearing salts', *Minerals Engineering*. Elsevier Ltd, 23(15), pp. 1220–1226. doi: 10.1016/j.mineng.2010.08.016.

Targan, Ş. and Tirtom, V. N. (2014) 'Arsenic removal from aqueous system using modified chestnut shell', *Desalination and Water Treatment*, (October), pp. 1–8. doi: 10.1080/19443994.2014.942377.

USACE (2001) *Adsorption Design Guide*. doi: DG 1110-1-2.

Wang, Y., Gao, B. Y., Yue, W. W. and Yue, Q. Y. (2007) 'Preparation and utilization of wheat straw anionic sorbent for the removal of nitrate from aqueous solution', *Journal of Environmental Sciences*, 19(11), pp. 1305–1310. doi: 10.1016/S1001-0742(07)60213-7.

Witter, A. and Jones, D. (1999) 'Chemical Characterization of Organic Constituents from Sulphide-Rich Produced Water Using Gas Chromatography / Mass Spectrometry', 18(9), pp. 1920–1926.

Wu, C.-H., Kuo, C.-Y., Lin, C.-F. and Lo, S.-L. (2002) 'Modeling competitive adsorption of molybdate, sulfate, selenate, and selenite using a Freundlich-type multi-component isotherm', *Chemosphere*, 47(3), pp. 283–292. doi: 10.1016/S0045-6535(01)00217-X.

Wu, C.-H., Lo, S.-L. and Lin, C.-F. (2000) 'Competitive adsorption of molybdate, chromate, sulfate, selenate, and selenite on γ -Al₂O₃', *Colloids and Surfaces A: Physicochemical and Engineering Aspects*, 166(1-3), pp. 251–259. doi: 10.1016/S0927-7757(99)00404-5.

Yang, J.-S., Kim, Y.-S., Park, S.-M. and Baek, K. (2014) 'Removal of As(III) and As(V) using iron-rich sludge produced from coal mine drainage treatment plant.', *Environmental science and pollution research international*, 21(18), pp. 10878–89. doi: 10.1007/s11356-014-3023-4.

Yang, Y., Lin, X., Wei, B., Zhao, Y. and Wang, J. (2013) 'Evaluation of adsorption potential of bamboo biochar for metal-complex dye: equilibrium, kinetics and artificial neural network modeling', *International Journal of Environmental Science and Technology*, 11(4), pp. 1093–1100. doi: 10.1007/s13762-013-0306-0.

Yao, Y. (2013) 'Sorption of Phosphate and Other Contaminants on Biochar and Its Environmental Implications.'

Yao, Y., Gao, B., Fang, J., Zhang, M., Chen, H., Zhou, Y., Creamer, A. E., Sun, Y. and Yang, L. (2014) 'Characterization and environmental applications of clay–biochar composites', *Chemical Engineering Journal*. Elsevier B.V., 242, pp. 136–143. doi: 10.1016/j.cej.2013.12.062.

Yao, Y., Gao, B., Inyang, M., Zimmerman, A. R., Cao, X., Pullammanappallil, P. and Yang, L. (2011) 'Removal of phosphate from aqueous solution by biochar derived from anaerobically digested sugar beet tailings', *Journal of Hazardous Materials*. Elsevier B.V., 190(1-3), pp. 501–507. doi: 10.1016/j.jhazmat.2011.03.083.

Chapter 2. Characterization of Biochar - Review

Yashodha G. Marambage, Kelly A. Hawboldt

Faculty of Engineering and Applied Science, Memorial University of Newfoundland,

St. John's, NL, Canada. A1B3X5

Abstract

Biochar has been studied as an adsorbent for removal of contaminants from water in a number of studies due to its low cost, availability, and adsorptive characteristics. Biochar can be generated in a number of ways, in this work we have focussed on biochar from the pyrolysis of woody biomass. This chapter reviews the properties of biochar as a function of pyrolysis conditions and biomass structure. Adsorption capacities of biochar in removal of aqueous contaminants are summarized. The surface area and pore size analysis, density analysis, SEM analysis, thermal analysis, elemental analysis, FTIR analysis and XRD-structural and mineralogical analysis have been discussed in detail with examples from literature. Physical properties largely influence the adsorption characteristics of biochar where the biochar with high porosity and high surface area have been identified as very good adsorbents. Chemical properties such as surface functional groups and surface charge of biochar determine the affinity of target contaminants on the biochar surface. In most batch adsorption experiments on biochar, high temperature and low pH of the solution have induced adsorption capacity. However, apart from the solution properties, the adsorption capacity of a particular adsorption system strongly depends on the compatibility in between the biochar and the target contaminant.

2.1 Introduction

Biochar is a carbon rich solid formed during thermal decomposition of biomass under limited or zero supply of oxygen. Biochar can be produced from feedstocks such as forestry residues, wood waste, municipal solid waste, animal manures and agricultural by-products, such as straw, rice hull, seeds or fruit stones (Attila et al., 1996). Regardless of its nature, worldwide biomass can be identified mainly in five components; lipids, starch, cellulose, hemicelluloses, lignin, and proteins. Approximately 90% of global biomass availability is lignocellulosic biomass which consists of cellulose, hemicelluloses, and lignin (Pandey et al., 2011). This type of biomass can be generated from different waste streams such as crop residues, paper and wood industries which makes it more economical and environmentally friendly (Duku et al. 2011; Pandey et al. 2011). Availability, suitability of some waste materials and the global production of biochar from those materials are shown in table 2-1

Table 2-1 Availability, suitability of waste materials for biochar production (Lehmann, Gaunt and Rondon, 2006)

Waste Material	Availability	Suitability	Potential global production (Pgyr ⁻¹)
Forestry residues	Medium	High	0.04
Mill residues	High	High	0.05
Rice husks	High	Medium	0.04
Groundnut shells	High	High	0.002
Urban waste	High	High	0.03

The application of biochar derived from waste biomass as an adsorbent in wastewater treatment has the benefit of using one waste to treat another. Further, as the bio-char is a by-product of another process, production costs are low. Ideally, the biochar would be regenerated to minimize disposal costs; however, regeneration is not necessary to make the process viable, because biochar is not expensive and has a minimal impact on the environment. In order to assess the suitability of a particular biochar as an adsorbent or in any other application, its physical chemical and thermal properties should be analysed.

2.2 Pyrolysis of biomass

Wood and plant biomass are readily available as a cheap feedstock from the residues of agriculture and forestry processing and include bark, sawdust, saw chips, plant residues and nut shells. Wood based biomass has high lignin concentration which results in high biochar yield when pyrolysed and also wood biochar has shown a carbon content up to 80% (Duku et al., 2011). Wood has a polymeric structure consisting of carbohydrates (cellulose and hemicellulose) and lignin, with small amounts of organic chemicals and minerals. As a result, wood biochar is a combination of mainly carbon atoms, heteroatoms such as hydrogen and oxygen and mineral matter (Pastor-Villegas et al., 2006). The pyrolysis process involves various reactants, intermediates and products (Brunner and Roberts, 1980). Ash formed during the pyrolysis process (e.g., K_2O , P_2O_5 , MgO , Na_2O) may catalyze graphitization and polymerization (Uchimiya et al., 2011). Pyrolysis starts with initial dehydration, and then depolymerisation of cellulose and hemicellulose structure, depolymerisation of the lignin, C-O and C-C bond breakage

and forming some graphitic layers when the temperature is above 400°C (Byrne and Nagle, 1996).

During the pyrolysis of biomass, the growth of aromatic structures in the solid phase along with the polymerization process results in carbon enrichment. Further, the volatilization of organic compounds causes various structural changes including porosity development (Mayer et al., 2013). In addition to biochar, pyrolysis of biomass generates an aqueous low molecular weight acidic liquid (pyroligneous acid or tar), and a low-energy, combustible gas depending on the pyrolysis temperatures, heating rates, and residence time (Brewer, 2012). There are four modes of pyrolysis; fast, intermediate, slow, and gasification. The yield from each pyrolysis process is determined by the pyrolysis conditions of the process as shown in table 2-2.

Table 2-2 Typical product yields (dry basis) obtained by different modes of pyrolysis (Herbert et al. 2012 ; Duku et al. 2011; Maschio et al. 1992 ; Ahmad, Rajapaksha, et al. 2014 ;Bolan et al. 2013)

Mode	Pyrolysis Conditions				Yield (% wt)		
	Temperature (°C)	Residence time(s)	Particle size(mm)	Heating rate(°C/s)	biochar	Liquid	Gas
Fast	500-1000	<2	<1	10-200	12	75	13
Intermediate	Around 500	10-20	-	-	25	50	25
Slow	300-700	600-6000	5-50	0.1-1	35	30	35
Gasification	>800	10-20	-	-	10	5	85

Slow pyrolysis gives the highest biochar yield. Even within the same pyrolysis mode and feedstock, the biochar yield can vary depending on the operating temperature illustrated in figure 2-1 and figure 2-2.

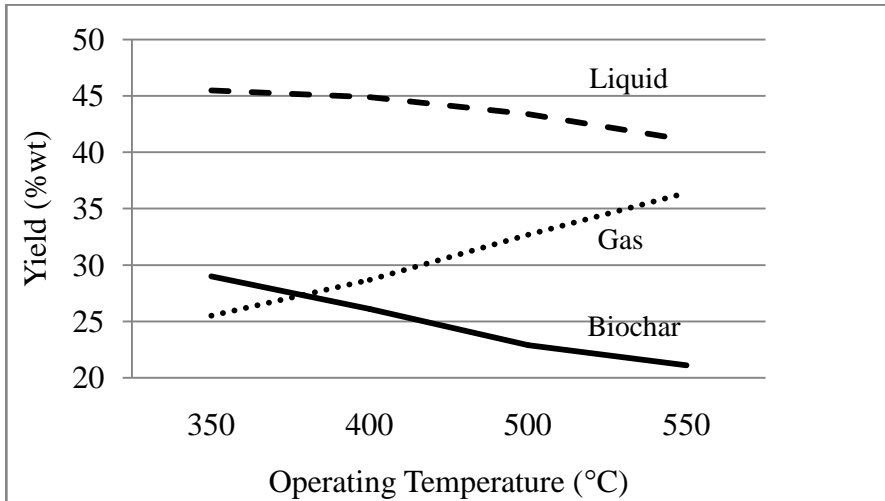


Figure 2-1 Yields of slow pyrolysis of wood (% wt)(Maschio et al., 1992)

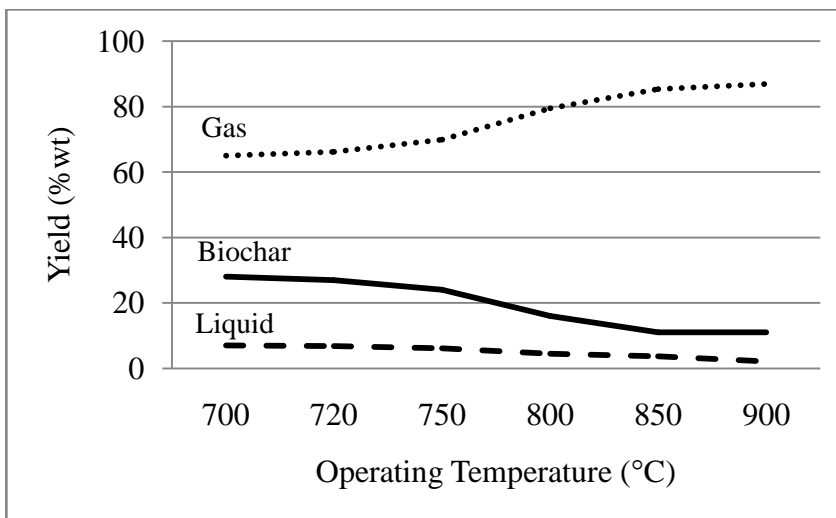


Figure 2-2 Yields of fast pyrolysis of hazel nut shells (% wt) (Maschio et al., 1992)

Figure 2-1 and 2-2 show that the biochar yield is low at high operating temperatures in both slow and fast pyrolysis modes. Fast pyrolysis of hazel nut shells has given a similar biochar yield, even at 700°C compared to the biochar yield of slow pyrolysed wood at 350°C of operating temperature. This suggests that the biochar yield also depends on the properties of the starting biomass. Pyrolysis conditions which favour high biochar yields have been identified as (i) high lignin, ash and nitrogen contents in the biomass, (ii) low pyrolysis temperature (<400 °C), (iii) high process pressure, (iv) long vapour residence time, (v) extended vapour/solid contact, (vi) low heating rate, (vii) large biomass particle size, and (viii) optimised heat integration (Duku et al., 2011).

2.3 Biochar as an Adsorbent in Water Treatment

The most appropriate end use application of a biochar is a function of physical, chemical, and thermal characteristics such as pore structure, density, moisture content, calorific value, fixed carbon, oxygen, hydrogen, nitrogen, volatiles, ash content, and cellulose/lignin ratio of feedstock result from pyrolysis process (Duku et al., 2011). According to the literature, high pyrolysis temperatures (>400⁰C) generally produce biochar with high surface area, micro porosity, and hydrophobicity therefore effective in adsorption of organic contaminants. Biochar obtained at lower temperatures (<400⁰C) are more suitable for removing inorganic/polar organic contaminants due to several properties such as oxygen containing functional groups and electrostatic attraction (Ahmad et al., 2014a).

Biochar has strong adsorption affinity for organic contaminants and heavy metals due to the porous structure and heterogeneous surface chemistry (Song et al., 2014). Heterogeneous surfaces are very important in adsorption since they have a large surface area due to micropores, mesopores, and macropores with a variety of adsorption sites. Specially wood biochar has a disorganized pore structure with a heterogeneous surface which makes it a very good adsorbent (Pastor-Villegas et al., 2007). The surface of wood char consists of the faces of graphene sheets and mostly on the edges, various functional groups such as O-containing carboxyl, hydroxyl, and phenolic surface functional groups which makes it an effective contaminant sorbent (Pastor-Villegas et al. 2007; Ahmad, Rajapaksha, et al. 2014). Table 2-3 summarizes some of the literature on biochar use as adsorbents in wastewater treatment:

Table 2-3 Biochar source, production method, and application for removal of aqueous contaminants

Biochar feedstock	Pyrolysis Conditions	Contaminant	Adsorption capacity (mg/g)	Temp	pH	Reference
Hardwood	450 °C, fast	Cu ²⁺	6.79	22	7	(Chen et al., 2011)
Hardwood	450 °C, fast	Zn ²⁺	4.54	22	8	(Chen et al., 2011)

Biochar feedstock	Pyrolysis Conditions	Contaminant	Adsorption capacity (mg/g)	Temp	pH	Reference
Corn straw	600 ⁰ C, slow	Cu ²⁺	12.52	22	5	(Chen et al., 2011)
Corn straw	600 ⁰ C, slow	Zn ²⁺	11.0	22	8	(Chen et al., 2011)
Root of rose	450 ⁰ C, 10 ⁰ C/min	Cd ²⁺ , Cr ²⁺ , Cu ²⁺ , Pb ²⁺	60	30	4	(Khare et al., 2013)
Stem of eucalyptus	450 ⁰ C 10 ⁰ C/min	Cd ²⁺ , Cr ²⁺ , Cu ²⁺ , Pb ²⁺	60	30	4	(Khare et al., 2013)
Bamboo char	1000 ⁰ C	Metal-complex dye	401.88	40	1	(Yang et al., 2013)
Coconut shell	400 ⁰ C for 2h	Oxalic Acid	0.09	-	-	(Rahman et al., 2006)
Coconut shell	400 ⁰ C for 2h	Maleic acid	0.15	-	-	(Rahman et al., 2006)
sugar beet tailings	600 ⁰ C, slow	PO ₄ ³⁻	133.085	Room T	5.2	(Yao et al., 2011)

Biochar feedstock	Pyrolysis Conditions	Contaminant	Adsorption capacity (mg/g)	Temp	pH	Reference
Buffalo weed char	300 ⁰ C, 10 ⁰ C/min	C ₂ HCl ₃	71.57	25	7	(Ahmad et al., 2014b)
Buffalo weed char	700 ⁰ C, 7 ⁰ C/min	C ₂ HCl ₃	91.15	25	7	(Ahmad et al., 2014b)
Coconut coir pith char	700 ⁰ C	SO ₄ ²⁻	4.9	35	4	(Namasivayam and Sangeetha, 2008)
Jatropha husk	700 ⁰ C for 1h	Nitrate	0.64	30	3	(Namasivayam et al., 2007)
Jatropha husk	700 ⁰ C for 1h	Phosphate	0.92	30	3	(Namasivayam et al., 2007)
Jatropha husk	700 ⁰ C for 1h	Thiocyanate	0.16	30	3	(Namasivayam et al., 2007)
Jatropha husk	700 ⁰ C for 1h	Selenite	0.75	30	2	(Namasivayam et al., 2007)
Jatropha husk	700 ⁰ C for 1h	Chromium (VI)	1.017	30	2	(Namasivayam et al., 2007)

Biochar feedstock	Pyrolysis Conditions	Contaminant	Adsorption capacity (mg/g)	Temp	pH	Reference
Jatropha husk	700 ⁰ C for 1h	Nickel(II)	9.7	30	5	(Namasivayam et al., 2007)
Jatropha husk	700 ⁰ C for 1h	Vanadium(V)	0.75	30	4	(Namasivayam et al., 2007)
Jatropha husk	700 ⁰ C for 1h	2-Chlorophenol	1	30	2	(Namasivayam et al., 2007)
Jatropha husk	700 ⁰ C for 1h	Bisphenol	1.13	30	2	(Namasivayam et al., 2007)
Jatropha husk	700 ⁰ C for 1h	Acid brilliant blue	1.48	30	10	(Namasivayam et al., 2007)
Jatropha husk	700 ⁰ C for 1h	Acid violet	2.05	30	5.9	(Namasivayam et al., 2007)
Jatropha husk	700 ⁰ C for 1h	Congo red	1.05	30	7	(Namasivayam et al., 2007)
Jatropha husk	700 ⁰ C for 1h	Direct red 12B	1.25	30	2	(Namasivayam et al., 2007)
Jatropha husk	700 ⁰ C for 1h	Methylene blue	1.38	30	10	(Namasivayam et al., 2007)

Biochar feedstock	Pyrolysis Conditions	Contaminant	Adsorption capacity (mg/g)	Temp	pH	Reference
Jatropha husk	700 ⁰ C for 1h	Procion orange	0.225	30	2	(Namasivayam et al., 2007)
Corn straws	600 ⁰ C for 3h	Cu ²⁺	19.6	25		(Song et al., 2014)
Peanut hull	300 ⁰ C for 5h	Pb ²⁺	1.04	Room T		(Xue et al., 2012)
Palm bark	400 ⁰ C, 5 ⁰ C/min	Methylene blue dye	2.66	40	5-9	(Sun et al., 2013)
Eucalyptus	400 ⁰ C, 5 ⁰ C/min	Methylene blue dye	2.06	40	5-9	(Sun et al., 2013)

Typically the maximum adsorption capacity has been obtained when the adsorption experiments are carried out at temperatures greater than 20 ⁰C, and the optimum pH varies according to the target contaminant and the chemistry of biochar. Acidic conditions (pH is between 2 to 5) have favoured the contaminant adsorption of most of the biochar samples. The adsorption capacity strongly depends on the biochar characteristics and the affinity of the contaminants on the biochar surface. Table 2-3 shows that in most cases, slow pyrolysis process has been carried out for biochar production. Comparing the results of the adsorption experiments for adsorption of aqueous Cu²⁺ and Zn²⁺ performed on slow

pyrolysed and fast pyrolysed biochar, high adsorption capacities have been obtained from biochar obtained from slow pyrolysis (Chen et al., 2011). Biochar produced at high pyrolysis temperatures, has shown high adsorption capacity compared to those generated from low pyrolysis temperatures. As examples, bamboo char produced at 1000°C had an adsorption capacity of 401.88 mg/g for a metal-complex dye while coconut shell char produced at 400°C has shown adsorption capacities of 0.09 mg/g and 0.15mg/g for oxalic acid and maleic acid respectively.

2.4 Characterization of Biochar

The adsorption capacity, selectivity, regenerability, adsorption kinetics, compatibility, and the cost of the adsorption system are the most important factors for any adsorption application (Knaebel, 2004). These factors are all tied to the adsorption properties of the char. As an example, the bulk density affects the pore size distribution and efficiency of adsorption process whereas porosity affects the holding capacity since greater surface area provides more space for the contaminant (Mayer et al., 2013). Biochar characterization can be carried out using a number of methods such as SEM analysis, ICP-elemental analysis, FTIR, TGA-thermal analysis, XRD-structural and mineralogical analysis, elemental (carbon, hydrogen, nitrogen, oxygen) and stable isotope analysis, surface area, and pore size distribution analysis (EPA, 2013).

2.4.1 Surface area, total pore volume and pore size distribution

The physical properties of biochar depend on the source biomass and on the pyrolysis process (fast, slow, etc.). The variation of BET surface area (Brunauer-Emmett-Teller) of

wood char produced from pitch pine at different final temperatures and ramp rates is shown in figure 2-3 (Brown et al., 2006).

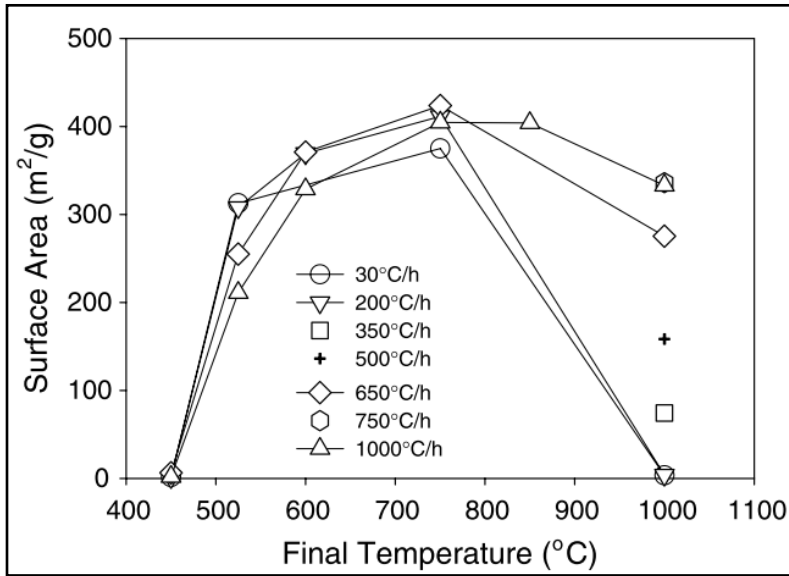


Figure 2-3 BET surface areas of pine wood char as a function of production temperature under various ramp rates (Brown et al., 2006).

According to figure 2-3, at 750°C, the BET surface area was approximately 400m²/g and for the same biomass at the lowest temperature studied (450°C), and at the highest temperature studied (1000°C), the surface area was less than 10m²/g. This suggests that the BET surface area strongly depends on the final temperature. The surface area did not significantly vary with different heating rates when the final temperature was below 600°C, however at final temperatures above 800°C, high heating rates gave high surface areas. The surface area can also vary within the same pyrolysis conditions depending on the starting biomass. Biochar produced from slow pyrolysis of different agricultural and

wood residues (bagasse, cocopeat, paddy straw, palm kernel shell, wood stem, and wood bark), heated from room temperature to 500 °C at approximately 10°C/min showed a wide variation of microscopic surface areas measured (Lee et al., 2013). Bagasse, cocopeat, paddy straw, palm kernel shell, wood stem, and wood bark exhibited surface areas of 202 m²/g, 13.7 m²/g, 45.8 m²/g, 191 m²/g, 326 m²/g, and 13.6 m²/g respectively (Lee et al., 2013). Table 2-4 summarizes additional BET surface area results from different biochars.

Table 2-4 BET Surface area, pore size and total pore volume of different biochar

Biochar	Pyrolysis Conditions		BET-N ₂ Surface area(m ² /g)	Avg. Pore size(nm)	Total pore volume V _{tot} (cm ³ /g)	Reference
	Final Temp.	Heating rate (°C/min)				
Buffalo weed char	300	7	3.98	4.56	0.01	(Ahmad et al., 2014b)
	700	7	9.25	5.63	0.02	
Coconut coir pith	700	-	167	2.75	0.1217	(Namasivayam and Sangeetha, 2008)
Oat hulls	300	3.6	0.1	3.2	0.009	(González et al., 2013)
	500	3.6	6.6	2.2	0.012	
Pine bark	300	3.6	1.9	3.1	0.008	
	500	3.6	63	3.1	0.028	

Biochar	Pyrolysis Conditions		BET-N ₂	Avg. Pore	Total pore	Reference
	Final Temp.	Heating rate (°C/min)	Surface area(m ² /g)	size(nm)	volume V _{tot} (cm ³ /g)	
Corn straws	600	slow pyrolysis for 3 h	61	23.7	0.036	(Song et al., 2014)
Maple-wood char	400	Slow	340	-	0.15	(Braidia et al., 2003)
Pine bark	350	100	<1	-	-	(Mitchell et al., 2015)
	450	100	19.6	-	-	
	600	100	259.4	-	-	
Pinewood	350	100	<1	-	-	(Mitchell et al., 2015)
	450	100	<1	-	-	
	600	100	407.8	-	-	
Poplar wood	350	100	<1	-	-	(Mitchell et al., 2015)
	450	100	<1	-	-	
	600	100	279.6	-	-	
Switch grass	500	15 (Slow)	50.2	-	-	(Brewer, 2012)
	500	Fast	21.6	-	-	
	760	Gasification	31.4	-	-	

Biochar	Pyrolysis Conditions		BET-N ₂	Avg. Pore	Total pore	Reference
	Final Temp.	Heating rate (°C/min)	Surface area(m ² /g)	size(nm)	volume V _{tot} (cm ³ /g)	
Corn	500	15 (Slow)	20.9	-	-	(Brewer, 2012)
Stover	500	Fast	7.0	-	-	
	730	Gasification	23.9	-	-	
Hardwood	500	15 (Slow)	19.7	-	-	(Brewer, 2012)
Willow char	410-480	30	1.4 - 5.4	-	-	(Mayer et al., 2013)

Note: Before BET analysis, oat hulls and pine bark samples have been vacuum degassed at 160 °C for 16 h, switch grass, corn stover, and hardwood samples have been vacuum degassed at 300°C for 4-16 hours and willow char has been degassed at 220 °C for 12 h.

Surface areas are in the range of 100–350 m²/g however there are biochars with very low surface area (1-50 m²/g) depending on the pyrolysis conditions, starting biomass, and ash content. The final temperature of the pyrolysis process has a significant impact on the surface area and porosity. When the final temperature is increased (above 500°C), the biochar increases in surface area due to the better removal of volatile components. Wood biochar shows high surface area compared to the other feedstock while slow pyrolysis results in higher surface areas compared to other pyrolysis modes. Adsorbents must be

highly porous and/or composed of very fine particles to achieve the large surface areas (>100m²/g) required (Rouquerol, 1999)..

2.4.2 Biochar Density (solid /true density and bulk density)

The density of biochar can be identified as solid density and bulk density. Solid density is the density at molecular level, related to the degree of packing of the carbon structure and bulk density involves all particles and includes the macroporosity within each particle and the interparticle voids (Downie, 2011). Solid or true density, also known as particle density, increases with ash (mineral) content and process temperature (Brewer, 2012). It has been proposed that the particle density can be used to estimate the charring temperature. As temperature and reaction time increase, the degree of graphitization increases and particle density of biochar can approach that of solid graphite which is around 2.25 g/cm³ (Brewer, 2012). Solid density as a function of final temperature of pyrolysis process is shown in figure 2-4.

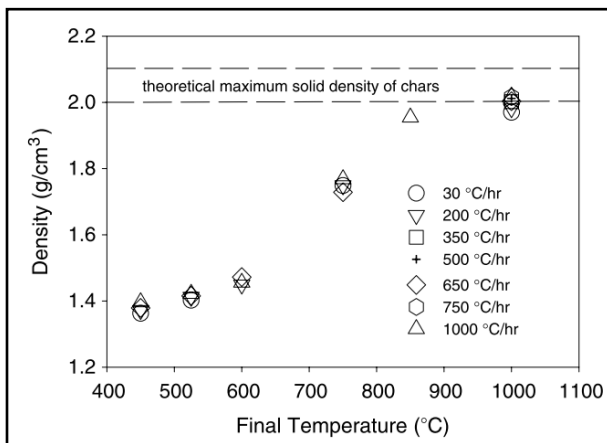


Figure 2-4 Solid density as a function of final temperature of pyrolysis process (Brown et al., 2006).

Figure 2-4 shows that the particle density is independent of the ramp rate and it is a function of the final temperature of the sample. With the increasing final temperature, low-density disordered carbon converts into high density carbon structure which results in high particle density (Brown et al., 2006). Particle density and bulk density of some biochars are shown in Table 2-5.

Table 2-5 Particle density and bulk density of some biochar in literature

Biochar	Pyrolysis Conditions		Particle density (g/cm ³)	Bulk density (g/cm ³)	Reference
	Final Temp	Heating rate (°C/min)			
Switch grass	500	15 (Slow)	1.76	-	(Brewer, 2012)
	500	Fast	1.78	-	
	760	Gasification	2.06	-	
Corn Stover	500	15 (Slow)	1.54		
	500	Fast	1.85		
	730	Gasification	1.92		
Hardwood	500	15 (Slow)	1.60		
Bamboo char	500	10 (Slow)	1.74	0.05	(Hernandez- menaetal., 2014)
Willow char	410- 480	30	-	0.15-0.18	(Mayer et al. 2013)

Particle densities of biochars are around 1.5 g cm^{-3} to 2.06 g cm^{-3} which are significantly lower than that of graphite (2.25 g cm^{-3}) because of the high porosity of biochar. As the final temperature increases, the biochar decreases in density due to the development of pore structure for the same feedstock. Minerals present in the original biomass impacts density, particle density can drastically increase as minerals are denser than most forms of carbon (Brewer, 2012).

2.4.3 Char particle structure and surface topography

Surface morphology (surface geometry, structural differences and pore development) of biochar strongly influences the adsorptive capability of biochar. As an example, activated carbon with micropores (<2 nm diameter) has high surface area and therefore can be used as an adsorbent for gases and solvents of small diameter molecules. Specific adsorption applications can be identified for those with mesopores (2-50nm diameter) and macropores (>50nm diameter) as shown in table 2-6 (Wildman et al., 1991).

Table 2-6 Pore Categories (Wildman et al. 1991; Lehmann and Joseph 2010)

Category	Pore diameter	Surface area (m^2g^{-1})	Volume (cm^3g^{-1})	Adsorption Application
Microspores	<2nm	750-1360	0.2-0.5	Molecules of small dimensions (Gases, common solvents)
Mesopores	2-50nm	138-750	0.5-0.6	Adsorption of larger molecules
Macropores	>50nm	51-138	0.6-1	Serve as feeder pores for the transport of adsorbate molecules.

A scanning electron microscope (SEM) image which shows macroporous structure of a wood biochar produced by slow pyrolysis is shown in figure 2-5. The biochar sample has been chromium coated and imaged with a beam energy of 20kV on a FEI Quanta 200 SEM (Downie, 2011).

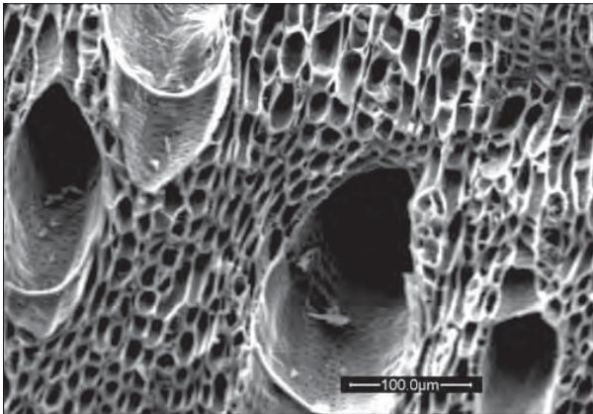


Figure 2-5 SEM image of wood biochar produced by slow pyrolysis (Downie, 2011).

This SEM image shows that wood biochar consists of pores with different sizes and shapes illustrating the heterogeneity of the chars. The porosity of biochar is high because the volatile matter is released during the carbonization of biomass creating pores, cracks and holes on the biochar surface (Özçimen and Ersoy-Meriçboyu, 2010). The cell cavities can have 100 nm diameters to over 150 μm diameter, depending on the structure and handling of the original biomass (Wildman et al., 1991). The pore structure also changes according to the starting biomass. The pore structures of biochar samples prepared from different woods ranging from primitive to hardwood examined by SEM illustrate macroporosity is associated with the original botanical structure and cell cavities (Wildman et al., 1991). Lee et al. (2013) explained that the large longitudinal pores which

can be seen in SEM images of biochar obtained from bagasse, is originated from the vascular structure of the raw biomass (Lee et al., 2013). The study analyzed six types of biochar using SEM as shown in figure 2-6.

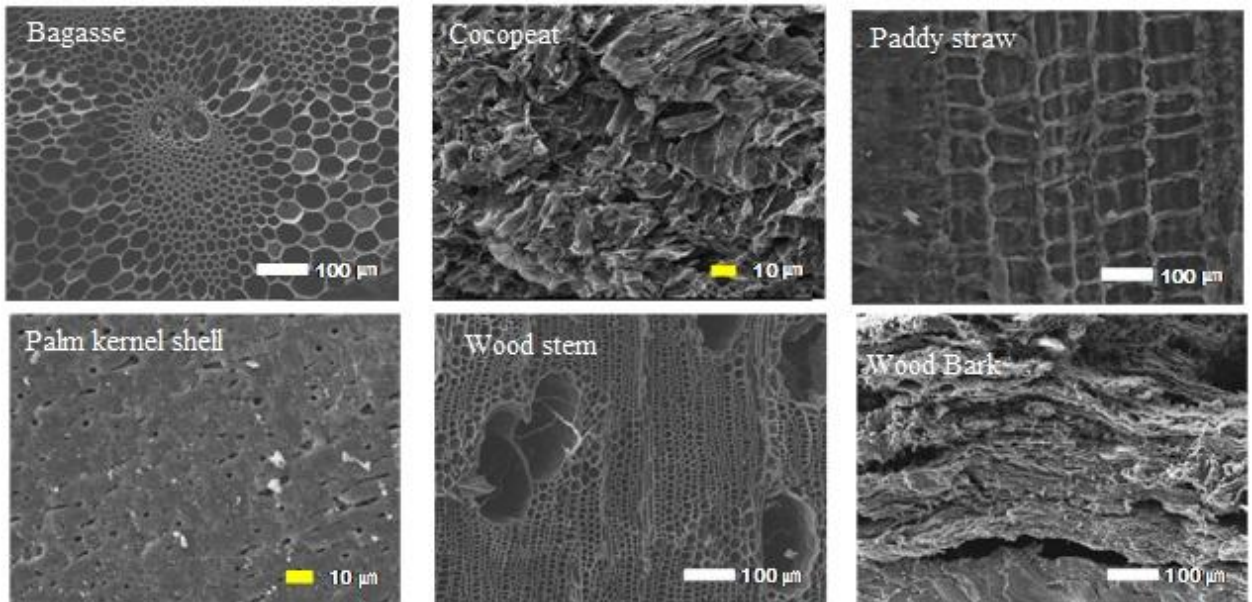


Figure 2-6 SEM images of biochar obtained at 500 °C (Lee et al., 2013)

These biochar samples (figure 2-6) show completely different surface geometry and a pore development. Wood bark char has the most irregular surface structure compared to others; biochar of paddy straw shows a structure of thin-walled plates, cocopeat biochar shows some deep fractures without pores on it, and the biochar of palm kernel shell exhibits dense and compact structure with a few small pores.

According to SEM illustrations, the original plant structure is visible in all of the chars while increased porosity from volatiles escaping during pyrolysis process can also be seen.

2.4.4 Moisture, ash, volatile matter, and fixed carbon content

Quantifying the amount moisture, ash, volatiles and fixed carbon in biochar is done by thermo gravimetric analysis (TGA). Table 2-7 summarizes the results of several studies done using different TGA analyses for biochar.

Table 2-7 Proximity Analysis using TGA studied in some of the literature

Biochar	Moisture % (w/w)	Ash% (w/w)	Volatile matter% (w/w)	Fixed Carbon% (w/w)	Reference
Cottonseed Hull Chars	5.3-9.92	3.1-9.2	11.42-69.3	22.3-70.3	(Uchimiya et al., 2011)
corn straws		5.02			(Song et al., 2014)
Switch grass	0.9-2.7	52.5- 54.6	7.1-17.4	26.4-39.5	(Brewer, 2012)
Corn Stover	1-1.8	32.4- 49.7	11.1-14.9	34.4-54.7	(Brewer, 2012)
Hardwood	2.6	13.9	19.7	63.8	(Brewer, 2012)
Bamboo char	6.5	3.9	8.1	81.5	(Hernandez-menaet al., 2014)
Bagasse	1.3	8.57	9.17	80.97	(Lee et al., 2013)
Cocopeat	2.55	15.9	14.3	67.25	(Lee et al., 2013)

Biochar	Moisture % (w/w)	Ash% (w/w)	Volatile matter% (w/w)	Fixed Carbon% (w/w)	Reference
Paddy straw	2.07	52.37	6.46	39.10	(Lee et al., 2013)
Palm kernel shell	0	6.86	12.29	80.85	(Lee et al., 2013)
Wood stem	1.46	2.28	12.79	83.47	(Lee et al., 2013)
Wood bark	0.36	12.84	18.14	68.66	(Lee et al., 2013)

During the carbonization process, biochar is subjected to a decrease in volatile matter and an increase in fixed carbon content and ash content. The ash content of biochar samples depends on the mineral content (Özçimen and Ersoy-Meriçboyu 2010). Therefore switch grass and paddy straw should contain high mineral content compared to other biochar. Bamboo char, palm kernel, wood stem have the highest fixed carbon content and show very low moisture content. Biochars with high moisture content have low carbon content compared to bamboo char, palm kernel, wood stem.

2.4.5 Elemental composition

The composition of carbon, hydrogen, nitrogen, and sulphur are determined using an elemental analyzer. Elemental composition (CHNSO) can be determined by dry combustion using a CHNSO analyser where O% is calculated by difference. CHNSO test results of some biochar are shown in table 2-8.

Table 2-8 CHNSO Analysis in some biochar found in literature

Biochar	C % (w/w)	H % (w/w)	N %(w/w)	S %(w/w)	O % (w/w)	Reference
Wood biochar	83.16	3.24	0.4	0.47	7.24	(Zhang et al., 2014)
Rice husk	51.06	2.6	0.66	0.22	17.62	(Zhang et al., 2014)
Poplar char	75.5-75.8	3.6-4.2	10-11		13-15.2	(Pereira et al., 2011)
Pine char	76.7-84.7	3.5-4.6	0.6		7.1-14.5	(Pereira et al., 2011)
Willow Char	66.2-79.1	3.5	1.5-1.7		8.2-23.1	(Pereira et al., 2011)
Willow Char	85.2	2.44	1.28		11.07	(Mayer et al., 2013)
corn straws	85.3	1.75	0.8	2.01	5.16	(Song et al., 2014)
Switch grass	39.4-38.7	1.3-2.5	0.7-0.6	0.002- 0.21		(Brewer, 2012)
Corn Stover	37.8-62.8	2.5-2.9	0.8-1.3	0.05- 0.06		(Brewer, 2012)
Hardwood	65.3	2.6	0.6	0.05		(Brewer, 2012)
Bamboo char	82.1	2.72	0.54	0.00116	14.6	(Hernandez-menaet al., 2014)

Biochar	C % (w/w)	H % (w/w)	N %(w/w)	S %(w/w)	O % (w/w)	Reference
Bamboo char	83.29	3.08	0.4	0.35	11.56	(Zhang et al., 2014)
Bagasse	85.59	2.82	1.11		10.48	(Lee et al., 2013)
Cocopeat	84.44	2.88	1.02		11.67	(Lee et al., 2013)
Paddy straw	86.28	3.12	3.25		7.35	(Lee et al., 2013)
Palm kernel shell	87.85	2.91	1.11		8.14	(Lee et al., 2013)
Wood stem	89.31	2.57	0.78		7.34	(Lee et al., 2013)
Wood bark	84.84	3.13	1.83		10.20	(Lee et al., 2013)

According to table 2-8, biochar is highly carbonaceous, with carbon contents above 80% in most cases. During the pyrolysis of biomass, O: C ratio and H: C ratio decrease as oxygen and hydrogen are removed as O and H containing volatiles. Then the char oxidize in the environment and gain oxygen containing surface functional groups, increasing the O/C ratio (Brewer, 2012). Results of elemental analysis can be used to estimate the aromaticity (H: C) and polarity (O: C, (O+N): C which are indicators of degree of graphitization and the functional groups present on the biochar (Uchimiya et al., 2011). Rice husk char shows high O: C content which suggests oxygen containing functional

groups on the biochar surface. Elemental analysis of poplar char shows high amount of nitrogen containing functional groups on the poplar char surface. Wood biochar, rice husk char, corn straws char, and bamboo char have functional groups containing oxygen, nitrogen, and sulphur. Low ratios of H: C of most of the wood biochar shows high aromaticity of biochar structure.

2.4.6 Functional groups/ Surface functionality

Fourier transform infrared spectroscopy (FTIR) is frequently used to identify and qualitatively determine functional groups in biochar samples (Brewer, 2012). Generally carbon adsorbents are considered as non-polar and therefore adsorb selectively non-polar compounds, but if the biochar surface consists of functional groups with polar substances such as oxygen, unique adsorptive properties can be recognized (Pastor-Villegas et al., 2007). Surface functionality can be observed using FTIR spectrophotometer.

Figure 2-7 shows the results of a FTIR analysis for two different commercial wood char originating from holm-oak wood (EnC) and eucalyptus wood (EuHC) (Pastor-Villegas et al., 2007).

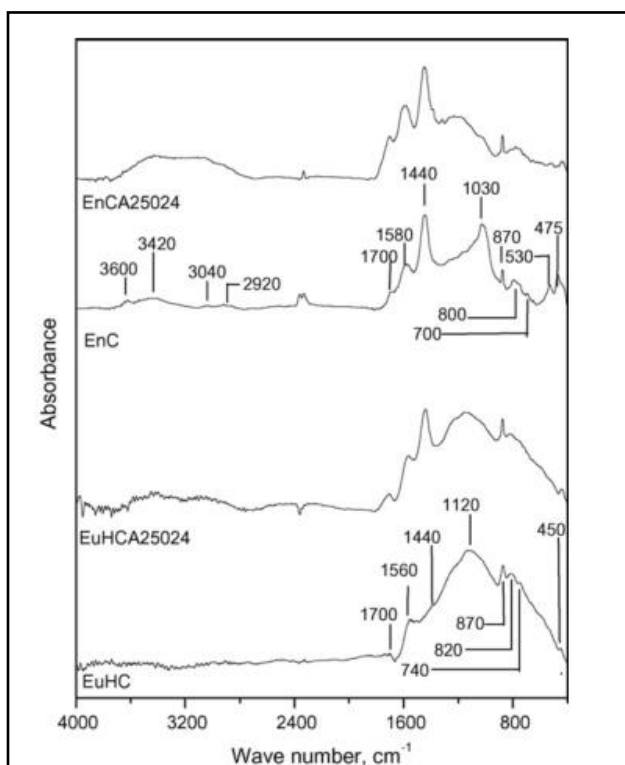


Figure 2-7 FTIR spectra for holm-oak wood char (EnC) and ceucalyptus wood char (EuHC) (Pastor-Villegas et al., 2007)

The FTIR spectra in figure 2-7 revealed O–H bonds, aromatic C–H groups, aliphatic C–H bonds, aromatic C–H groups, and asymmetric vibrations of CH₂ groups in biochar. Some of the bonding groups and structures according to their wave numbers of adsorption are listed in table 2-9.

Table 2-9 Bonding groups and structures according to the wave number (Fu et al. 2009)

Wave number (cm ⁻¹)	Infrared absorption	Atomic groups and structures
3200-3700	O-H stretching	Hydroxyl
2800-3000	C-H stretching	Aliphatic structures
1650-1770	C=O stretching	Carbonyl
1610-1680	C=C stretching	Olefinic structures
1450-1600	C=C stretching	Aromatic structures
1420-1480	C-H bending	Aliphatic structures
1360-1430	O-H and C-H bending	Hydroxyl, acid, phenol, olefins, methyl
1200-1300	C-O stretching	Unsaturated ethers
1000-1200	C-H out-of-plane bending	Aromatic structures
1000-1160	C-O stretching	Saturated ethers
1050-1160	C-O stretching	Tertiary hydroxyl
1070-1120	C-O stretching	Secondary hydroxyl
1000-1060	C-O stretching	Primary hydroxyl
625-1000	C-H out-of-plane bending	Olefinic and aromatic structures

Starting biomass and biochar samples produced from apricot stone, hazelnut shell, grape seed and chestnut shell have been analysed using FTIR spectra and recorded in the transmission mode between 4000 and 650 cm^{-1} . The functional groups which were identified from the FTIR spectrum of the biochar samples are given in table 2-10.

Table 2-10 Functional groups of biochar samples determined by the FTIR analysis (Özçimen and Ersoy-Meriçboyu, 2010)

Wave numbers (cm^{-1})	Functional groups
Hazelnut shell biochar	
3387	-OH stretching
1577	Aromatic C=C ring stretching
1373	Aliphatic CH ₃ deformation
1137	Aromatic CO- stretching
1021	Aliphatic ether C-O and alcohol C-O stretching
869	1 adjacent H deformation
794	2 adjacent H deformation
738	4 adjacent H deformation
Apricot stone biochar	
2972	Aliphatic CH stretching
1582	Aromatic C=C ring stretching

Wave numbers (cm ⁻¹)	Functional groups
Apricot stone biochar	
1393	Aliphatic CH ₃ deformation
1233	Aromatic CO– stretching
1112	Aromatic CO– stretching
1069	Aliphatic ether C–O and alcohol C–O stretching
859	1 adjacent H deformation
791	2 adjacent H deformation
730	4 adjacent H deformation
Grape seed biochar	
2977	Aliphatic CH stretching
2896	Aliphatic CH stretching
2587	Aromatic C=C ring stretching
1421	Aromatic C=C ring stretching
1074	Aliphatic ether C–O and alcohol C–O stretching
872	1 adjacent H deformation
Chestnut shell biochar	
2891	Aliphatic CH stretching
1582	Aromatic C=C ring stretching
1416	Aromatic C=C ring stretching
1160	Aromatic CO– stretching

Wave numbers (cm ⁻¹)	Functional groups
Apricot stone biochar	
872	1 adjacent H deformation
809	2 adjacent H deformation
725	4 adjacent H deformation

Biomass samples did not show peaks corresponding to an aromatic C-H stretching vibration which indicates that there is no adjacent aromatic hydrogen in biochar samples. Hazel nut char showed OH bonds and more O containing groups compared to other biochar. With increasing pyrolysis temperature, biochar samples show more aromatic and carbonaceous properties and loss of hydroxyl, aliphatic C-H, carbonyl, and olefinic C=C groups (Fu et al., 2009).

2.4.7 Crystalline structure and mineralogical composition

X-ray diffraction (XRD) method is performed to observe the crystalline structure and mineralogical composition of biochar. Abdulrazzaq et al.(2014) obtained X-ray diffraction profiles of empty fruit bunches biochar produced from slow pyrolysis, wood biochar of kilning mangrove wood logs produced from gasification, and rice husk biochar (RHB) produced from gasification. The results of slow pyrolysed biochar illustrate peak spacing at 6.560Å and 5.007 Å which represents crystallographic planes. Biochar from gasification rises to peak 2.08 Å, as it consists of graphene sheets within turbostratic carbon crystallites (Abdulrazzaq et al., 2014). The X-ray diffraction pattern of woody

biomass fly ash has showed that it consists crystalline phases such as lime, calcite, and quartz (Berra et al., 2011).

XRD technique has also been used in analysis of mineralogical composition of biochars. Studies have shown that RHB mainly consists of amorphous (noncrystalline) silica. The relevant XRD pattern is shown in figure 2-8.

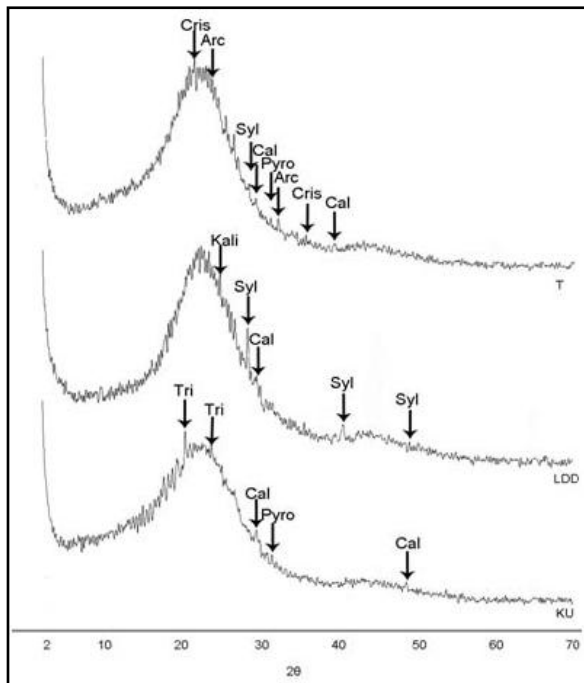


Figure 2-8 XRD Patterns of three types of Rice Husk Biochar (Arc=Archerite, Cal=Calcite, Cris=Cristobalite, Kali = Kalcinite, Pyro=Pyrocoprite, Syl=Sylvite, Tri=Tridymite) (Prakongkep et al., 2013).

Biochar from pistachio shells showed the presence of some mineral crystals, such as halite (NaCl) and kalcinite (KHCO_3) (Komnitsas et al., 2014). Kalcinite, which is a

highly soluble mineral phase, improves the quality of biochar and when biochar is used as an adsorbent, K can be exchanged with divalent ions (Komnitsas et al., 2014). A pine bark char sample showed the presence of quartz (SiO_2) and anorthite ($\text{CaAl}_2\text{Si}_2\text{O}_8$) and biochar samples derived from oat hull and canola straw showed low intensity peaks associated to sylvite (KCl) (González et al., 2013).

XRD reveals important structural properties and mineral composition of biochar. Many biochars showed similar broad XRD peak centred at 2θ - 22.5° which can be recognized as amorphous carbon as well as disordered cristobalite (Prakongkep et al. 2013; Liou 2004). In XRD patterns of biochar subjected to high charring temperature, intense peaks can be observed due to the increasing concentration of minerals and loss of organic compounds (González et al., 2013). However, broad peaks were observed in most of the biochar XRD patterns in past studies, indicating low degree of crystalline structure.

2.5 Conclusion

Biochar is a feasible and economical solution in waste water treatment since it can be produced using materials generated as by products from other processes. The characteristics of biochar discussed in past studies and adsorption capacities obtained, show that it has a potential to remove a number of aqueous pollutants. Most of the biochar has shown a high adsorption capacity in temperatures above room temperature and in low pH. Physical, chemical and thermal properties of biochar strongly depend on the composition and structure of starting biomass and pyrolysis conditions such as heating rate, residence time and final temperature. These variations have been studied in literature

88

using characterisation techniques such as BET, TGA, SEM, FTIR and XRD analysis. Characterisation of different biochar produced from plants and woody biomass were discussed in this paper. Some exhibit favourable adsorptive properties such as high surface area, high porosity and surface functional groups which induce adhesive properties depending on production conditions. Therefore, biochar adsorbents produced from waste streams would be an economical and a green solution for waste water treatment which requires further researches and proper engineering designs in order to be applied in modern industry.

2.6 Bibliography –Chapter 2

Abdulrazzaq, H., Jol, H., Husni, A. and Abu-bakr, R. (2014) ‘Characterization and Stabilisation of Biochars Obtained from Empty Fruit Bunch, Wood, and Rice Husk’, 9(2003), pp. 2888–2898.

Ahmad, M., Moon, D. H., Vithanage, M., Koutsospyros, A., Lee, S. S., Yang, J. E., Lee, S. E., Jeon, C. and Ok, Y. S. (2014) ‘Production and use of biochar from buffalo-weed (*Ambrosia trifida* L.) for trichloroethylene removal from water’, *Journal of Chemical Technology and Biotechnology*, 89(1), pp. 150–157. doi: 10.1002/jctb.4157.

Ahmad, M., Rajapaksha, A. U., Lim, J. E., Zhang, M., Bolan, N., Mohan, D., Vithanage, M., Lee, S. S. and Ok, Y. S. (2014) ‘Biochar as a sorbent for contaminant management in soil and water: a review.’, *Chemosphere*. Elsevier Ltd, 99, pp. 19–33. doi: 10.1016/j.chemosphere.2013.10.071.

Attila, B., Krisztina, L. and Lajos, N. (1996) ‘Adsorbents from Waste Materials’, 91, pp. 81–91.

Berra, M., Casa, G. De, Orso, M. D., Galeotti, L., Mangialardi, T., Paolini, A. E. and Piga, L. (2011) ‘Recycling of Biomass Ashes.’ Edited by H. Insam and B. A. Knapp. Berlin, Heidelberg: Springer Berlin Heidelberg, pp. 133–146. doi: 10.1007/978-3-642-19354-5.

Bolan, N. S., Thangarajan, R., Seshadri, B., Jena, U., Das, K. C., Wang, H. and Naidu, R. (2013) ‘Landfills as a biorefinery to produce biomass and capture biogas’, *Bioresource Technology*. Elsevier Ltd, 135, pp. 578–587. doi: 10.1016/j.biortech.2012.08.135.

Braida, W. J., Pignatello, J. J., Lu, Y., Ravikovitch, P. I., Neimark, A. V and Xing, B. (2003) ‘Sorption hysteresis of benzene in charcoal particles.’, *Environmental science & technology*, 37(2), pp. 409–17. Available at: <http://www.ncbi.nlm.nih.gov/pubmed/12564916>.

Brewer, C. E. (2012) ‘Biochar characterization and engineering.’

Brown, R. a., Kercher, A. K., Nguyen, T. H., Nagle, D. C. and Ball, W. P. (2006) ‘Production and characterization of synthetic wood chars for use as surrogates for natural sorbents’, *Organic Geochemistry*, 37(3), pp. 321–333. doi: 10.1016/j.orggeochem.2005.10.008.

Brunner, P. H. and Roberts, P. V (1980) ‘The Significance of Heating Rate on Char Yield and Char Properties in the Pyrolysis of Cellulose’, 18.

Byrne, C. and Nagle, D. (1996) 'Carbonization of Wood for Advanced Materials.', 35(2), pp. 259–266.

Chen, X., Chen, G., Chen, L., Chen, Y., Lehmann, J., McBride, M. B. and Hay, A. G. (2011) 'Adsorption of copper and zinc by biochars produced from pyrolysis of hardwood and corn straw in aqueous solution', *Bioresource Technology*, 102(19), pp. 8877–8884. doi: 10.1016/j.biortech.2011.06.078.

Downie, A. (2011) 'Biochar Production and Use: Environmental Risks and Rewards.'

Duku, M. H., Gu, S. and Hagan, E. Ben (2011) 'Biochar production potential in Ghana - A review', *Renewable and Sustainable Energy Reviews*, 15, pp. 3539–3551. doi: 10.1016/j.rser.2011.05.010.

EPA (2013) 'Biochar Research at Western Ecology Division.'

Fu, P., Hu, S., Sun, L., Xiang, J., Yang, T., Zhang, A. and Zhang, J. (2009) 'Structural evolution of maize stalk/char particles during pyrolysis.', *Bioresource technology*. Elsevier Ltd, 100(20), pp. 4877–83. doi: 10.1016/j.biortech.2009.05.009.

González, M. E., Cea, M., Sangaletti, N., González, a., Toro, C., Diez, M. C., Moreno, N., Querol, X. and Navia, R. (2013) 'Biochar Derived from Agricultural and Forestry Residual Biomass: Characterization and Potential Application for Enzymes Immobilization', *Journal of Biobased Materials and Bioenergy*, 7(6), pp. 724–732. doi: 10.1166/jbmb.2013.1373.

Herbert, L., Hosek, I., Kripalani, R. and Vanasupa, A. L. (2012) 'The Characterization and Comparison of Biochar Produced From a Decentralized Reactor Using Forced Air and Natural Draft Pyrolysis', (June).

Hernandez-mena, L., Pécora, A. A. B. and Beraldo, A. L. (2014) 'Slow Pyrolysis of Bamboo Biomass: Analysis of Biochar Properties', 37, pp. 115–120. doi: 10.3303/CET1437020.

Khare, P., Dilshad, U., Rout, P. K., Yadav, V. and Jain, S. (2013) 'Plant refuses driven biochar: Application as metal adsorbent from acidic solutions', *Arabian Journal of Chemistry*. King Saud University. doi: 10.1016/j.arabjc.2013.11.047.

Knaebel, K. S. (2004) 'Adsorbant Selection', *Adsorption Research Inc*.

Komnitsas, K., Zaharaki, D., Pylotis, I., Vamvuka, D. and Bartzas, G. (2014) 'Assessment of pistachio shell biochar quality and its potential for adsorption of heavy metals', pp. 1–12.

Lee, Y., Park, J., Ryu, C., Gang, K. S., Yang, W., Park, Y.-K., Jung, J. and Hyun, S. (2013) 'Comparison of biochar properties from biomass residues produced by slow pyrolysis at 500°C.', *Bioresource technology*. Elsevier Ltd, 148, pp. 196–201. doi: 10.1016/j.biortech.2013.08.135.

Lehmann, J. and Joseph, S. (2010) *Biochar for Environmental Management*.

Liou, T.-H. (2004) 'Preparation and characterization of nano-structured silica from rice husk', *Materials Science and Engineering: A*, 364(1-2), pp. 313–323. doi: 10.1016/j.msea.2003.08.045.

Maschio, G., Koufopoulos, C. and Lucchesi, a. (1992) 'Pyrolysis, a promising route for biomass utilization', *Bioresource Technology*, 42, pp. 219–231. doi: 10.1016/0960-8524(92)90025-S.

Mayer, Z., Eltom, Y., Stennett, D., Schr, E. and Apfelbacher, A. (2013) 'Characterization of Engineered Biochar for Soil Management', 33(2). doi: 10.1002/ep.

Mitchell, S. M., Subbiah, M., Ullman, J. L., Frear, C. and Call, D. R. (2015) 'Journal of Environmental Chemical Engineering Evaluation of 27 different biochars for potential sequestration of antibiotic residues in food animal production environments', *Biochemical Pharmacology*. Elsevier B.V., 3(1), pp. 162–169. doi: 10.1016/j.jece.2014.11.012.

Namasivayam, C. and Sangeetha, D. (2008) 'Application of coconut coir pith for the removal of sulfate and other anions from water', *Desalination*, 219(1-3), pp. 1–13. doi: 10.1016/j.desal.2007.03.008.

Namasivayam, C., Sangeetha, D. and Gunasekaran, R. (2007) 'Removal of anions, heavy metals, organics and dyes from water by adsorption onto a new activated carbon from *Jatropha* husk, an agro-industrial solid waste', *Process Safety and Environmental Protection*, 85(B2), pp. 181–184. doi: 10.1205/psep05002.

Özçimen, D. and Ersoy-Meriçboyu, A. (2010) 'Characterization of biochar and bio-oil samples obtained from carbonization of various biomass materials', *Renewable Energy*, 35(6), pp. 1319–1324. doi: 10.1016/j.renene.2009.11.042.

Pandey, A., Larroche, C., Ricke, S., Dussap, C.-G. and Gnansounou, E. (2011) *Biofuels : alternative feedstocks and conversion processes*.

Pastor-Villegas, J., Meneses Rodríguez, J. M., Pastor-Valle, J. F. and García García, M. (2007) 'Changes in commercial wood charcoals by thermal treatments', *Journal of Analytical and Applied Pyrolysis*, 80(2), pp. 507–514. doi: 10.1016/j.jaap.2007.05.001.

Pastor-Villegas, J., Pastor-Valle, J. F., Rodríguez, J. M. M. and García, M. G. (2006) 'Study of commercial wood charcoals for the preparation of carbon adsorbents', *Journal of Analytical and Applied Pyrolysis*, 76(1-2), pp. 103–108. doi: 10.1016/j.jaap.2005.08.002.

Pereira, C., Kaal, J., Camps Arbostain, M., Pardo Lorenzo, R., Aitkenhead, W., Hedley, M., Macías, F., Hindmarsh, J. and Maciá-Agulló, J. a. (2011) 'Contribution to characterisation of biochar to estimate the labile fraction of carbon', *Organic Geochemistry*. Elsevier Ltd, 42(11), pp. 1331–1342. doi: 10.1016/j.orggeochem.2011.09.002.

Prakongkep, N., Gilkes, R. J., Wiriyakitnateekul, W. and Duangchan, A. (2013) 'The Effects of Pyrolysis Conditions on the Chemical and Physical Properties of Rice Husk Biochar', 3(3), pp. 97–103.

Rahman, M. A., Asadullah, M., Haque, M. M., Motin, M. A., Sultan, M. B. and Azad, M. A. K. (2006) 'Preparation and Characterization of Activated Charcoal as an Adsorbent', 22(3), pp. 133–140.

Rouquerol, F. (1999) *Adsorption by Powders and Porous Solids*. San Diego: Academic Press, San Diego.

Song, Z., Lian, F., Yu, Z., Zhu, L., Xing, B. and Qiu, W. (2014) 'Synthesis and characterization of a novel MnOx-loaded biochar and its adsorption properties for Cu²⁺ in aqueous solution', *Chemical Engineering Journal*. Elsevier B.V., 242, pp. 36–42. doi: 10.1016/j.cej.2013.12.061.

Sun, L., Wan, S. and Luo, W. (2013) 'Biochars prepared from anaerobic digestion residue, palm bark, and eucalyptus for adsorption of cationic methylene blue dye: Characterization, equilibrium, and kinetic studies', *Bioresource Technology*. Elsevier Ltd, 140, pp. 406–413. doi: 10.1016/j.biortech.2013.04.116.

Uchimiya, M., Wartelle, L. H., Klasson, K. T., Fortier, C. a and Lima, I. M. (2011) 'Influence of pyrolysis temperature on biochar property and function as a heavy metal sorbent in soil.', *Journal of agricultural and food chemistry*, 59(6), pp. 2501–10. doi: 10.1021/jf104206c.

Wildman, J., Speakman, S., Street, G. and Zhe, L. W. N. (1991) 'Origins and functions of macroporosity activated carbons from coal and wood precursors', 70, pp. 655–661.

Xue, Y., Gao, B., Yao, Y., Inyang, M., Zhang, M., Zimmerman, A. R. and Ro, K. S. (2012) 'Hydrogen peroxide modification enhances the ability of biochar (hydrochar) produced from hydrothermal carbonization of peanut hull to remove aqueous heavy

metals: Batch and column tests', *Chemical Engineering Journal*. Elsevier B.V., 200-202, pp. 673–680. doi: 10.1016/j.cej.2012.06.116.

Yang, Y., Lin, X., Wei, B., Zhao, Y. and Wang, J. (2013) 'Evaluation of adsorption potential of bamboo biochar for metal-complex dye: equilibrium, kinetics and artificial neural network modeling', *International Journal of Environmental Science and Technology*, 11(4), pp. 1093–1100. doi: 10.1007/s13762-013-0306-0.

Yao, Y., Gao, B., Inyang, M., Zimmerman, A. R., Cao, X., Pullammanappallil, P. and Yang, L. (2011) 'Removal of phosphate from aqueous solution by biochar derived from anaerobically digested sugar beet tailings', *Journal of Hazardous Materials*. Elsevier B.V., 190(1-3), pp. 501–507. doi: 10.1016/j.jhazmat.2011.03.083.

Zhang, J., Lü, F., Luo, C., Shao, L. and He, P. (2014) 'Humification characterization of biochar and its potential as a composting amendment', *Journal of Environmental Sciences*. The Research Centre for Eco-Environmental Sciences, Chinese Academy of Sciences, 26(2), pp. 390–397. doi: 10.1016/S1001-0742(13)60421-0.

Chapter 3. Biochar Characterization Results and Discussion

Yashodha G. Marambage, Kelly A. Hawboldt

Faculty of Engineering and Applied Science, Memorial University of Newfoundland,

St. John's, NL, Canada. A1B3X5

Abstract

Biochar samples produced through fast pyrolysis of bark, hardwood sawdust, and softwood sawdust were characterized through a series of tests. Physical properties such as surface area, porosity, total pore volume, pore width and surface morphology of biochar were investigated using BET-N₂ analysis and SEM analysis. Density and pH of the biochar samples were determined using laboratory experiments. Carbon content and ash content were determined by TGA analysis. C, H, N, S content were determined by elemental analysis, ATR-FTIR analysis and XRD analysis were performed to find out functional groups and mineralogical composition respectively. Hardwood char samples at 450 °C showed the highest BET surface area (43.23m²/g) and the highest pore volume (0.003161 cm³/ g). SEM images of biochar revealed a highly heterogeneous structure with small cracks and pores. Bulk density of the biochar samples was 0.3 g/cm³. All biochar samples showed alkaline pH. TGA results showed that softwood char has the highest moisture content, highest unburned carbon content and lowest ash content compared to bark and hardwood char. Elemental analysis showed that the biochar samples have H: C ratio of 0.05 which is a result of a carbonaceous, graphite- like structure. Functional groups in biochar structure were observed using FTIR analysis and

XRD analysis which demonstrated that the biochar samples have less crystalline structures and they have mineral compounds mainly kalicinite, chloromagnesite, calcite and quartz.

3.1 Introduction

Physical, chemical and thermal properties determine the potential of biochar as an adsorbent in water treatment. During the pyrolysis process, biomass undergoes complex chemical reactions, causing significant heterogeneity in the resulting biochar to the microscopic scale, even within the same biochar sample (Lehmann and Joseph, 2010). Therefore, the specific properties influencing adsorption capacity of biochar is obtained by a series of standard characterisation techniques. This study focuses on the biochar produced using wood residues from forestry industry. Wood char is a porous carbon material with a heterogeneous surface and can be used as an adsorbent because of its disorganized pore structure and the presence of functional groups (Pastor-Villegas et al., 2007). Treating wastewater using biochar sourced from wood waste is a two-fold solution to environmental problems as it reduces the volume of the wastes.

3.2 Materials and methods

Biochar were obtained from three different biomass (bark, softwood saw dust, and hardwood saw dust) from wood residues. Feedstock particle size was less than 2 mm. All biochar samples were produced in a 2-4 kg/h auger pyrolysis reactor at a temperature of 450 °C with a residence time of 3 minutes. The intended product of this fast pyrolysis process was bio oil and biochar was generated as a by product with a yield of 15-17 %

(bio char generation rate wa 300-600 gh⁻¹). Biochar samples were crushed in the miller into fine particles and the moisture content of biochar samples was below 10%. Biochar samples were kept in the oven at 75 °C overnight before analysis.

The microscopic surface area and porous properties of biochar were measured by Micromeritics TriStar II Plus surface area and porosity analyzer in the Inco Innovation Center at Memorial University. Nitrogen gas was used resulting adsorption isotherms at 77 K. The samples were vacuum-degassed at 230°C overnight before the test.

Bulk density of biochar was calculated from the volume of a measuring cylinder filled with the biochar samples. The weight of an empty 100 mL measuring cylinder (m_1) was recorded and then it was closely packed with biochar (up to 100 mL mark) and the total weight (m_2) was measured. Bulk density was calculated as follows.

$$\text{Bulk density of biochar} = \frac{(m_2 - m_1)g}{100 \text{ cm}^3} \quad (3-1)$$

The morphology of biochar was analyzed by Scanning Electron Microscopy (SEM) using FEI MLA 650F in Micro Analysis Facility at Core Research Equipment & Instrument Training Network (CREAIT). Samples for SEM analysis were mounted on Carbon adhesive tabs of 12mm diameter which were put on Aluminium stubs. Carbon evaporator was used to coat transparent conductive carbon layer on samples to avoid the formation of electric charge on the surface during scanning.

The pH of biochar samples was measured using a biochar suspension with 1:20 ratio of biochar weight to deionised water weight(Lee et al., 2013). The mixture was kept in

shaker for 20 min at 180 rpm at room temperature to make it homogeneous. Resulting solution pH was measured using a calibrated digital pH meter.

TGA was performed using Thermo Gravimetric Analyzer (TGA Q500) at the Centre for Chemical Analysis, Research and Training (C-CART) at Memorial University. Samples were loaded on to a platinum pan and heated to 600°C at a ramping rate of 20°C/min under inert (N₂) atmosphere at 50 mL/min gas flow minimize oxidation. At 600°C, the gas inflow was switched into air input with 50 mL/min flow rate and the samples were combusted in air at the same ramping rate to measure the ash content. Elemental analysis (C, N, H, S, and O) was performed in G.G Hatch stable isotope laboratory in University of Ottawa. Samples were weighed into tin capsules and loaded with standards into a micro cube elemental analyser. Samples were flash combusted with oxygen at 1800°C and carried by helium through columns of reducing/oxidizing chemicals to get N₂, CO₂, H₂O and SO₂. The gases were trapped within an adsorption column, released separately and were detected by thermal conductivity detector.

ATR-FTIR analysis was done using Bruker Tensor 27 FTIR spectrometer at Centre for Chemical Analysis, Research and Training (C-CART) in Department of Chemistry, Memorial University. IR spectrum was obtained in the wavelength range of 4000 cm⁻¹ to 400 cm⁻¹. XRD analysis was carried out using the Rigaku Ultima IV X-ray diffractometer at the Earth Resources Research and Analysis Facility (TERRA) at Memorial University. X-ray diffraction patterns were obtained in 2θ scanning mode and Cu- K_α radiation (40 kV, 44 mA) with 0.1° step size inside 5°-100° range.

3.3 Results and discussion

3.3.1 N₂ adsorption isotherms, specific surface area, pore characteristics

N₂ adsorption isotherm plots obtained for all three samples are illustrated in Figure 3-1.

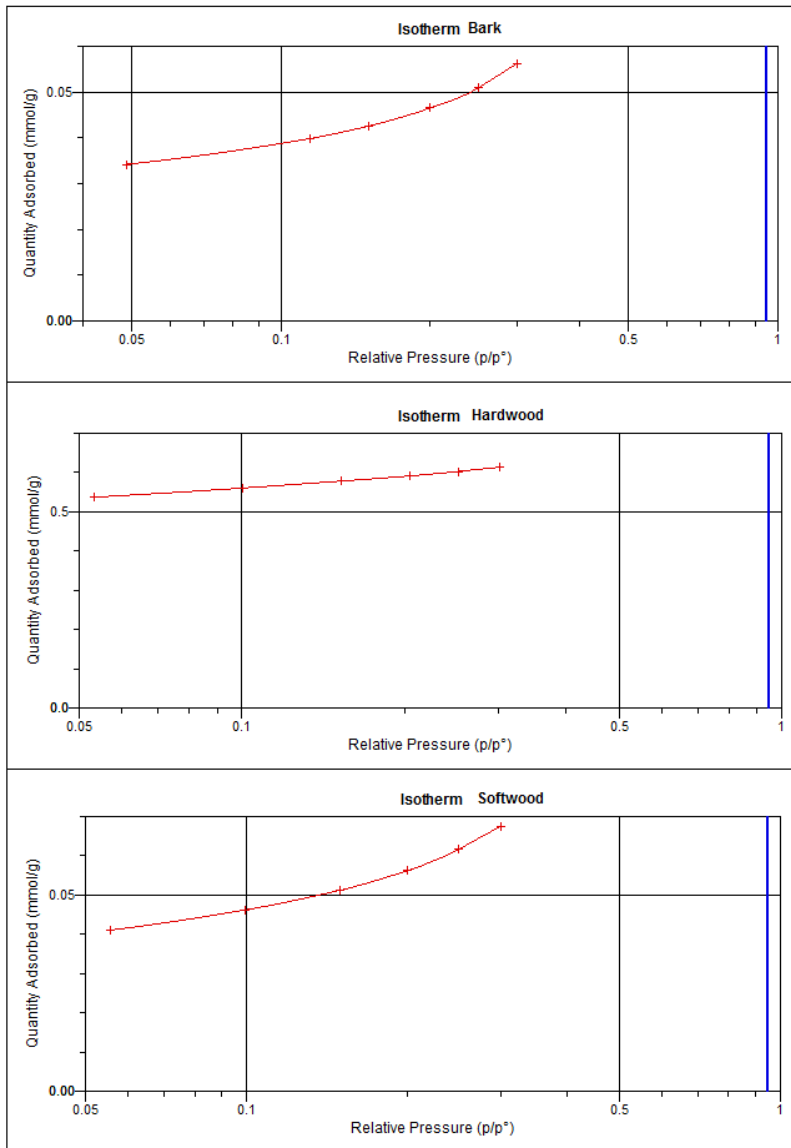


Figure 3-1 Comparison of BET- N₂ adsorption isotherms for bark, hardwood and softwood biochar

All isotherms are almost linear at the beginning and then convex to the p/p° axis at the end, and therefore can be identified as type II isotherms according to the IUPAC classification (Rouquerol et al., 1999). In a study done with eucalyptus wood biochar, type II isotherms have been observed and the density of surface groups is relatively high in biochars resulting in type II isotherms (Pastor-Villegas et al., 2007). Since all isotherms show high adsorption capacities at the elevated relative pressure, the biochar is mostly macroporous (Rouquerol et al., 1999). Macroporous biochars exhibit low surface areas (51-138 m^2/g) compared to the surface area of micro porous biochar (750-1360 m^2/g) (Lehmann and Joseph, 2010). Porosity and surface area characteristics of biochar samples are shown in table 3-1.

Table 3-1 Results of BET analysis

Sample	Specific surface area (m^2/g)		Total pore volume (cm^3/g)	Pore Width (nm)
	BET	Langmuir		
Bark	4.03	6.31	0.0014	2.12
Hardwood	43.23	61.80	0.0032	2.16
Softwood	4.78	7.75	0.0014	2.18

Hardwood shows the highest BET surface area and highest pore volume. Brown *et al.*, (2006) found that regardless of ramp rate, wood biochars produced at low final temperatures (450 °C), have surface areas of less than 10 m^2/g , and when the final temperature of pyrolysis process is in between 600–750°C surface areas increase to

400m²/g (Brown et al., 2006). The low surface areas obtained from the biochar samples can be a result of less microporosity as higher temperatures and longer retention times are required for the development of micropores (Lehmann and Joseph, 2010). In literature also, wood derived carbon are recognized as adsorbents with high proportions of macropores and mesopores, which serve as feeder pores for the transport of adsorbate molecules to microporous sites, and facilitate adsorption of larger molecules respectively (Wildman et al., 1991).

3.3.2 Biochar density

Bulk densities of biochar samples were obtained as 0.33g/cm³, 0.33g/cm³, and 0.30g/cm³ for bark char, hardwood char, and softwood char respectively. These values are close to the values found in literature for commercial wood char used as adsorbents; 0.37g/cm³ forholm-oak wood char, and 0.30 g/cm³ for eucalyptus wood char (Pastor-Villegas et al., 2006). The low bulk densities obtained for the biochar samples illustrate that the carbon samples are highly branched and porous with more void space (Sivakumar et al., 2012). For carbons used in gas adsorption, bulk density values range from 0.40 to 0.50 g/cm³ (Pastor-Villegas et al., 2006).

3.3.3 SEM analysis

According to the SEM images shown in figure 3-2, the structure of the biochar was found to be highly heterogeneous with very small amount of pores present on the surface of the biochar. Samples contain several tiny cracks and holes formed because of the release of volatile matter during carbonization (Özçimen and Ersoy-Meriçboyu, 2010).

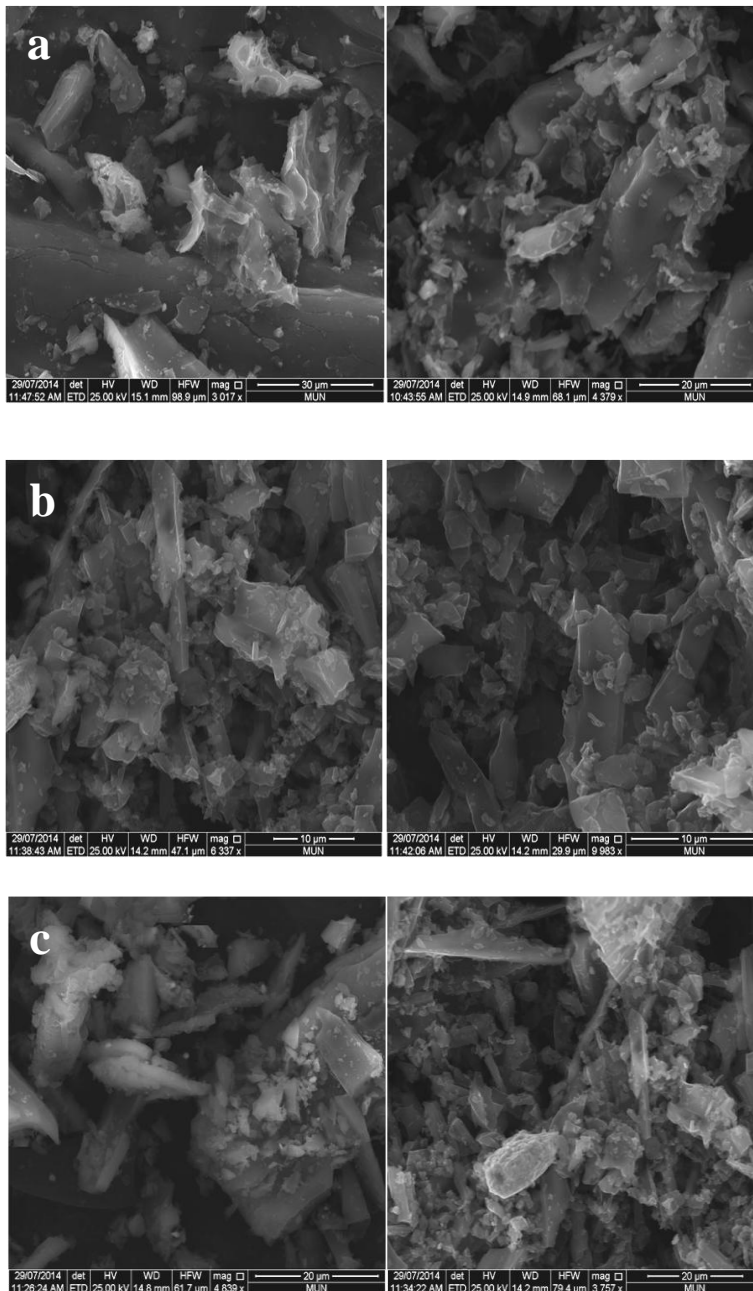


Figure 3-2 SEM images of biochar from (a) Bark, (b) Hardwood, (c) Softwood

Biochar structure becomes more porous and low in density with the release of volatile components during the carbonization. Low conductivity of wood is another reason for the

102

cracks, because during heat ramp up, the surface of wood is exposed to a higher temperature than the internal structure, generating an extreme tension during the pyrolysis process which can cause fractured surfaces (Byrne and Nagle, 1996). According to the SEM analysis, bark char shows more cracks and holes compared to hardwood and softwood char. Although large pores may not be directly related to the microscopic surface area or adsorption process, those can act as routes for adsorption process and provide a matrix on which smaller pores develop (Lee et al., 2013). However, all biochar samples analysed here exhibit an irregular surface with some cracks without showing any clue of the vascular structure of the raw biomass.

3.3.4 pH of biochar

pH of biochar samples were obtained as 9.0, 9.0, and 8.6 for bark char, hardwood char, and softwood char respectively. The pH of biochar depends on the feedstock type and the pyrolysis process conditions (Ahmad et al., 2014a). Bark char and hardwood char have the same pH while the softwood char is lower, but has not deviated largely from the other two. Similar results were obtained on different biochar which showed pH values in between 6.0 to 12 (Ahmad et al., 2014a). Biochar samples exhibit alkaline pH, which can be due to three factors; organic functional groups, carbonates, and inorganic alkalis present in biochar (Lee et al., 2013).

3.3.5 Thermo gravimetric analysis

The TGA plots for the weight percentage and the derivative weight percentage obtained with respect to temperature are shown in Figure 3-3.

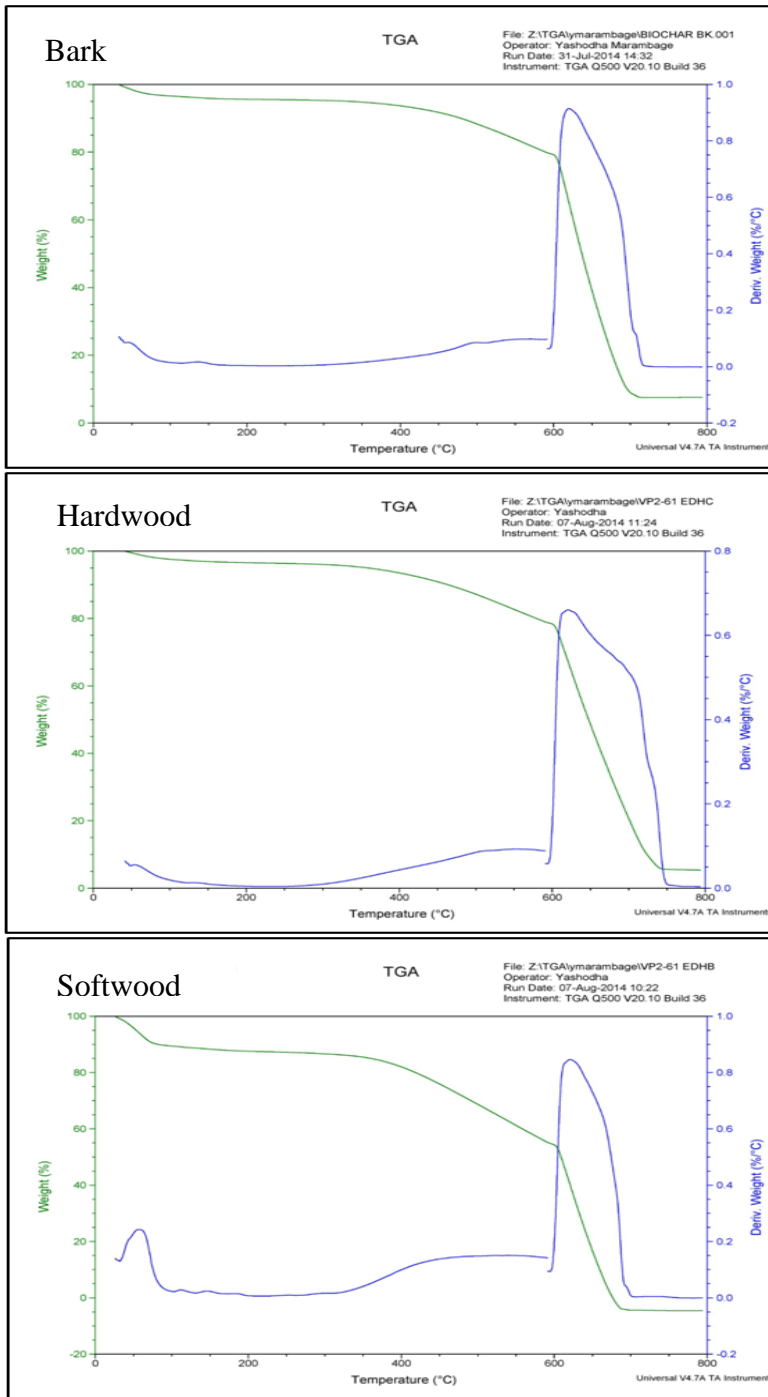


Figure 3-3 TGA plots for the weight percentage and the derivative weight percentage vs. temperature

Moisture content is the percentage of weight loss from the biochar at 110 °C (Harris et al., 2013). According to the above graphs, the moisture contents\ of bark, hardwood and softwood char samples are 4%, 3% and 11% respectively. The weight loss in the range of 300–500°C shows the percentage of volatile carbon (Insam and Knapp, 2011). Bark, hardwood and softwood char samples have volatile carbon content of 7%, 8%, and 17% respectively. In 250-400°C temperature range, there is no apparent weight loss in biochar samples, because at low temperatures, there can be a weight increase caused by catalyst oxidation, reducing the observable weight loss due to carbon oxidation (Aguado et al., 2013). The peak of the derivative of weight loss, just after 600°C represents the oxidation due to air flow on the sample. The oxidation is completed at 725°C and 750 °C for bark and hardwood respectively and the ash content are 12% and 6% respectively. Low ash content of softwood char indicates that the inorganic mineral in this biochar is low (Fang et al., 2014).

3.3.6 Elemental composition

The results of elemental analysis are shown in Table 3-2.

Table 3-2 Elemental analysis results of biochar and the comparison of ratios

Sample	C (wt %)	H (wt %)	O (wt %)	N (wt %)	S (wt %)	H:C ratio	O:C ratio	(O+N):C ratio
Bark	67.22	3.61	26.12	0.31	0.02	0.0537	0.388	0.393
Hardwood	72.79	3.70	18.77	0.28	0.01	0.0508	0.258	0.262
Softwood	71.90	4.31	20.82	0.21	0.00	0.0599	0.289	0.292

Elemental analysis associated ratios are often used to assess biochar production, where H:C and O:C ratios are used to measure the degree of aromaticity and maturation (Lehmann and Joseph, 2010). According to literature, cellulose and lignin have a H: C ratio of 1.5 and biochar formed at temperatures above 400 °C have H: C ratios less than 0.5 (Lehmann and Joseph, 2010). Decreasing H: C ratio and H: O ratio of wood biochar demonstrate the depolymerisation of biomass into smaller dissociation products of lignin and cellulose (Ahmad et al., 2014a). Low H:C ratio of hardwood reflects high levels of hydrogen removal which strongly depends on the final pyrolysis temperature (Brown et al., 2006). All biochar samples tested have H: C ratio around 0.05 where softwood has the highest ratio indicating low aromaticity and hardwood shows the lowest ratio indicating high aromaticity. Very low H: C ratios of all biochar samples shows that a few C is either directly bonded to H or connected through an OH group, indicating a more graphite-like structure (Lehmann and Joseph, 2010). Low O: C ratios relate to lower polarity of biochars derived, decrease of the surface hydrophobicity, which results in reduced affinity for water molecules. (Ahmad *et al.*, 2014; Fang *et al.*, 2014). High polarity indexes [(O +N)/C] cause biochar to have high hydrophobicity, and thus, surfaces will be covered with a layer of water in aqueous solutions (Fang et al., 2014). All biochar samples show favourable polarity index (O+N): C ratios indicating existence of polar-groups as adsorption sites.

3.3.7 ATR (Attenuated Total Reflection)-FTIR Results

FTIR plots for biochar samples are shown in Figure 3-4.

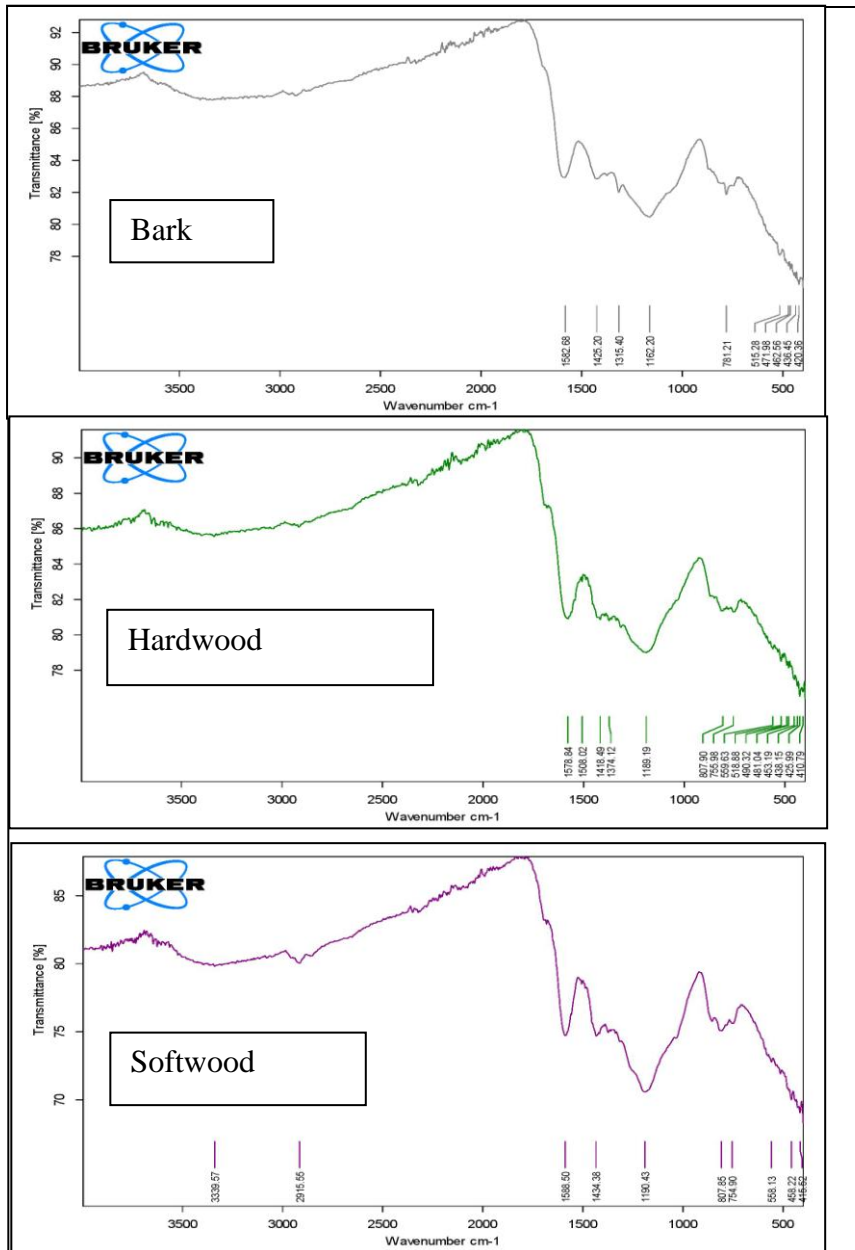


Figure 3-4 ATR-FTIR results for bark, hardwood and softwood char in the wavelength range of 4000 cm^{-1} to 400 cm^{-1} .

Biochar samples have broad peaks in between 3500-3200 cm^{-1} correspond to OH stretching, indicating the extensive dehydration of cellulosic components (Keiluweit et al., 2010). All biochar samples show similar FTIR patterns, except softwood has a peak at 2915.55 cm^{-1} correspond to aliphatic C-H stretching (Abdulrazzaq et al., 2014). Strong peaks in between 1648 and 1540 cm^{-1} showed a high-intensity region of C=C ring stretching, representing the decrease in aromaticity during gasification (Abdulrazzaq et al., 2014). The strong bands in between 1300 and 900 cm^{-1} exhibit that the amount of ether-type (C-O-C) structure is significant in biochar samples (Pastor-Villegas et al., 2007). Bark and hardwood char show peaks between 1360–1430 cm^{-1} which represent O–H and C–H bending can be due to hydroxyl, acid, phenol, olefinesor methyl groups (Fu et al., 2009). There are multiple peaks in the range of 1600-700 cm^{-1} indicating the presence of lignin and cellulose derived transformation products in biochar samples (Keiluweit et al., 2010). Peaks observed in the region of 1000–625 cm^{-1} are compatible with C–H vibrations in olefinic or aromatic structures (Fu et al., 2009). Multiple peaks are observed in the region 900–700 cm^{-1} , which are compatible with out-of-plane C–H deformation in aromatic systems with adjacent-hydrogen atoms (Pastor-Villegas et al., 2007).

3.3.8 X-Ray Diffraction analysis

XRD patterns obtained are shown in figure 3-5 (Intensity vs. $2\theta^\circ$) and the results after the analysis are summarised in table 3-3.

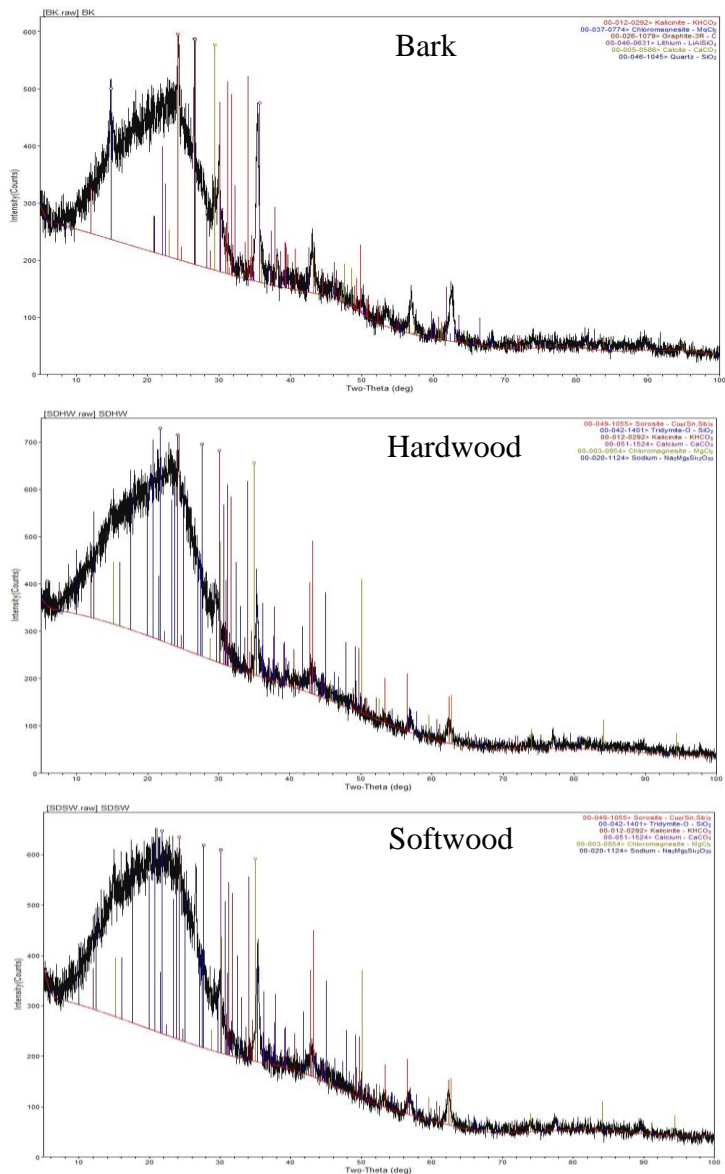


Figure 3-5 XRD patterns of biochar obtained with Cu- $K\alpha$ radiation (40 kV, 40 mA) and

0.1° step size within 5° - 100°)

Table 3-3 XRD Results

Biochar Sample	Mineral	Chemical formula
Bark	Kalicipite	KHCO_3
	Chloromagnesite	MgCl_2
	Calcite	CaCO_3
	Quartz	SiO_2
	Graphite	C
	α -eucryptite	LiAlSiO_4
Hard wood	Kalicipite	KHCO_3
	Chloromagnesite	MgCl_2
	Calcite	CaCO_3
	Quartz	SiO_2
	Sorosite	$\text{Cu}_6(\text{Sn,Sb})_5$
	Silicate mineral	$\text{Na}_2\text{Mg}_5\text{Si}_{12}\text{O}_{30}$
Soft wood	Kalicipite	KHCO_3
	Chloromagnesite	MgCl_2
	Calcite	CaCO_3
	Quartz	SiO_2
	Sorosite	$\text{Cu}_6(\text{Sn,Sb})_5$
	Silicate mineral	$\text{Na}_2\text{Mg}_5\text{Si}_{12}\text{O}_{30}$

In all XRD patterns, broad peaks were observed, indicating less crystalline and amorphous structure and low crystal size (González et al., 2013). Also they showed an elevated background between 14° to 26° , due to the presence of organic matter (Cao and Harris, 2010). Kalicinite, chloromagnesite, calcite and quartz were detected as common mineral phases in all biochar samples. The detection of calcite in these biochar samples indicates why the biochar samples are alkaline (González et al., 2013). XRD pattern of hardwood and softwood char show the presence of sorosite and also a silicate mineral containing Na and Mg. All biochar samples show kalicinite (KHCO_3), a highly soluble mineral phase which can be useful if biochar is used as an adsorbent to exchange K with divalent ions (Komnitsas et al., 2014).

3.4 Conclusion

The biochar samples produced from fast pyrolysis showed similar characteristics to those which have been used as adsorbents in literature. Biochar samples are chemically and physically heterogeneous due to the complexity of pyrolysis process. Low BET surface area obtained was due to the high proportion of macro pores on the biochar surface and it was also explained by the “Type II” isotherms obtained which is an indication of macro pores. However, SEM images also showed large cracks and pores confirming above facts and the biochar may be suitable for an adsorbent since the macroporous surface structure can provide routes to adsorptive molecules, even though surface area is low. Hardwood showed the highest BET surface area, pore volume and an insignificant upward curve in its N_2 isotherm, while bark and softwood char showed greater upward curve indicating

their less adsorptive properties. Density of all biochar samples were around 0.3 g/m^2 and showed alkaline pH which is similar to the biochar adsorbents studied in literature. All biochar samples tested have H: C ratio around 0.05 where softwood has the highest ratio indicating low aromaticity and hardwood shows the lowest ratio indicating high aromaticity. High H: C ratio of softwood obtained from elemental analysis was explained in FTIR analysis where low aromaticity was observed with the highest intensity region relevant to C=C rings. In the FTIR pattern for hardwood, high amount of peaks were observed in the region representing C-H bonds explaining high aromaticity and low H: C ratio. Bark and hardwood char showed oxygen containing groups which can improve the adsorptive characteristics of biochar. XRD patterns revealed that the biochar samples contain kaliginite (KHCO_3) which can be useful if biochar is used as an adsorbent and mineral phases such as chloromagnesite, calcite and quartz were also present.

3.5 Bibliography- Chapter 03

Abdulrazzaq, H., Jol, H., Husni, A. and Abu-bakr, R. (2014) 'Characterization and Stabilisation of Biochars Obtained from Empty Fruit Bunch, Wood, and Rice Husk', 9(2003), pp. 2888–2898.

Aguado, R. C., Chen, D. and Zhu, J. (2013) *Catalytic conversion of biomass*. Norwegian University of Science and Technology Department.

Ahmad, M., Rajapaksha, A. U., Lim, J. E., Zhang, M., Bolan, N., Mohan, D., Vithanage, M., Lee, S. S. and Ok, Y. S. (2014) 'Biochar as a sorbent for contaminant management in soil and water: a review.', *Chemosphere*. Elsevier Ltd, 99, pp. 19–33. doi: 10.1016/j.chemosphere.2013.10.071.

Brown, R. a., Kercher, A. K., Nguyen, T. H., Nagle, D. C. and Ball, W. P. (2006) 'Production and characterization of synthetic wood chars for use as surrogates for natural sorbents', *Organic Geochemistry*, 37(3), pp. 321–333. doi: 10.1016/j.orggeochem.2005.10.008.

Byrne, C. and Nagle, D. (1996) 'Carbonization of Wood for Advanced Materials.', 35(2), pp. 259–266.

Cao, X. and Harris, W. (2010) 'Bioresource Technology Properties of dairy-manure-derived biochar pertinent to its potential use in remediation', *Bioresource Technology*. Elsevier Ltd, 101(14), pp. 5222–5228. doi: 10.1016/j.biortech.2010.02.052.

Fang, Q., Chen, B., Lin, Y. and Guan, Y. (2014) 'Aromatic and hydrophobic surfaces of wood-derived biochar enhance perchlorate adsorption via hydrogen bonding to oxygen-containing organic groups', *Environmental Science and Technology*, 48, pp. 279–288. doi: 10.1021/es403711y.

Fu, P., Hu, S., Sun, L., Xiang, J., Yang, T., Zhang, A. and Zhang, J. (2009) 'Structural evolution of maize stalk/char particles during pyrolysis.', *Bioresource technology*. Elsevier Ltd, 100(20), pp. 4877–83. doi: 10.1016/j.biortech.2009.05.009.

González, M. E., Cea, M., Sangaletti, N., González, a., Toro, C., Diez, M. C., Moreno, N., Querol, X. and Navia, R. (2013) 'Biochar Derived from Agricultural and Forestry Residual Biomass: Characterization and Potential Application for Enzymes Immobilization', *Journal of Biobased Materials and Bioenergy*, 7(6), pp. 724–732. doi: 10.1166/jbmb.2013.1373.

Harris, K., Gaskin, J., Cabrera, M., Miller, W. and Das, K. (2013) 'Characterization and Mineralization Rates of Low Temperature Peanut Hull and Pine Chip Biochars', *Agronomy*, 3, pp. 294–312. doi: 10.3390/agronomy3020294.

Insam, H. and Knapp, B. (2011) *Recycling of Biomass Ashes*. Springer Heidelberg Dordrecht London New York. doi: 10.1007/978-3-642-19354-5.

Keiluweit, M., Nico, P., Johnson, M. and Kleber, M. (2010) ‘Dynamic Molecular Structure of Plant Biomass-derived Black Carbon (Biochar).’

Komnitsas, K., Zaharaki, D., Pylotis, I., Vamvuka, D. and Bartzas, G. (2014) ‘Assessment of pistachio shell biochar quality and its potential for adsorption of heavy metals’, pp. 1–12.

Lee, Y., Park, J., Ryu, C., Gang, K. S., Yang, W., Park, Y.-K., Jung, J. and Hyun, S. (2013) ‘Comparison of biochar properties from biomass residues produced by slow pyrolysis at 500°C.’, *Bioresource technology*. Elsevier Ltd, 148, pp. 196–201. doi: 10.1016/j.biortech.2013.08.135.

Lehmann, J. and Joseph, S. (2010) *Biochar for Environmental Management*.

Özçimen, D. and Ersoy-Meriçboyu, A. (2010) ‘Characterization of biochar and bio-oil samples obtained from carbonization of various biomass materials’, *Renewable Energy*, 35(6), pp. 1319–1324. doi: 10.1016/j.renene.2009.11.042.

Pastor-Villegas, J., Meneses Rodríguez, J. M., Pastor-Valle, J. F. and García García, M. (2007) ‘Changes in commercial wood charcoals by thermal treatments’, *Journal of Analytical and Applied Pyrolysis*, 80(2), pp. 507–514. doi: 10.1016/j.jaap.2007.05.001.

Pastor-Villegas, J., Pastor-Valle, J. F., Rodríguez, J. M. M. and García, M. G. (2006) ‘Study of commercial wood charcoals for the preparation of carbon adsorbents’, *Journal of Analytical and Applied Pyrolysis*, 76(1-2), pp. 103–108. doi: 10.1016/j.jaap.2005.08.002.

Rouquerol, F., Rouquerol, J. and Sing, K. (1999) *Adsorption by Powders and Porous Solids*.

Sivakumar, V., Asaithambi, M. and Sivakumar, P. (2012) ‘Physico-chemical and adsorption studies of activated carbon from Agricultural wastes’, 3(1), pp. 219–226.

Wildman, J., Speakman, S., Street, G. and Zhe, L. W. N. (1991) ‘Origins and functions of macroporosity activated carbons from coal and wood precursors’, 70, pp. 655–661.

Chapter 4. Adsorption of Sulphate Using Wood Biochar

Yashodha G. Marambage, Kelly A. Hawboldt

Faculty of Engineering and Applied Science, Memorial University of Newfoundland,

St. John's, NL, Canada. A1B3X5

Abstract

The potential of wood based biochar as an adsorbent for removal of sulphate in water was investigated through a series of batch adsorption experiments. Biochar produced by fast pyrolysis of bark, hardwood sawdust, and softwood sawdust were used as adsorbents in sodium sulphate solutions prepared in specific concentrations (sulphate concentrations from 300-1800 mg/L) and at pH=4. Experiments were carried out to analyse adsorption isotherms, adsorption kinetics, and thermodynamics. The highest adsorption capacity obtained for hardwood char, softwood char and bark char were 11.81 mg/g, 9.44 mg/g, and 7.94 mg/g respectively at 10 °C and pH=4 for an initial sulphate concentration of 1500 mg/L. The adsorption of sulphate on biochar is an exothermic process. Experimental data was better fitted in pseudo second order kinetic model compared to pseudo first order kinetic model. Adsorption process was described using the Freundlich isotherm model which showed model constants of 0.839 mg/g, 0.839mg/g, and 0.834 mg/g respectively for bark, hardwood, and softwood char. Thermodynamic parameters for the adsorption process were calculated using Van't Hoff equation and negative Gibbs free energy values were obtained suggesting a favourable spontaneous adsorption reaction for all biochar types. ΔH (kJ/mol) and ΔS (kJ/K/mol) values obtained for bark char were -38.577 and -115

0.114 respectively, for hardwood char were -57.899 and -0.177 respectively, and for softwood were -57.832 and -0.179 respectively.

4.1 **Introduction**

Removal of sulphur compounds in waste water streams is a concern especially in oil and gas industry, mining and metallurgical industry, as well as in other industries involving effluents with sulphur compounds such as in the production of fertilisers, dyes, glass, paper, soaps, textiles, fungicides, leather, and metals (Silva, Cadorin and Rubio, 2010). Due to the high solubility and stability of sulphate in aqueous solutions, removal of this anion is complex (Namasivayam and Sangeetha, 2008). Current industrial treatment methods for sulphur compounds include chemical precipitation, biological treatment, and adsorption (Cao *et al.*, 2011). Chemical precipitation involves large costs with high amounts of sludge generation and biological treatment methods require long residence times, large areas and management of organic residuals (Silva, Cadorin and Rubio, 2010). Reverse osmosis, electrodialysis, and nanofiltration or membrane filtration can be used, but those are expensive and limited as waste water volumes increase (Silva, Cadorin and Rubio, 2010). Compared to other sulphur treatment techniques, adsorption processes consume less energy, giving nearly 100% of product water recovery, and no chemicals are required for a normal adsorptive process (RPSEA, 2009). Zeolite, organoclay, activated alumina, activated carbon and biochar are some adsorbents used in industrial water treatment systems (Guerra, Dahm and Dunderf, 2011). Adsorbents derived from

biochar make the process more environmentally friendly and highly cost effective (Yao, 2013).

There are recent studies done on removal of sulphur compounds using magnetite, γ - Al_2O_3 , goethite, shrimp shell waste, and modified sugarcane bagasse as adsorbents but a very few research studies are available on biochar based adsorbents in sulphur removal (Geelhoed et al., 1997; Mulinari and da Silva, 2008; Roonasi and Holmgren, 2009; Wu et al., 2000; Moret and Rubio, 2003). As an example, activated carbon from coconut coir pith, (activated using ZnCl_2) was investigated as an adsorbent for removal of sulphate from water and sulphur removal varied from 54% to 90% in the optimum pH range of 3.0–9.0 (Namasivayam and Sangeetha, 2008). Hong et al. (2014) studied removal of sulphate from acid mine drainage water (AMD) using wood based activated carbon, modified by grafting polypyrrole and a maximum of 44.7 mg/g of sulphate adsorption was achieved (Hong *et al.*, 2014). Both studies are on activated carbon, improved using different chemicals which can make the adsorbent more expensive and may also require a proper way of disposal. Therefore, a biochar based adsorbent with minimum or no chemicals involved would be a cost effective and environmental friendly technique for removal of sulphur compounds from industrial waste streams.

This study investigates biochar produced from wood residues as an adsorbent to remove sulphur compounds from water. Throughout the world, wood residues are generated in large quantities as a waste product; as an example, in the United States in 2001, 234 million metric tons of wood residues has been generated from various sources including

traditional timber extraction (Nzokou, Simons and Weatherspoon, 2011). It is estimated that wood residues accounts for about 17% of the total residues received at municipal landfills in the United States (Nzokou, Simons and Weatherspoon, 2011). In saw mills, after receiving the wood logs, about 12% of waste is generated in the form of bark and sawdust constitutes another 12% of the log input (Koopmans and Koppejan, 1997). Biochar for adsorption experiments of this study were obtained as bark, softwood sawdust, and hardwood sawdust which were generated as waste from saw mills.

Biochar samples were characterised using standard methods including BET-N₂ analysis, elemental analysis, Fourier transform infrared (FTIR) spectroscopy, scanning electron microscopy (SEM), and XRD (X-ray diffraction) analysis and the adsorption performance for removal of sulphate, including adsorption isotherms, adsorption kinetics, and adsorption thermodynamics were evaluated by batch adsorption experiments.

4.2 Materials and methods

4.2.1 Characterization of biochar

Biochar for adsorption experiments were obtained from three different biomass (bark, softwood saw dust, and hardwood saw dust) from wood residues. Feedstock particle size was less than 2 mm. All biochar samples were produced in a 2-4 kg/h auger pyrolysis reactor at a temperature of 450 °C with a residence time of 3 minutes. The intended product of this fast pyrolysis process was bio oil and biochar was generated as a by product with a yield of 15-17 % (bio char generation rate wa 300-600 gh⁻¹).

Biochar samples were kept in the oven at 75 °C overnight before each test.

Physical properties such as surface area, porosity, total pore volume, pore width and surface morphology of biochar were measured using BET-N₂ analysis and SEM analysis. Density and pH of the biochar samples were determined. Carbon content and ash content were determined by TGA analysis. C, H, N, S, and O content were determined by elemental analysis, ATR-FTIR analysis and XRD analysis. The detailed characterization methodology and discussion on results are in Chapter 3.

4.2.2 Batch adsorption experiments

Batch adsorption experiments were conducted in a rotary shaker (Innova 4230 refrigerated incubator shaker). 1g of biochar and 100mL of sulphate solution with the desired concentration were added to a 250mL flask. Sulphate solutions were prepared using sodium sulphate anhydrous powder (Na₂SO₄) ≥99.0% from Sigma-Aldrich Canada Co. The pH of the solution was adjusted with 0.1 M HCl (Sigma-Aldrich Canada Co.) and/or 0.1M NaOH (Sigma-Aldrich Canada Co.) using a calibrated digital pH meter (“Oakton pH Testr 10” with ±0.1pH accuracy) to ensure the desired pH before adding biochar. The samples in tightly closed flasks were mixed for 1 hour at 250 rpm in the rotary shaker at the specified temperature. Triplicates were run with 100ml sulphate solutions using the same procedure. The mixtures were filtered using vacuum filtration to separate the spent biochar. The concentrations of the sulphur compounds in the aqueous phase were analyzed using the ICP-OES instrument (“Perkin-Elmer Optima 5300 DV” Inductively Coupled Plasma – Optical Emission Spectrometer using a Cetac ASX-520

auto sampler) in Core Research Equipment and Instrument Training (CREAIT) network at Memorial University of Newfoundland.

Adsorption capacity was calculated using the following equation.

$$\text{Adsorption capacity } (q_e) \text{ (mg/g)} = (C_i - C_e) \times \frac{V}{m} \quad (4-1)$$

C_i = Initial concentration of adsorbate (mg/L)

C_e = Equilibrium adsorbate concentration (mg/L)

V = Volume of the solution (L)

m = Mass of the adsorbent (g)

4.2.3 Adsorption kinetic studies

Pseudo first order kinetic model and pseudo second order kinetic model were used to describe the adsorption kinetics.

The first-order rate expression is outlined below (Qiu *et al.*, 2009).

$$\log(q_e - q_t) = \log q_e - \frac{K_1 t}{2.303} \quad (4-2)$$

Where q_t (mg/g) is the amount of the adsorbate adsorbed at time t (min), K_1 (min^{-1}) is the rate constant of pseudo first order adsorption and q_e (mg/g) is the adsorption capacity at equilibrium. A linear relationship in the plot of $\log(q_e - q_t)$ versus t is expected if first-order kinetics is applicable

The second-order kinetic model is as follows (Qiu *et al.*, 2009).

$$\frac{t}{q_t} = \frac{1}{K_2 q_e^2} + \frac{t}{q_e} \quad (4-3)$$

Where q_t (mg/g) is the amount of the adsorbate adsorbed at time t (min), K_2 (g/mg min) is the rate constant of pseudo second order adsorption and q_e (mg/g) is the adsorption capacity at equilibrium. A linear relationship in the plot of t/q_t versus t is expected if second-order kinetics is applicable.

The initial adsorption rate h ($\text{mg g}^{-1}\text{min}^{-1}$) when t approaches 0, was determined from K_2 and q_e value using the following equation:

$$h = K_2 q_e^2 \quad (4-4)$$

4.2.4 Adsorption isotherm studies

Freundlich Isotherm model and Langmuir isotherm model were used to analyse adsorption experiments.

The Freundlich Isotherm model was obtained using below equation.

$$q_e = K_F C_e^{\frac{1}{n}} \quad (4-5)$$

q_e = Amount of solute adsorbed per unit weight of adsorbent at equilibrium (mg/g dry weight)

C_e = Equilibrium concentration of the solute in the solution (mg/L)

K_F = Freundlich constant (mg/g/min)

$1/n$ = A measure of intensity of adsorption.

Linearization of the Freundlich model gives

$$\log(q_e) = \log(K_F) + \frac{1}{n} \log(C_e) \quad (4-6)$$

A log-log plot of q_e versus C_e gives an intercept of $\log K_F$ and a slope of $1/n$.

The Langmuir isotherm model was obtained using below equation.

$$q_e = \frac{Q_a^0 K_L C_e}{1 + K_L C_e} \quad (4-7)$$

q_e = Amount of solute adsorbed per unit weight of adsorbent at equilibrium (mg/g dry weight)

C_e = Equilibrium concentration of the solute in the solution (mg/L)

K_L = Langmuir constant related to the affinity of the binding sites (L/mg)

Q_a^0 = Maximum adsorption capacity for forming monolayer (mg/g).

Linearization of the Langmuir model gives:

$$\frac{C_e}{q_e} = \frac{1}{K_L Q_a^0} + \frac{C_e}{Q_a^0} \quad (4-8)$$

A Langmuir system exhibits a straight line when plotting $\frac{C_e}{q_e}$ versus C_e with an intercept of

$\frac{1}{K_L Q_a^0}$ and a slope of $\frac{1}{Q_a^0}$.

4.2.5 Adsorption thermodynamic studies

The thermodynamics parameters for the adsorption process were calculated using the distribution coefficients at different temperatures.

$$K_D = \frac{q_e}{C_e} \quad (4-9)$$

K_D = distribution coefficient (L/kg)

q_e = quantity of the adsorbate adsorbed per unit mass of solid (mg/kg)

C_e = equilibrium concentration of adsorbate in the solution (mg/L)

The K_D values were used to determine the thermodynamic parameters such as standard Gibbs free energy change, enthalpy change (ΔH), and entropy change (ΔS):

$$\Delta G = \Delta H - T\Delta S \quad (4-10)$$

$$\Delta G = -RT\ln K_D \quad (4-11)$$

R = universal gas constant (8.314 Jmol⁻¹K⁻¹)

T = absolute temperature (K)

The ΔH and ΔS were obtained from the intercept and slope of the Van't Hoff equation of ΔG vs. T

$$\ln K_D = \frac{\Delta S}{R} - \frac{\Delta H}{R} \times \frac{1}{T} \quad (4-12)$$

4.3 Results and discussion

4.3.1 Effect of the biochar type and the temperature

Batch adsorption experiments were carried out for the three biochar samples (bark, softwood sawdust, and hardwood saw dust) in order to analyse the effect of starting biomass on adsorption of sulphate on biochar. The most suitable pH was determined as 4 by carrying out a series of pH experiments. This pH value was supported according to a past study done on removal of sulphate using activated carbon from coconut coir pith at pH=4 (Namasivayam and Sangeetha, 2008). At initial sulphur concentration [S] of 548 mg/L and at pH=4, the results obtained from batch adsorption experiments at different temperatures are shown in table 4-1 (Standard deviation of the results obtained for final sulphur concentration is $\pm 2\%$).

Table 4-1 Effect of the temperature on adsorption of sulphate by different biochar types

Sample name (10g/L dose)	Temperature (°C)	Final [S] (mg/L)	Sulphur removal (mg/L)	Adsorption capacity (mg/g)
Bark char	10	468.6	79.4	7.94
	20.1	511.75	36.25	3.62
	30	518.33	29.67	2.97

Sample name (10g/L dose)	Temperature (°C)	Final [S] (mg/L)	Sulphur removal (mg/L)	Adsorption capacity (mg/g)
Hardwood char	10	429.9	118.1	11.81
	20.1	483.75	64.25	6.42
	30	521.73	26.27	2.63
Softwood char	10	453.62	94.38	9.44
	20.1	495.15	52.85	5.29
	30	527.65	20.35	2.03

The highest adsorption capacities obtained for hardwood char, softwood char and bark char were 11.81 mg/g, 9.44 mg/g, and 7.94 mg/g respectively at 10 °C. This can be explained by the BET-N₂ analysis results where hardwood char showed the highest BET surface area of 43.23m²/g and the highest pore volume of 0.0032 cm³/g. Due to higher porosity, hardwood char has adsorbed more sulphur molecules compared to other two. This is a very good adsorption capacity as the biochar is not activated, compared to the 4.9 mg/g of maximum sulphate adsorption capacity from the activated carbon from coconut coir pith and 7.23mg/g of maximum sulphate adsorption capacity for a wood-based activated carbon (Namasivayam and Sangeetha, 2008; Hong et al., 2014).

With increasing temperature, all biochar showed decreasing adsorption capacities. Figure 4-1 illustrates the results of adsorption capacity with increasing temperature for three biochar types. Standard deviation of $\pm 2\%$ of adsorption capacity is illustrated in the graphs.

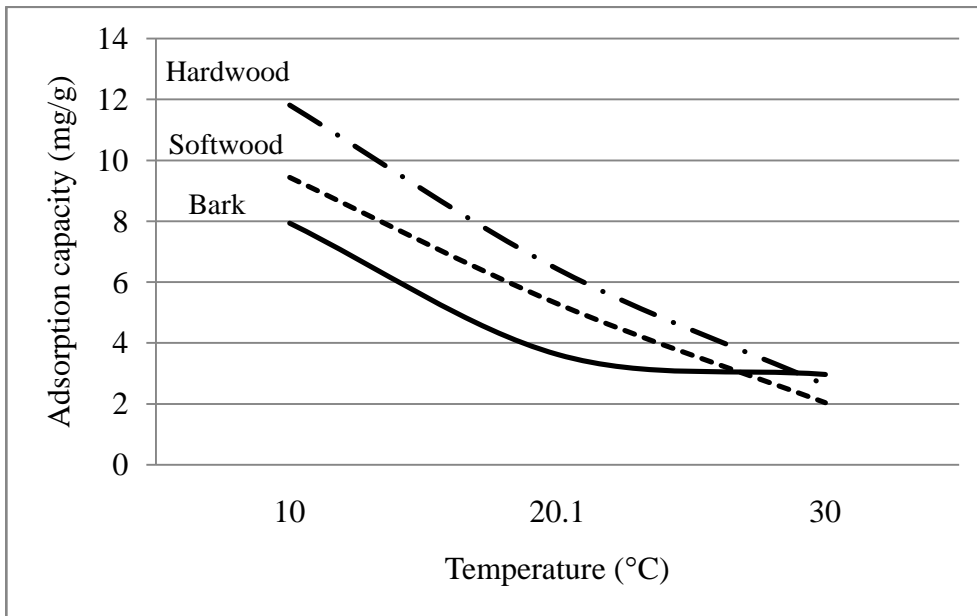


Figure 4-1 Adsorption capacity vs. Temperature and biochar type

As shown in figure 4-1, biochar showed better adsorbent characteristics in low temperatures. Hardwood char showed highest adsorption capacity compared to other two biochar types at all temperatures below 30 °C. At 30 °C, bark char showed better adsorption compared to softwood char, which showed higher adsorption capacity in lower temperatures. The relationship of temperature to adsorption process is discussed in later under adsorption thermodynamics.

4.3.2 Adsorption Kinetics

Batch adsorption experiments were carried out for the three biochar samples (bark, softwood sawdust, and hardwood sawdust) at pH=4 and at 10°C. At selected time intervals (15min, 30min and 45 min) up to a maximum of 1 hour, samples were extracted from the rotary shaker and tested for the remaining sulphur content in the solution. The results obtained for adsorption capacities at different time intervals are shown in table 4-2(Standard deviation of the results obtained for final sulphur concentration is $\pm 2\%$).

Table 4-2 Effect of mixing time on adsorption of sulphate by different biochar types

Sample name (10g/L dose)	Time (t) (min)	Final [S] (mg/L)	Sulphur removal (mg/L)	Adsorption capacity (mg/g)
Bark char	15	484.37	63.62	6.36
	30	473.25	74.75	7.47
	45	471.7	76.3	7.63
	60	468.6	79.4	7.94
Hardwood char	15	480.3	67.7	6.77
	30	460.2	87.8	8.78
	45	433.7	114.3	11.43
	60	429.9	118.1	11.81
Softwood char	15	486.1	61.9	6.19
	30	480.55	61.74	6.74
	45	473.25	67.45	7.48
	60	453.62	94.37	9.44

The results obtained were plotted as shown in figure 4-2. Standard deviation of $\pm 2\%$ of adsorption capacity is illustrated in the graphs.

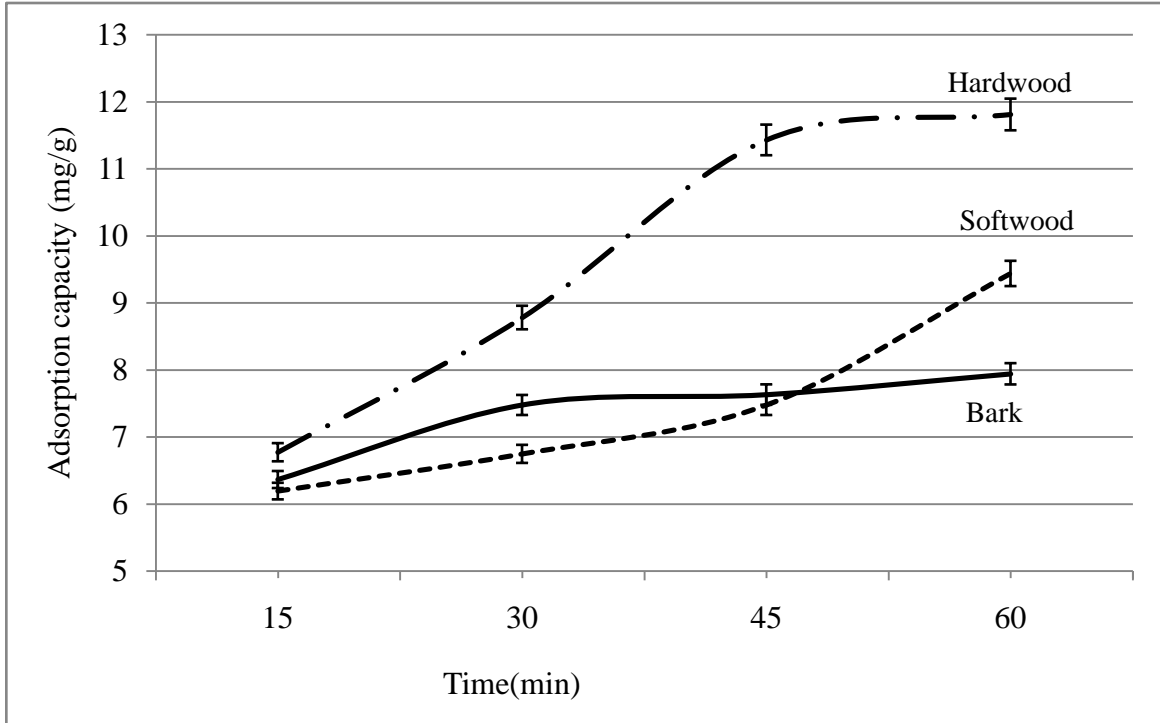


Figure 4-2 Adsorption capacity vs. Mixing time and biochar type

The results showed that for bark and hardwood char, there is a rapid increase of adsorption rate at the beginning of the mixing and at 60 minutes, the mixture has reached equilibrium. Softwood char, which showed different kinetics, has an increasing adsorption rate with time until equilibrium is achieved at 60 minutes mixing time. In past studies, it has been shown that the sulphate adsorption is, kinetically, a very fast process, as for chitin-based shrimp shells, 15 minutes was sufficient to attain the maximum uptake of sulphate ions (Moret and Rubio, 2003). On a coconut coir pith based activated carbon,

the amount of sulphate adsorption increased with time and reached equilibrium at 30 minutes (Namasivayam and Sangeetha, 2008). Similar to those studies, the rate of adsorption of sulphate on the bark and hardwood char samples was rapid in the initial stages and gradually decreased until the equilibrium reached at 60 minutes suggesting the possible monolayer coverage of sulphate on the surface of biochar (Namasivayam and Sangeetha, 2008). Softwood char has a low adsorption capacity at the beginning compared to the other two biochars, but after 45 minutes, the adsorption capacity has increased compared to bark char. The adsorption rates can be further explained using two kinetics models.

Pseudo first order model and pseudo second order model were used to further describe the kinetics of adsorption process according to the equations (4-2) and (4-3) respectively as shown in table 4-3 and table 4-4. A linear relationship in the plot of $\log (q_e - q_t)$ vs. t is expected if first order kinetics is applicable and a linear relationship in the plot of t/q_t versus t is expected if second-order kinetics is applicable.

Table 4-3 First order kinetic model plots

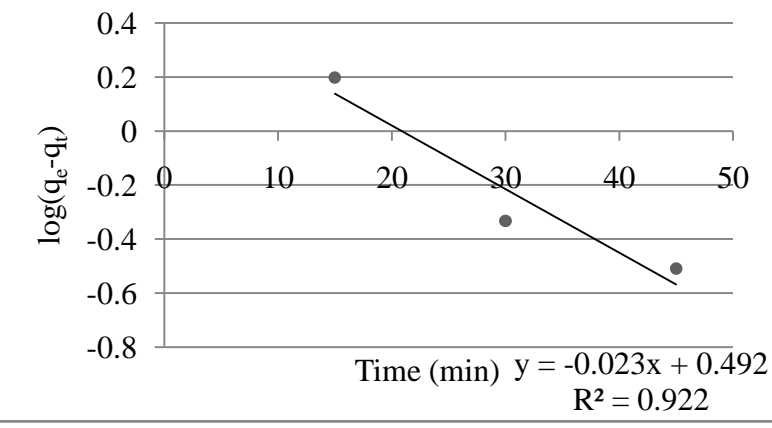
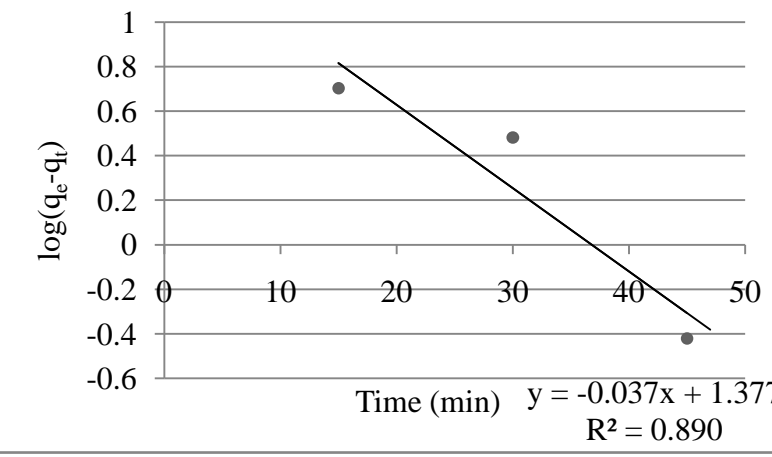
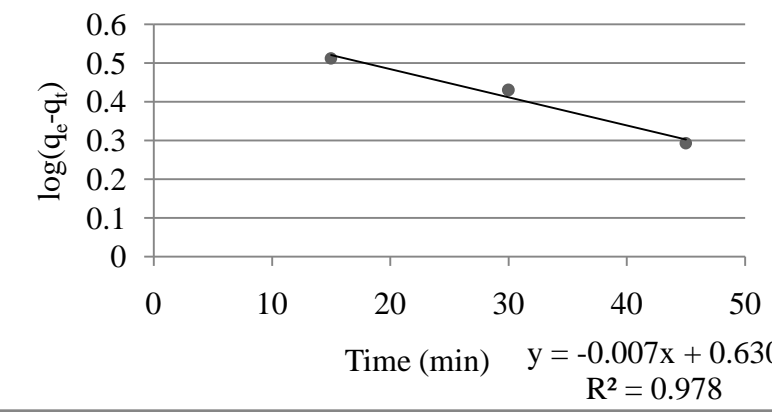
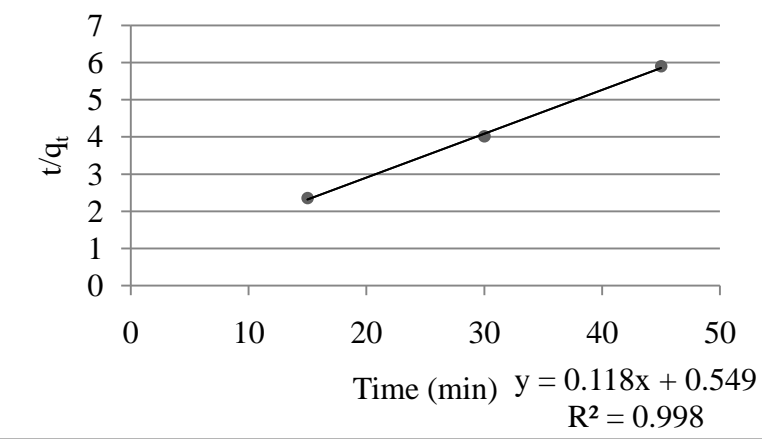
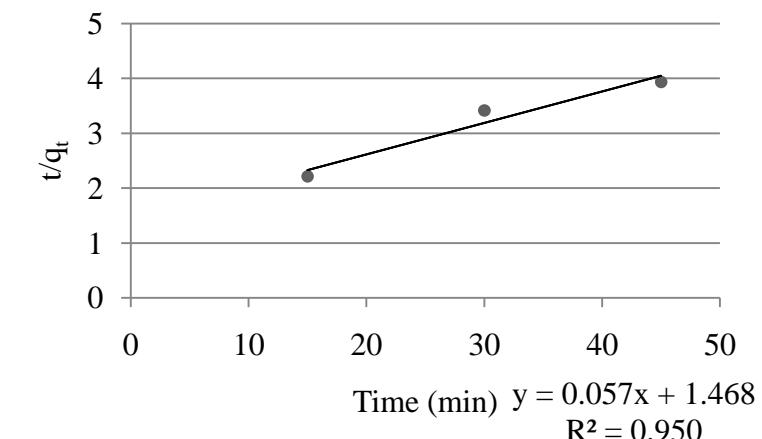
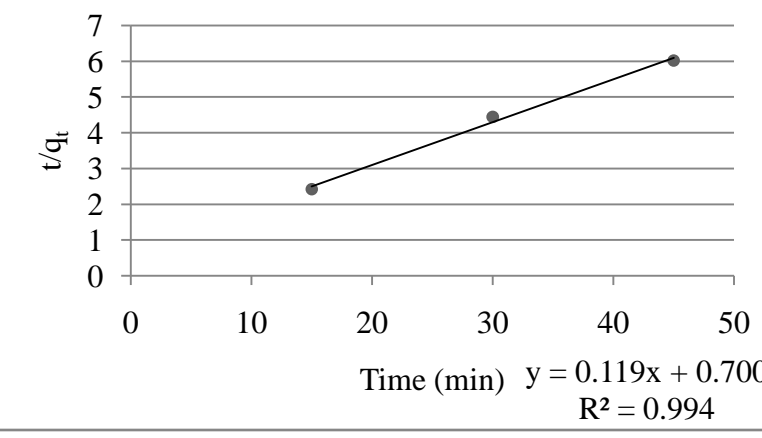
Bark char	 <p>Time (min) $y = -0.023x + 0.492$ $R^2 = 0.922$</p>	
Hardwood sawdust char	 <p>Time (min) $y = -0.037x + 1.377$ $R^2 = 0.890$</p>	
Softwood sawdust char	 <p>Time (min) $y = -0.007x + 0.630$ $R^2 = 0.978$</p>	

Table 4-4 Second order kinetic model plots

Bark char	 <p>Time (min) $y = 0.118x + 0.549$ $R^2 = 0.998$</p>
Hardwood sawdust char	 <p>Time (min) $y = 0.057x + 1.468$ $R^2 = 0.950$</p>
Softwood sawdust char	 <p>Time (min) $y = 0.119x + 0.700$ $R^2 = 0.994$</p>

Kinetic plots show that the experimental data has better agreement with the pseudo second order kinetic model. To compare the suitability of these two models, values of q_e , K_1 , and K_2 were calculated from the slopes and intercepts of relevant plots according to the equations (4-2) and (4-3). The calculated results are shown in table 4-5 as a comparison with experimental results.

Table 4-5 Comparison of the first and second order adsorption rate constants and calculated and experimental q_e values

Biochar	q_e (mg/g) (Experi.)	First order kinetics			Second order kinetics		
		K_1 (min^{-1})	q_e (mg/g) (Calc)	R^2	K_2 (g/mg/min)	q_e (mg/g) (Calc)	R^2
Bark char	7.94	0.053	3.10	0.922	0.025	8.47	0.998
Hardwood sawdust char	11.81	0.085	23.82	0.890	0.002	17.54	0.950
Softwood sawdust char	9.44	0.016	4.27	0.978	0.020	8.40	0.994

According to the above data, in first order kinetic model, calculated q_e values do not agree with the experimental q_e values obtained. Therefore, sulphate adsorption on these biochar samples does not follow the first order kinetic model. Comparatively, calculated q_e values from the second order kinetic model have more agreement with the experimental q_e values. The R^2 values are also higher and very much closer to 1 in second order kinetic

model suggesting higher linear agreement with the model equation. Therefore, it is concluded that sulphate adsorption on these biochar samples follows second order kinetic model. Similarly, the adsorption of sulphate (initial concentration of 80mg/L) on activated coconut coir pith also followed the second-order kinetic model with a K_2 value of 0.043 g/mg/min at 35°C and pH=4 (Namasivayam and Sangeetha, 2008). The pseudo second order kinetic model assumes that the rate limiting step may be a chemical reaction involving valence forces through sharing or exchange of electrons between adsorbent and adsorbate (Qiu *et al.*, 2009). Therefore, sulphate adsorption process on these biochar samples can be a chemical reaction in between the functional groups on biochar surface and sulphate molecules.

The rate of a reaction is defined as the change in concentration of a reactant or product per unit time (Ho, 2006). The initial adsorption rate h ($\text{mg g}^{-1}\text{min}^{-1}$), when t approaches 0, was determined from K_2 and q_e value using the equation 4-4. The initial adsorption rates (h) for bark, hardwood and softwood char are 1.82 mg/g/min, 0.86 mg/g/min, 1.43 mg/g/min respectively. Bark and softwood have high initial adsorption rate demonstrating a rapid attraction of sulphate molecules which can be a result of the high polarity according to the results obtained from elemental analysis (high (O+N): C ratio). Although hardwood char has the highest adsorption capacity due to the high porosity, it has the slowest initial adsorption rate and the lowest K_2 , because hardwood char showed the highest aromaticity (lowest H: C ratio) and the lowest polarity (low (O+N): C ratio) making the surface of the biochar more hydrophobic, while reducing the attraction of sulphate molecules which are hydrophilic (Ahmad *et al.*, 2014)

4.3.3 Adsorption isotherms

Batch adsorption experiments were carried out for the three biochar samples (bark, softwood sawdust, and hardwood saw dust) at pH=4 and at 10°C, using different initial S concentrations (100mg/L, 400 mg/L, 500mg/L and 600mg/L). Results obtained are shown in table 4-6 (Standard deviation of the results obtained for final sulphur concentration is $\pm 2\%$).

Table 4-6 Adsorption capacities obtained from different initial sulphate concentrations

Sample name (10g/L dose)	Initial [S] (mg/L)	Final [S] (mg/L)	Adsorption capacity (mg/g)
Bark char	100	97.55	0.24
	400	331.47	6.85
	500	468.6	3.14
	600	445.58	15.44
Hardwood char	100	99.42	0.06
	400	321.25	7.87
	500	429.9	7.01
	600	449.80	15.02
Softwood char	100	95.48	0.45
	400	344.70	5.53
	500	453.62	4.64
	600	422.43	17.76

The adsorption isotherms for sulphur adsorption by biochar samples are plotted in figure 4-3.

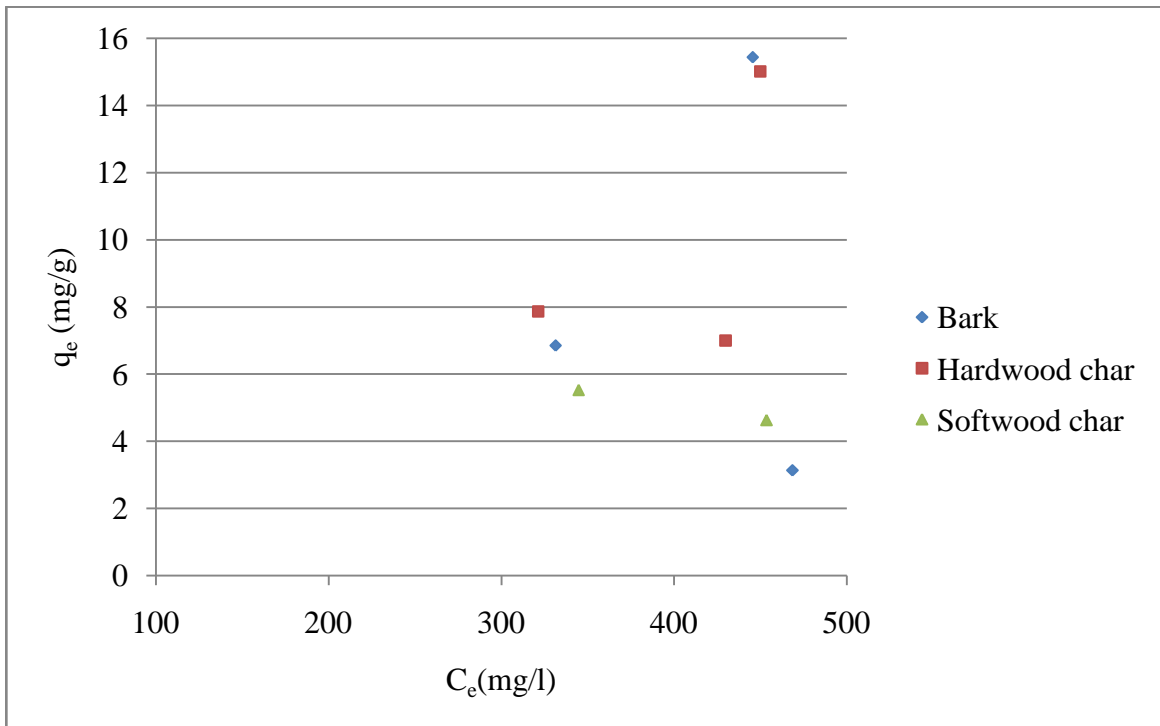


Figure 4-3 Sulphate adsorption isotherm data at pH=4 and 10°C for different biochar

As shown, the adsorption capacity increases quickly at higher sulphate concentrations because the amount of sulphate adsorbed increased. The adsorption capacities of bark char and softwood char are much lower than that of hardwood char, suggesting that hardwood char is the most effective adsorbent at higher concentrations. At lower concentrations, bark char and softwood char showed higher adsorption capacities than hardwood. The adsorption data pattern in figure 4-3 suggest a Freundlich isotherm model with $n > 1$ (Rouquerol, 1999). However, the results were fitted to linear equations of

Freundlich isotherm (equation 4-6) and Langmuir isotherm (equation 4-8) both by plotting $\log q_e$ against $\log C_e$ and C_e/q_e against C_e respectively. The related parameters of Langmuir and Freundlich models were evaluated for further analysis of adsorption isotherms as shown in table 4-7.

Table 4-7 Freundlich and Langmuir equation constants and correlation coefficients for adsorption of sulphate by biochar

Biochar	Freundlich model			Langmuir model		
	K_F (mg/g)	n	R^2	K_L (l/mg)	Q_a^0 (mg/g)	R^2
Bark char	0.839	5.319	0.999	-0.0019	-1.200	0.695
Hardwood	0.839	5.319	0.999	-0.0023	-0.204	0.875
Softwood	0.834	5.291	0.999	-0.0018	-2.336	0.744

The above results confirm that the experimental data properly fit into the Freundlich isotherm model with R^2 value of 0.999. The negative response for Langmuir model suggests that there is no monolayer adsorption (the active sites present on the surface of biochar are not homogenous) and the agreement with Freundlich model suggests a heterogeneous adsorption model due to the variety of sulphur compounds adsorbed in various forms or due to the diversity of sorption sites (Namasivayam and Sangeetha, 2008; Harikishore Kumar Reddy and Lee, 2014). The adsorption of sulphate on activated coconut coir pith followed both Freundlich and Langmuir isotherm models, where Freundlich constants were $K_F = 1.48$ and $n = 3.24$ at 35°C (Namasivayam and Sangeetha, 2008). Sulphate adsorption on $\gamma\text{-Al}_2\text{O}_3$ also followed the Freundlich isotherm model with

$K_F = 28.87$ and $n=0.123$ at 25°C (Wu *et al.*, 2002). Bark and hardwood char show high K_F values compared to softwood char, indicating the higher adsorption ability (Ahmad *et al.*, 2014). The inverse of n ($1/n$) is a measure of intensity of adsorption. The $1/n$ values between 0 and 1 indicate that adsorption of sulphate onto these biochar samples was favourable under the experimental conditions studied (Harikishore Kumar Reddy and Lee, 2014)

4.3.4 Adsorption thermodynamics

Thermodynamic parameters for adsorption reaction were obtained using the results of batch adsorption experiments carried out at different temperatures for the three biochar samples (bark, softwood sawdust, and hardwood saw dust) at initial sulphur concentration [S] of 548 mg/L, at 10°C and $\text{pH}=4$. The results obtained are shown in table 4-1 and were fitted to linear equation 4-12 (Van't Hoff equation) by plotting $\ln(K_D)$ vs. $1/T$ as shown in figure 4-4.

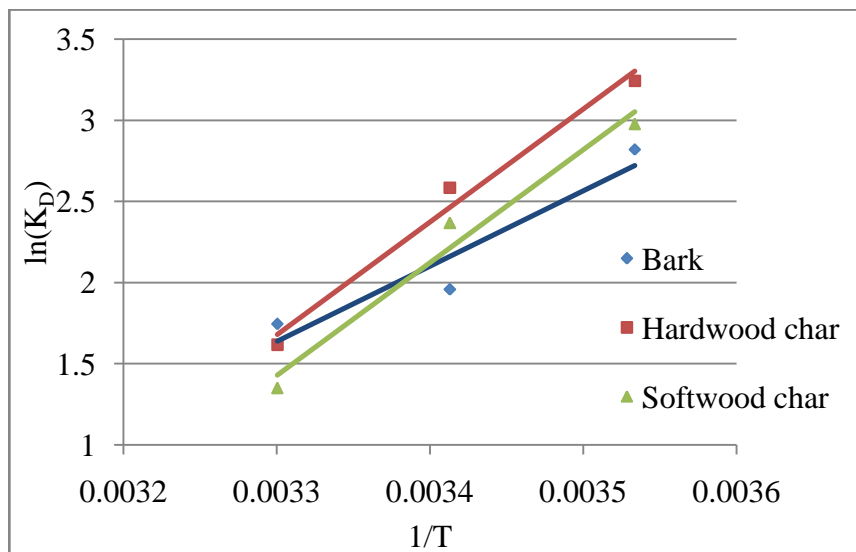


Figure 4-4 Van't Hoff plot for adsorption of sulphate on biochar
137

From the intercept and slope of the plot, ΔH and ΔS were obtained and ΔG was calculated using equation 4-10. Thermodynamic parameters obtained are shown in table 4-8.

Table 4-8 Thermodynamic parameters

Biochar	Temperature (°C)	K_D (L/kg)	ΔG (kJ/mol)	ΔH (kJ/mol)	ΔS (kJ/K/mol)
Bark char	10	16.77	-6.413	-38.577	-0.114
	20	7.08	-5.277		
	30	5.72	-4.140		
Hardwood sawdust char	10	25.66	-7.783	-57.899	-0.177
	20	13.28	-6.011		
	30	5.03	-4.240		
Softwood sawdust char	10	19.64	-7.198	-57.832	-0.179
	20	10.67	-5.409		
	30	3.86	-3.620		

It is concluded that the adsorption of sulphate on biochar is a favourable spontaneous process, as the total Gibbs free energy of the system decreases during the process ($\Delta G < 0$) for all biochar types. ΔS has become negative during adsorption because the degree of freedom of the molecule or the randomness of the molecule decreases as the sulphate molecules transfer on to the solid (biochar surface) from the aqueous solution. Negative ΔH represents the exothermic nature of an adsorption, where the adsorption capacities

decrease with increasing temperature (Yang *et al.*, 2014). This is because when the molecules are adsorbed on the adsorbent, heat can be generated due to the forces of attraction. Similar thermodynamic behaviour has been obtained in the study of As (III) adsorption on modified chestnut shell where the negative value of $\Delta H(-103.816 \text{ kJ mol}^{-1})$ and the negative value of $\Delta S(-314.36 \text{ JK}^{-1} \text{ mol}^{-1})$ indicated exothermic adsorption process and a negative value of $\Delta G(-6.792 \text{ kJ mol}^{-1})$ showed a spontaneous adsorption reaction (Targan and Tirtom, 2014).

4.4 Conclusion

Biochar was produced from fast pyrolysis of three types of wood residues (bark, hardwood sawdust, softwood sawdust) and used as adsorbents in removal of sulphate from water. Batch adsorption experiments carried out in laboratory showed that wood biochar can be used as an adsorbent as a replacement for expensive and chemically modified industrial adsorbents such as activated carbon. Compared to the other studies has been carried out on sulphate removal using biochar adsorbents without any chemical activation, these wood biochar showed better maximum adsorption capacities. Hardwood char showed highest adsorption capacity compared to other two because of higher surface area and porosity. Bark and softwood char showed high adsorption rates as the adsorbent surfaces exhibited high polarity and less aromaticity. Adsorption capacities decreased with increasing temperature. Adsorption process was described using pseudo second order kinetic model and the rate determining step of sulphate adsorption was determined as a chemical reaction in between the functional groups on biochar surface and sulphate

molecules. Adsorption results agreed with Freundlich isotherm model and suggested a heterogeneous adsorption model. Thermodynamic parameters showed that the adsorption process is spontaneous, thermodynamically favourable and exothermic with decreasing randomness in the system.

4.5 Bibliography- Chapter 04

Ahmad, M., Moon, D. H., Vithanage, M., Koutsospyros, A., Lee, S. S., Yang, J. E., Lee, S. E., Jeon, C. and Ok, Y. S. (2014) 'Production and use of biochar from buffalo-weed (*Ambrosia trifida* L.) for trichloroethylene removal from water', *Journal of Chemical Technology and Biotechnology*, 89(1), pp. 150–157. doi: 10.1002/jctb.4157.

Cao, W., Dang, Z., Zhou, X.-Q., Yi, X.-Y., Wu, P.-X., Zhu, N.-W. and Lu, G.-N. (2011) 'Removal of sulphate from aqueous solution using modified rice straw: Preparation, characterization and adsorption performance', *Carbohydrate Polymers*. Elsevier Ltd., 85(3), pp. 571–577. doi: 10.1016/j.carbpol.2011.03.016.

Geelhoed, J. S., Hiemstra, T. and Van Riemsdijk, W. H. (1997) 'Phosphate and sulfate adsorption on goethite: Single anion and competitive adsorption', *Geochimica et Cosmochimica Acta*, 61(12), pp. 2389–2396. doi: 10.1016/S0016-7037(97)00096-3.

Guerra, K., Dahm, K. and Dunderf, S. (2011) *Oil and Gas Produced Water Management and Beneficial Use in the Western United States*.

Harikishore Kumar Reddy, D. and Lee, S.-M. (2014) 'Magnetic biochar composite: Facile synthesis, characterization, and application for heavy metal removal', *Colloids and Surfaces A: Physicochemical and Engineering Aspects*. Elsevier B.V., 454, pp. 96–103. doi: 10.1016/j.colsurfa.2014.03.105.

Ho, Y.-S. (2006) 'Review of second-order models for adsorption systems.', *Journal of hazardous materials*, 136(3), pp. 681–9. doi: 10.1016/j.jhazmat.2005.12.043.

Hong, S., Cannon, F. S., Hou, P., Byrne, T. and Nieto-delgado, C. (2014) 'Sulfate removal from acid mine drainage using polypyrrole-grafted granular activated carbon', *Carbon*. Elsevier Ltd, 73(29), pp. 51–60. doi: 10.1016/j.carbon.2014.02.036.

Koopmans, A. and Koppejan, J. (1997) 'Agricultural and forest residues - Generation, utilization and availability', *Regional Consultation on Modern Applications of Biomass Energy*, (January 1997), pp. 6–10.

Moret, a. and Rubio, J. (2003) 'Sulphate and molybdate ions uptake by chitin-based shrimp shells', *Minerals Engineering*, 16(8), pp. 715–722. doi: 10.1016/S0892-6875(03)00169-9.

Namasivayam, C. and Sangeetha, D. (2008) 'Application of coconut coir pith for the removal of sulfate and other anions from water', *Desalination*, 219(1-3), pp. 1–13. doi: 10.1016/j.desal.2007.03.008.

Nzokou, P., Simons, J. and Weatherspoon, A. (2011) 'Wood residue processing and utilization in southeastern Michigan, U.S', *Arboriculture and Urban Forestry*, 37(1), pp. 13–18.

Qiu, H., Lv, L., Pan, B., Zhang, Q., Zhang, W. and Zhang, Q. (2009) 'Critical review in adsorption kinetic models', *Journal of Zhejiang University SCIENCE A*, 10(5), pp. 716–724. doi: 10.1631/jzus.A0820524.

Roonasi, P. and Holmgren, A. (2009) 'An ATR-FTIR study of sulphate sorption on magnetite; rate of adsorption, surface speciation, and effect of calcium ions.', *Journal of colloid and interface science*. Elsevier Inc., 333(1), pp. 27–32. doi: 10.1016/j.jcis.2008.12.080.

Rouquerol, F. (1999) *Adsorption by Powders and Porous Solids*. San Diego: Academic Press, San Diego.

RPSEA (2009) *An Integrated Framework for Treatment and Management of Produced Water*.

Silva, R., Cadorin, L. and Rubio, J. (2010) 'Sulphate ions removal from an aqueous solution: I. Co-precipitation with hydrolysed aluminum-bearing salts', *Minerals Engineering*. Elsevier Ltd, 23(15), pp. 1220–1226. doi: 10.1016/j.mineng.2010.08.016.

Targan, Ş. and Tirtom, V. N. (2014) 'Arsenic removal from aqueous system using modified chestnut shell', *Desalination and Water Treatment*, (October), pp. 1–8. doi: 10.1080/19443994.2014.942377.

Wu, C.-H., Kuo, C.-Y., Lin, C.-F. and Lo, S.-L. (2002) 'Modeling competitive adsorption of molybdate, sulfate, selenate, and selenite using a Freundlich-type multi-component isotherm', *Chemosphere*, 47(3), pp. 283–292. doi: 10.1016/S0045-6535(01)00217-X.

Wu, C.-H., Lo, S.-L. and Lin, C.-F. (2000) 'Competitive adsorption of molybdate, chromate, sulfate, selenate, and selenite on γ -Al₂O₃', *Colloids and Surfaces A: Physicochemical and Engineering Aspects*, 166(1-3), pp. 251–259. doi: 10.1016/S0927-7757(99)00404-5.

Yang, J.-S., Kim, Y.-S., Park, S.-M. and Baek, K. (2014) 'Removal of As(III) and As(V) using iron-rich sludge produced from coal mine drainage treatment plant.', *Environmental science and pollution research international*, 21(18), pp. 10878–89. doi: 10.1007/s11356-014-3023-4.

Yao, Y. (2013) 'Sorption of Phosphate and Other Contaminants on Biochar and Its Environmental Implications.'

Chapter 5. Summary

This study investigated the potential of wood biochar as an adsorbent in removal of sulphur compounds from offshore produced water.

Chapter 1 consists of a comprehensive literature review on the composition of produced water and the current treatment technologies. It also provides a review specifically on current industrial sulphur removal methods and studies on adsorption of sulphur compounds and other types of contaminants. Adsorption kinetics, isotherms, and thermodynamics are also discussed providing examples from past studies. The literature review shows that biochar can be a potential adsorbent for the removal of sulphur compounds from produced water using a compact, robust, and remotely operated adsorption unit.

Chapter 2 is a literature review on characterisation of biochar. It includes a discussion of past studies where biochar was used as an adsorbent in removal of contaminants from waste water. A comparison of the biochar characterisation results from past studies is carried out. This analysis illustrates that the biochar adsorbents can be used in waste water treatment and requires further research and proper engineering designs.

Chapter 3 discusses the characterisation results obtained for wood biochar produced through fast pyrolysis of bark, hardwood sawdust and softwood sawdust. The results obtained from standard characterisation methods such as BET analysis, SEM analysis, XRD analysis, and FTIR analysis were analysed for predicting the favourable adsorptive properties. The analysis shows that all biochar samples are heterogeneous in porous

structure and in distribution of adsorption sites and due to the high porosity and the favourable surface chemistry, wood biochar can be used as an adsorbent.

Chapter 4 discusses the results obtained from a series of batch adsorption tests to analyse sulphate adsorption capacity of wood biochar in different adsorption conditions. The highest adsorption capacities obtained for hardwood char, softwood char and bark char are 11.81 mg/g, 9.44 mg/g, and 7.94 mg/g respectively at 10 °C and pH=4. Calculations are carried out to determine the suitable adsorption kinetic model, isotherm model, and the thermodynamic parameters. The analysis connects the batch adsorption test results with the characterisation results obtained in chapter 3. The adsorption reaction of sulphate on wood biochar follows a pseudo second order kinetic model and the adsorption process agrees the Freundlich isotherm model. The thermodynamic parameters show that the adsorption is thermodynamically favourable.

The study shows that the biochar obtained from fast pyrolysis of bark, hardwood sawdust, and softwood sawdust have the potential to be used as adsorbents in sulphate removal from produced water. In order to use wood biochar as an industrial adsorbent and to improve the adsorptive properties, more work has to be carried out in future as summarized below.

5.1 **Future work and recommendations**

Biochar adsorption capacity for sulphur containing anions can be increased through chemical modifications. The chemical treatments should be selected to increase one or more of the properties such as porosity, anion exchange capacity, positively charged surface functional groups, and hydrophilic surface characteristics.

Produced water can contain various compounds other than the target contaminant. Therefore experiments should be carried out to examine the interference of the other compounds in the adsorption of sulphate on biochar.

The characterisation procedure can be carried out on spent biochar also in order to further analyse the adsorption mechanism and confirm the adsorption capacities obtained from batch adsorption tests.

In order to introduce this adsorption process to industry, the environmental impact on used biochar needs to be assessed and also a proper disposal method should be determined. Laboratory scale column experiments can be used to simulate the system and to assess the efficiency and the effectiveness of the adsorption process. Finally, a compact adsorption unit has to be designed which can be operated remotely for offshore platforms.

5.2 **Challenges**

The main challenge in this research was finding a suitable analytical method to analyse the sulphate concentration in the solution. Many samples were tested using the ICP-MS (Inductively Coupled Plasma-Mass Spectrometry) technique, but the error of the data was at least 10%. It was concluded that the results were subjected to the disturbances from the

other compounds leached from biochar, with similar molar masses to sulphate. Therefore the analysis of tests was then repeated with ICP-OES (Inductively Coupled Plasma-Optical Emission Spectrometry) which doesn't involve molar masses in measurement. Initially ICP-OES method also gave higher [S] results than expected, but the error between replicates was always below 2%. The reason was found to be the carryover of sulphur compounds as sulphur was sticking around in the system. This problem was overcome by flushing the system every time after and before a sample was run in the instrument. If the elemental analysis were performed on spent biochar to determine the amount of adsorbed sulphate, these issues would not have occurred, but in that scenario, the biochar surface is extremely heterogeneous and the adsorption process is also heterogeneous, which can make the elemental composition less accurate and diverge. One fast and inexpensive way of measuring sulphate is by using a sulphate ion selective electrode.

Heterogeneous nature of the biochar was a challenge in performing characterisation experiments as well as batch adsorption experiments. The biochar sample was mixed thoroughly before every experiment and triplicates were run in batch adsorption tests in order to increase the homogeneity. Although the bulk sample was mixed, as the characterisation tests were carried out using a very small amount of biochar, the effect of heterogeneity on the results could not be reduced considerably.

Another significant challenge was the lack of the previous studies on sulphate removal using biochar. There are many studies on removal of other contaminants using biochar, but there is a few in sulphate removal. It was a challenge to perform experiments since a

lot of trial experiments had to be carried out to determine the best adsorption parameters. There were no enough data in literature to compare the kinetic results, isotherm models and thermodynamic parameters in the sulphate adsorption system. Therefore, the studies on removal of similar anions using biochar were used to compare the results and plan adsorption experiments.

Appendix

Appendix A: Characterisation of produced water from various studies

Parameter	Bahadori,2013		Fakhrul,2009		Allen,1993		Heavy metal	Fakhrul,2009		Allen, 1993
	Oily waste water	Stripped sour water	Oil-Field	Gas-field	World	North sea		Oil-Field	Gas-field	North sea
Density (kg/m ³)			1014-1140		1014 – 1140	1014 - 1085	Calcium	13-25800	9400-51300	7,455mg/l
Temperature(⁰ C)	30–60	30-35			18-69.5		Sodium	132-97000	37500-120000	47,833
Surface Tension (dynes/cm)			43-78		43 -78	None quoted	Potassium	24-4300	149-3870	2,344
Turbidity							Magnesium	8-6000	1300-3900	674
Conductivity (ohms/cm)				136000 - 586000			Iron	<0.1-100	39-680	43

Parameter	Bahadori,2013		Fakhrul,2009		Allen,1993		Heavy metal	Fakhrul,2009		Allen, 1993
	Oily waste water	Stripped sour water	Oil-Field	Gas-field	World	North sea		Oil-Field	Gas-field	North sea
Alkalinity(mg/l)				0-285			Aluminium	310-410	<0.5-83	
Hardness (ppm)							Boron	5-95	<56	
Salinity (ppm)							Barium	1.3-650	9.65-1740	20
TOC (mg/L)			0-1500	67-38000	0-1500	100 - 1000	Cadmium	<0.005-0.2	<0.02-1.21	
COD (mg/L)	300–1200	200–500	1220	2600-120000	1220	None quoted	Chromium	0.02-1.1	<0.03	
BOD	300–500	100–300	4 – 37 ppm	75-2870			Copper	<0.002-1.5	<0.02-5	
TSS (mg/L)	300–800	10–20	1.2-1000	8-5484	1.2 - 1000	None quoted	Lithium	3-5	18.6-235	
pH	7-8	7-8	4.3-10	3.1-6.47	4.3 - 10	6.7 -7.3	Manganese	<0.004-175	3.59-63	

Parameter	Bahadori,2013		Fakhrul,2009		Allen,1993		Heavy metal	Fakhrul,2009		Allen, 1993
	Oily waste water	Stripped sour water	Oil-Field	Gas-field	World	North sea		Oil-Field	Gas-field	North sea
TDS (mg/l)	150–5000	50–150		139000 - 360000		150 456 mg/l	Lead	0.002-8.8	<0.2-10.2	
Total oil (IR; mg/L)			2-565	2.3-38.8	2 - 565	2 - 64	Strontium	0.02-1000	<6200	660
Volatile (BTX; mg/L)			0.39-35		0.39 - 35	4.5 - 35	Titanium	<0.01-0.7		
Base/ neutrals (mg/L)			<140		<140	<140	Zinc	0.01-35	<0.02-5	
Bases (µg/L)			275		275	Detected	Arsenic	<0.005-0.3	<0.005-151	
Chloride (mg/L)	50–2000	-	80-200000	81500-167448	80 - 200,000	12,400 - 81,000	Mercury	<0.001-0.002		
Bicarbonate (mg/L)			77-3990		77 - 3990	420 - 1430	Silver	<0.001-0.15	0.047-7	
Sulphate (mg/L)			<2-1650	<0.1-47	<2 - 1650	18 - 1650	Beryllium	<0.001-0.004		

Parameter	Bahadori,2013		Fakhrul,2009		Allen,1993		Heavy metal	Fakhrul,2009		Allen, 1993
	Oily waste water	Stripped sour water	Oil-Field	Gas-field	World	North sea		Oil-Field	Gas-field	North sea
Ammoniacal nitrogen (mg/L)	20-50	40-80	10-300		10 - 300	10 - 250	Bromide		150-1149	
Sulphite (mg/L)			10		10	No quoted	Nickel		<0.08-9.2	
Total polar (mg/L)			9.7-600		9.7 - 600	25 -520				
Higher acids(mg/L)			<1-63		<1- 63	0.1 - 53				
Phenols (mg/L)	5-20	20-80	0.009-23		0.009 - 23	2 - 23				
VFA's (volatile fatty acids) (mg/L)			2-4900		2 - 4900	200 - 930				
Dissolved H ₂ S (mg/l)	5-10	10-40				100				
Dissolved CO ₂ (mg/l)					44-265					

